Harmonic and Narrowband Disturbance Rejection for Linear Time-Periodic Plants

Daniel G. Cole

Dissertation submitted to the Faculty of the
Virginia Polytechnic Institute and State University
in partial fulfillment of the requirements of the degree of

Doctor of Philosophy
in
Mechanical Engineering

Harry H. Robertshaw, Ph.D., Chair
William T. Bauman, Ph.D.
Harley H. Cudney, Ph.D.
Mary E. F. Kasarda, Ph.D.
Dean T. Mook, Ph.D.

October 19, 1998
Blacksburg, Virginia

Keywords: periodic systems, $\mathcal{H}_\infty$ control, disturbance rejection

Harmonic and Narrowband Disturbance Rejection for Linear Time-Periodic Plants

by

Daniel G. Cole

Chair, Harry H. Robertshaw, Ph.D.
Department of Mechanical Engineering

(ABSTRACT)

This research investigates the harmonic and narrowband disturbance rejection problem for linear time-periodic (LTP) systems. The consequence of disturbances on LTP systems is similar to their linear time-invariant (LTI) counterparts, but is complicated by the interaction of the disturbance and plant acting at different frequencies, which manifests itself in the modulation of the disturbance signal. The result, for an m-periodic plant and disturbance containing a single tone, is that the output contains m tones.

Using various disturbance rejection architectures, harmonic and narrowband disturbance rejection is investigated for linear time-periodic plants. Included are classical and multivariable feedback controllers, fixed-gain feedforward designs using finite impulse response (FIR) filters and $\mathcal{H}_\infty$ synthesis tools, and adaptive feedforward controllers. The objective of time-periodic, narrowband, disturbance rejection seeks to place a zero in the controlled system's disturbance path and align the zero direction, defined by the null space of the controlled system at the disturbance frequency, with the disturbance.

In this research, constraints on controlled system ∞-norms specify nominal performance and robust stability objectives. Periodic controllers are found using existing LTI $\mathcal{H}_\infty$ control theory, and causality is sastified using two techniques which can be added easily to $\mathcal{H}_\infty$ solvers: loop-shifting and Q-parameterization. The resulting controllers are high-gain, narrowband-pass, periodic filters; the closed-loop sensitivity has a zero at the disturbance frequency, and the disturbance is in the sensitivity's null space. It is also shown that classical designs do not achieve the same performance levels as periodic controllers.

Similar developments are made using the feedforward disturbance rejection architecture. Objectives are given which minimize the weighted ∞-norm of the controlled system. Such feedforward controllers achieve perfect disturbance rejection. A multivariable equivalent of the tapped-delay line is used in the description of periodic FIR filters. In addition, periodic FIR filters are made adaptive using an algorithm similar to filtered-X least mean square (LMS) but modified for periodic systems.

Dedicated to

my

Mother & Father

Acknowledgements

After a dozen years of undergraduate and graduate education, making a list of individuals whom I should thank is a considerable task. To be sure, it would be impossible to acknowledge each teacher who gave me some new insight into the world, and I would forget, most certainly, the countless people who have helped along the way. Thus, to all of the people whom I thoughtlessly overlook, you have my most sincere gratitude. Please know that no task such as this can be accomplished alone and your assistance, in whatever for it took, is what made this accomplishment possible.

Of course, there are some people who have directly influenced this work, me, and my engineering philosophy. First is my committee; thank you Drs. Baumann, Cudney, Kasarda, and Mook for your time and consideration of this research. Also, I would like to thank Dr. Reinholtz and Dr. Inman for their financial support during the later part of my graduate studies. Thank you Will Saunders for your personal and professional friendship. I will always be indebted for the opportunities we have shared, and only hope I can, in some small way, repay you for them. And finally, thank you Harry Robershaw for your friendship, patience, guidance and advice. Few advisors would have allowed a student explore and discover their chosen topic without constraint; I consider this to be among the greatest fortunes of my studies. I will always be grateful for the opportunity to know and work with you.

Contents

List of Figures

List of Tables

Nomenclature

m	plant period
$h[n,t]$	impulse response function
$y[k]$	discrete-time signal
$\hat{y}[k]$	lifted signal
$\hat{y}_l[k]$	lth (block) entry in $\hat{y}[k]$
z	$\mathcal{Z}$-transform variable
$\hat{z}$	lifted $\mathcal{Z}$-transform variable
β	uncertainty weight or flapping angle
γ	$\mathcal{H}_\infty$ bound or Lock inertia number
ε	offset ratio
θ	blade cyclic pitch
$\hat{\lambda}$	inflow ratio
μ	advance ratio
ρ	controller weight
$\overline{\sigma}$	maximum singular value
$\underline{\sigma}$	minimum singular value
$\hat{\phi}_i$	ith lifted sinusoidal vector
φ	azimuth angle
ω	frequency
A_k, B_k, C_k, D_k	time-periodic system matrices
$\hat{A}, \hat{B}, \hat{C}, \hat{D}$	lifted system matrices
$\mathcal{E}$	estimation operator
$\mathbf{F}$	feedforward controller
$\mathcal{F}_l$	lower linear fractional transformation
$\mathcal{F}_u$	upper linear fractional transformation

$\mathbf{G}$	periodic system
$\hat{\mathbf{G}}$	lifted system
$\hat{\mathbf{G}}^{\star}$	lifted plant model
$\tilde{\mathbf{G}}$	harmonic-lifted system
$\mathbf{H}$	time-invariant filter or lifted impulse response function
J	cost function
$\mathbf{J}$	'central' controller
$\mathbf{K}$	generalized or feedback controller
L_2	space of signals with finite 2-norm
$\mathbf{L}$	loop-gain
$\mathfrak{L}_m$	Lifting operator
$\mathbf{P}$	generalized plant
$\mathbf{Q}$	Q-parameter
$\mathbf{S}$	closed-loop sensitivity or controlled disturbance path
$\mathcal{S}^n$	n-dimensional signal space
$\mathbf{T}$	closed-loop complimentary sensitivity
$W_{n,i}$	ith weighting matrix element at delay n
$\mathbf{W}_d$	input weighting matrix
$\mathbf{W}_y$	output weighting matrix
$\mathbf{1}$	unit-step
$\mathbf{\Delta}$	plant uncertainty
$\mathbf{\Lambda}$	delay operator
$\mathbf{\Pi}$	truncation operator
$\mathbf{\Phi}_\omega$	sinusoidal basis at frequency ω
Ω	plant-periodic frequency or rotor frequency
$\|\cdot\|$	vector Euclidian norm
$\|\cdot\|_2$	signal or system 2-norm
$\|\cdot\|_\infty$	system ∞-norm

Chapter 1

Introduction

A large variety of processes can be modeled by linear time-periodic (LTP) systems, including: rotary aerodynamics, multi-rate systems, structures with periodic loading, orbital dynamics, and cyclic and seasonal processes. The ability to enhance performance and stability of periodic systems has obvious merits; however, due to mathematical difficulties the development of control theory for LTP plants has lagged behind linear time-invariant (LTI) systems.

Classical developments in control theory such as disturbance rejection and stabilization have nearly no extension to LTP processes because of the apparent inability to transform such systems into the frequency domain where the majority of the analysis and synthesis tools are formulated. However, recent developments in system theory show an equivalence between LTP systems and corresponding LTI systems. Thus, it appears the wealth of control theory for LTI systems can be brought to bear on the periodic plant.

1.1 Periodic System Control

The time-periodic systems of interest here are of the form

$$\begin{aligned} x[k+1] &= A_k x[k] + B_k u[k] \\ y[k] &= C_k x[k] + D_k u[k] \end{aligned}$$

where the system matrices are m-periodic, meaning for all k

$$A_k = A_{k+m} \qquad B_k = B_{k+m}$$
$$C_k = C_{k+m} \qquad D_k = D_{k+m}$$

We are interested in studying discrete-time periodic systems for the following reasons: the ease of computer application and implementation; it is numerically simpler than continuous-time, matrix multiplies vs. matrix integration; and, the lifted system, discussed later, is a finite dimensional LTI representation of the periodic system. A sampled-data representation of continuous-time T-periodic system (continuous-time coefficients which have period T) results in a m-periodic discrete-time system; when sampling is synchronous with the system period, m is the number of samples per period T (see Appendix C).

The geometry and structure of LTP systems is well established in the literature [3, 46] with the theory of Floquet being the most widely known tool for analyzing the stability of periodic systems. Geometric concepts such as controllability (stabilizability), and observability (detectability) have received special attention [3, 4, 5, 19, 44, 54] due to their importance in control theory.

Control approaches such as eigenvalue assignment [1, 7, 25, 31, 41, 42, 51, 52] and deadbeat control [17, 20, 21] provide methods to adjust the system poles (Floquet multipliers). An important result is that periodic *output* feedback suffices for pole placement for periodic systems, something not achievable for LTI systems. Other research has focused on state estimation [7, 58], and output feedback [7, 45], where researchers have cast their results in periodic and 'lifted' domains.

Meyer and Burrus [38], and Khargonekar et al. [30] establish a canonical relationship between a discrete-time, linear, p-out, q-in, m-periodic system and a linear, mp-out, mq-in, time-invariant system; the LTI system is called the *lifted* system, or the *lift* of the LTP system. The direct relationship between the periodic system and the 'larger' time-invariant system is natural since it preserves both algebraic properties and system norms. It is this lifting process which will be utilized in the study of disturbance rejection of linear, time-periodic systems. The apparent advantage of the lifted system is that it allows us to pose system analysis and controller synthesis problems using time-invariant techniques. However, it should immediately be noticed that the larger system requires MIMO design and analysis tools.

Meyer and Burrus also discuss frequency domain analysis of periodic systems, using lifted representations. The frequency response of the periodic system is defined so that the system response is consistent with time-invariant frequency response representations.

1.2 Disturbance Rejection

The consequence of disturbances on LTP systems is similar to their LTI counterparts, but is complicated by the interaction of the disturbance and plant acting at different frequencies. This interaction manifests itself in the modulation of the disturbance signal by sinusoids at integer multiples of the plant frequency. The result, for an m-periodic plant and disturbance containing a single tone, is that the output contains m tones.

For a variety of periodic system problems the disturbance frequency occurs at or near the plant periodic frequency. In this situation, the system output contains tones at the disturbance frequency and its higher harmonics. This is, in fact, the motivation for the higher harmonic control (HHC) algorithm used initially for vibration reduction on helicopters.

Control theory related to disturbance rejection has focused in two main areas. One is related to the optimal rejection of bounded disturbances [8, 9, 10]. This method has focused on the minimization of system norms relating inputs with finite magnitude to outputs with finite magnitude, as compared to signals with finite energy which are a common focus for conventional control theory. Dahleh and others [8, 10] present the problem in general, non-square, time-invariant case, where the minimizing solution is obtained from a linear programming problem, and extend these results to periodic systems, using lifted descriptions, where constraints on the controller causality are introduced.

Grasselli and others [20, 22] study the disturbance localization problem. "A system is disturbance-localized if and only if the forced output response to every disturbance input function is null" [22]. Here a direct output feedback solution is given for the disturbance localization problem; however, although a dead-beat solution is given, there are no other guarantees on stability. Also, Grasselli [20] considers the problem in the periodic domain by considering controllable subspaces of a periodic system, and avoids lifted representations. Such formulations are much more complicated than similar methods using lifted systems, and they do not permit the insightful tools of frequency domain analysis.

Although not explicitly intended for periodic systems, classical control approaches such as higher-harmonic control have been implemented, most notably on helicopter rotors. This approach has been shown to be equivalent to the classical narrowband disturbance rejection problem [50]. Here, two lightly damped feedback compensator poles are placed at the disturbance frequency. For LTI systems, these poles become zeros in the closed-loop system, thus, providing disturbance attenuation; in addition, stability is ensured by requiring the departure angle from the complex poles to be 180°. This minimizes the sensitivity function in the region near the disturbance frequency, adding robustness to errors in the plant. Similar extensions have not been directly made in the periodic case because such systems do not have transfer function representations; however, favorable results (as much as 5 dB in helicopter vibration experiments) have been achieved.

The success of adaptive feedforward controllers for narrowband disturbance rejection is well documented in the LTI case. The difficulty of applying such techniques to the LTP problem is caused by, among other things, the inability of the LMS algorithm to track a nonstationary environment [13]. Filter weights must vary to account for time-variations in the cross-correlation between the filtered-X signal and the error, and the LMS algorithm has the difficulty of not only finding the minimum point of the error surface but tracking this point as it changes with time.

Despite the above research, there has been little coordinated effort into the control of periodic systems, especially in the area of disturbance rejection. The use of classical approaches has resulted not because of any effort to investigate periodic systems, but rather from their success with disturbance rejection on LTI systems, and even though favorable results have been achieved the question that needs to be asked is: can we achieve improved results if we account for the periodicity during controller design?

1.3 About this Research

This research investigates the harmonic and narrowband disturbance rejection problem for LTP systems. Vibration control problems for plants with periodic coefficients, such as helicopters, could benefit directly from this study. Here, periodicity is a result of the mechanics of the system, and cannot be avoided, and the necessity of disturbance compensating controllers might be required as an afterthought to system development. The ability to construct

disturbance rejecting controllers goes beyond the helicopter vibration problem, which is an underlying theme in this research and the motivator for this study of periodic systems.

There are potential applications to sampled-data systems with multiple sampling rates. Multi-rate systems, which belong to a general class of periodic systems, offer possibilities of increased robustness [30] and improved channel bandwidths [37]. Equal sampling over all channels gives the same bandwidth in every channel of the system. In order to not loose information, the Nyquist frequency must be above the maximum signal bandwidth, leading to over-sampling and increased costs with faster sample-holds. Also, sample rates can be tailored for individual sensors and actuators which have different response times.

The thesis of this research inquires whether we can achieve improved disturbance rejection results by accounting for system periodicity during controller design. The pursuit of this question requires both theory necessary for describing periodic systems and practical synthesis tools for building controllers.

The mathematical complexity of periodic systems has largely limited their study. However, the equivalence of time-periodic systems and corresponding, time-invariant, lifted systems permits the machinery of multivariable control theory to be used for analysis and synthesis. Thus, we can describe periodic systems using tools such as system norms, transfer function matrices, and Bode diagrams; in like manner, we can take advantage of the computational capabilites of state-variable representations for controller synthesis.

Much of current, linear, system theory can be directly applied to linear periodic systems without modification. Using the lifted representation, the computation of controllability gramians, observability gramians, and system 2-norms using the discrete-time Lyapunov equation can be done directly. In a similar fashion, the discrete-time algebraic Riccati equation can be used without alteration to calculate the system ∞-norm. The simplification of much of periodic system theory is the lifted representation's greatest benefit. However, the causality constraint, embodied in a lower triangular feedthrough matrix, is its greatest difficulty.

Among the many useful, multivariable, synthesis tools, $\mathcal{H}_\infty$ control was developed historically as the principal method for controller fabrication within robust control theory. In this research, constraints on controlled system ∞-norms specify nominal performance and robust stability objectives. Candidate periodic controllers, which meet appropriate control

objectives, can be found easily using existing LTI $\mathcal{H}_\infty$ control theory; however, many of these controllers cannot be realized since they do not satisfy the causality constraint. Two techniques are introduced which can be added easily to $\mathcal{H}_\infty$ solvers and can be used to make causal controllers: loop-shifting and Q-parameterization. In both cases, the critical step involves the minimization of a constant LFT over a set of lower triangular matrices. Thus, the fabrication of periodic controllers which meet appropriate objective is, at least, brought within the realm of practicality. The lifted representation allows for simplified system expression, simplified periodic system theory, and simplified controller development.

An LTP system responds to a sinusoidal input not only with a sinusoid at the excitation frequency, as LTI systems do, but also additional harmonics at higher frequencies spaced by multiples of the plant-periodic frequency. This behavior results from the modulation of the plant-periodic frequency with the input frequency by the time-periodic system. Thus, the narrowband disturbance rejection problem for LTP systems is considerably more complicated than its LTI counterpart, and we would expect periodic controllers to take better advantage of system structure.

Using various architectures, harmonic and narrowband disturbance rejection is investigated for linear time-periodic plants. Included are classical and multivariable feedback controllers, fixed-gain feedforward designs using FIR filters and $\mathcal{H}_\infty$ synthesis tools, and adaptive feedforward controllers. The objective of time-periodic, narrowband, disturbance rejection is similar to the time-invariant problem, which seeks to place a zero in the controlled system's disturbance path. In the time-invariant problem, this is achieved by placing a high-gain narrow bandpass filter in the feedback path for feedback architectures, or by appropriately inverting the control path while accounting for disturbance path dynamics in feedforward architectures (this includes adaptive feedforward schemes which implicitly measure the disturbance path). For the time-periodic problem, we must not only place a zero in the controlled system's disturbance path, achieved, in concept, using the same techniques as the time-invariant problem, but we must also ensure the zero direction, defined by the null space of the controlled system at the disturbance frequency, is coincident with the disturbance.

Classical designs, like higher harmonic control, which was originally developed for helicopter vibration control, do not achieve the desired objectives of narrowband disturbance rejection when applied to time-periodic plants. Such controllers are high-gain, narrowband-

pass filters, and, as a result, do place a zero in the periodic system's sensitivity; however, because of their structure, the disturbance, in general, does not lie in the closed-loop sensitivity's null space, resulting in transmission of the disturbance and poor performance. Classical controllers do eliminate the target frequency from the control system output, but with the potential penalty of amplifying other harmonics, and, as demonstrated in the case study (Section 6.3.1), may be limited by reduced stability margins which restrict controller gains and achievable performance.

In this research, $\mathcal{H}_\infty$ design methods are used to fabricate controllers, and control objectives are cast as constraints on the ∞-norm of the system sensitivity and complimentary sensitivity. The resulting controllers are high-gain, narrowband-pass, periodic filters. The closed-loop sensitivity has a zero at the disturbance frequency, and the disturbance is in its null space. This is achieved by proper selection of an input-weighting matrix, which is interpreted as a model of the disturbance, as opposed to the technique of output-weighting, which places the required zero but fails to match the disturbance direction with the sensitivity's null space.

Controllers designed using multivariable methods achieve improved performance over and exhibit larger robustness margins than the classical designs discussed previously. While classical designs reject only harmonics at the target frequency, $\mathcal{H}_\infty$ controllers realize perfect disturbance rejection over a wider bandwidth—nearly two and a half times as wide in our case study. Also, because robustness is considered directly during design, such controllers have considerably larger robustness margins. Our case study demonstrates, for example, an improvement in the lower bound estimates of the gain margin from $[-1.51, 1.83]$ dB to $[-5.94, 35.1]$ dB and the phase margin from ± 10.9 degrees to ± 58.8 degrees (both using the output sensitivity).

Similar nominal performance results can be achieved using the feedforward disturbance rejection architecture. This is expected. The disturbance, or at least a coherent reference to it, is available for measurement, and the controller alters the magnitude and direction of the disturbance so that when reintroduced via the control path there is cancelation in the system output.

Objectives are given which minimize the weighted ∞-norm of the controlled system; optimal controllers can be found using γ-iteration. Such feedforward controllers achieve

perfect disturbance rejection. In the case study, the controller achieves perfect rejection across the entire frequency range. Spectacular results, such as this, should not be considered the rule, however, due to uncertainties which exist in the disturbance path and control path transfer function matrices.

A multivariable equivalent of the tapped-delay line is used in the description of periodic FIR filters. Such filters allow constrollers to be implemented using simplified structures, and allow the designer to focus on system performance at target frequencies. Near perfect rejection is possible using periodic FIR filters. In addition, periodic FIR filters can be made adaptive using an algorithm similar to filtered-X LMS but modified for the multivariable problem. Although perfect rejection is in theory attainable using adaptive FIR filters, the achieved level of performance depends largely upon the time-constants which govern adaptation. The case study demonstrates nearly 25 dB rejection in 100 cycles; this performance exceeds classical feedback design, and adaptation happens quickly.

Organization

Much of the system theory developed during the course of this research relies heavily upon the lifted representation and LTI system theory. It is assumed that the reader has at least some familiarity with linear system theory and especially concepts connected to multivariable frequency response. Chapter 2 discusses system theory as it relates to LTP plants. Characteristics related to the time-invariant lifted representation are reviewed in connection to periodic systems, and harmonic and narrowband response of periodic systems is discussed in this framework.

Chapter 3 discusses disturbance rejection using feedback control architectures for the harmonic and narrowband problem. Control objectives and limitations for feedback and feedforward disturbance rejection are studied, and for the feedback case, time-invariant controllers, such as HHC, are reviewed and their performance with periodic systems is shown. These controllers will be compared with controllers which explicitly account for the plant periodicity at the design phase. $\mathcal{H}_\infty$ optimal controllers, which minimize the system gain at the frequency of interest, are discussed. Design considerations relevant to the narrowband problem and related to the optimization are illuminated.

In Chapter 4, feedforward control is used for narrowband disturbance rejection. Mul-

tivariable designs are found which minimize weighted disturbance-to-error gain of the controlled system. Controller optimimization is posed as a generalized regulator problem for use in $\mathcal{H}_\infty$ machinery. A definition of periodic finite impulse response (FIR) filters is made and used for narrowband disturbance rejection.

Also, this research poses a technique for accounting for the time-variations which previously have limited the performance of adaptive feedforward techniques. By posing the filtered-X LMS algorithm in the lifted domain, a MIMO LMS algorithm can be implemented which solves for the time-varying coefficients of the transversal filter. Chapter 4 discusses adaptive feedforward technique for use with periodic systems.

Chapter 5 discusses two techniques for making controllers calculated using $\mathcal{H}_\infty$ control theory causal lifted representations of periodic systems. Both methods operate on state-space models of the generalized plant and can be added easliy to existing $\mathcal{H}_\infty$ solvers. The first method accounts for controller casuality during loop-shifting, a process which considerably simplifies $\mathcal{H}_\infty$ theory and solutions. The second method uses Q-parameterization to design causal lifted controllers.

Finally, a case study of each control technique is developed using a simplified helicopter rotor model and is discussed in Chapter 6.

Chapter 2

Signals and Linear Periodic Systems

The primary stumbling block for the periodic system analysis has been the lack of computational tools. As outlined in the last chapter, the realm of periodic system theory and control is limited, and even the evaluation of important system characteristics such as system norms by evaluating periodic grammians or solving periodic Riccati equations for use in the bounded real lemma may be simple in concept but are considerably more difficult to execute in practice. At first glance, it would appear that the time-varying nature of periodic systems prohibits the use of analysis tools in the frequency domain and that they are permanently limited to time domain analysis. This would be unfortunate, since the success of control engineering is tied to frequency domain descriptions, namely transfer functions, and analysis and design tools such as Bode diagrams and loopshaping.

This chapter presents periodic system theory but does so using the equivalent LTI system mentioned previously. Section 2.1 presents the lifting operation in both time and frequency domains. Signal norms are defined and preservation of norms before and after lifting is shown. This fact is important to the definition and equivalence of norms for lowered and lifted systems. Finally, since this research is interested in the harmonic disturbance rejection, we present a useful framework for handling lifted harmonic signals.

Section 2.2 formally presents the lifted system and illustrates its time-invariance and causality. System norms are presented and shown to be equivalent for a periodic system and its lift. A state-space representation for a lifted system is given based upon a state-space model of its periodic system. This representation is then used within the established framework of modern and robust control theory to identify a frequency response for the

periodic (lifted) system. Throughout this discussion, important concepts to control theory such as system zeros, poles, controllability, and observability are presented and made relevant to periodic systems.

Finally, Section 2.3 gives an algorithm which allows the lifted representation of a periodic system to be implemented without needing an explicit periodic representation of the system.

2.1 Signals

The signals we are concerned with are functions of discrete-time, $y[k] : \mathbb{Z} \to \mathbb{R}^n$, where $\mathbb{Z}$ is the set of integers. The dimension of a signal is n, and a signal space $\mathcal{S}^n$ is the set of all signals with such dimension. Without much loss of generality, we will consider signals to be one sided, that is, $y[k] = 0$ for all $k < 0$.

2.1.1 Lifting

The following lifting operations, in the time and frequency domains, are discussed in Meyer and Burrus [38]. While time domain lifting is fairly straightforward, its frequency domain counterpart is more mathematically intense and the interested reader is refered to Meyer and Burrus for appropriate proofs.

Time Domain

We define the lifting operator, $\mathfrak{L}_m : \mathcal{S}^p \to \mathcal{S}^{mp}$ to be

$$y = \{y[0], y[1], \dots\} \longrightarrow \mathfrak{L}_m y = \hat{y} = \left\{ \begin{bmatrix} y[0] \\ y[1] \\ \vdots \\ y[m-1] \end{bmatrix}, \begin{bmatrix} y[m] \\ y[m+1] \\ \vdots \\ y[2m-1] \end{bmatrix}, \dots \right\}$$

The lth row of the larger *lifted* signal $\hat{y}(k)$ is of course

$$\hat{y}_l[k] = y[km + l]$$

It should be pointed out that time 0 $(\mathrm{mod}\, m)$ is the start of each cycle and therefore becomes the first entry in each vector of the lifted signal. If necessary we will discriminate between

matrix and temporal indices; however, it is notationally more convenient and conceptually straightforward to consider the signals position within the cycle.

It is apparent that the inverse lifting operator, $\mathfrak{L}_m^{-1}$, is a reordering of the lifted signal, $\hat{y}(k)$, into the *lowered* signal $y(k)$, and this inverse does exist.

Frequency Domain

We define the $\mathcal{Z}$-transform in the usual way for both the lowered and lifted signals.

$$y(z) = \sum_{k=0}^{\infty} y[k] z^{-k}$$
$$\hat{y}(\hat{z}) = \sum_{k=0}^{\infty} \hat{y}[k] \hat{z}^{-k}$$

For the lifted system each sample occurs once per cycle of the original signal, thus

$$\hat{z} = z^m$$

also, because $\hat{y}$ is a $mp \times 1$ vector, we find its lth row to be

$$\hat{y}_l(\hat{z}) = \sum_{k=0}^{\infty} y[km+l] \hat{z}^{-k} = \sum_{k=0}^{\infty} y[km+l] z^{-km}$$

Given the above definitions, it is possible to write the lifting and inverse lifting operations in the frequency domain. The first, which is intuitively more simple, is the inverse lifting operator.

$$y(z) = \mathfrak{L}_m^{-1} \hat{y}(\hat{z}) = \sum_{l=0}^{m-1} z^{-l} \hat{y}_l(z^m)$$

The objective of this operation is to take each row of the lifted signal, $\hat{y}_l(k)$, delay it according to its position around the period, and sum the signals together thereby reconstructing the original signal.

The frequency domain description of the lifting operation is as follows:

$$\hat{y}_l(\hat{z}) = \hat{y}_l(z^m) = \mathfrak{L}_m y(z) = \tfrac{1}{m} z^l \sum_{i=0}^{m-1} e^{j(i\Omega)l} y(z e^{j(i\Omega)})$$

where $\Omega = 2\pi/m$ is the plant-periodic frequency. An interpretation of this process is not as obvious as was for the inverse lifting operation. First, we must notice that the replacement $ze^{j(i\Omega)} \rightarrow z$ is the $\mathcal{Z}$-transform of $y[k]$ modulated with $e^{-j(i\Omega)k}$.

$$y(ze^{j(i\Omega)}) = \sum_{k=0}^{\infty} y[k] \left(ze^{j(i\Omega)}\right)^{-k} = \sum_{k=0}^{\infty} \left(e^{-j(i\Omega)k}\, y[k]\right) z^{-k}$$

Thus, we can write

$$\hat{y}_l(z^m) = \tfrac{1}{m} z^l \sum_{i=0}^{m-1} e^{j(i\Omega)l}\, \mathcal{Z}\left\{e^{-j(i\Omega)k}\, y[k]\right\}$$

which shows $\hat{y}_l(\hat{z})$ is the sum of the $\mathcal{Z}$-transform of $y[k]$ modulated with sinusoids at multiples of the plant-periodic frequency and phase shifted by $i\Omega l$. The final z^l is a time advance to make the correct starting time for the modulated sequence.

It is reasonably straight forward to prove that the two operations are indeed inverses [38].

2.1.2 Norms and Spaces of Signals

Time Domain

The size of a signal will be measured by a 2-norm defined over an infinite time interval. The Euclidian norm is $\|y\| = \sqrt{y'y}$, and the 2-norm of a signal is

$$\|y\|_2 = \left\{ \sum_{k=0}^{\infty} \|y[k]\|^2 \right\}^{\frac{1}{2}}$$

where according to this definition y may be a lifted or a lowered signal.

It is important to notice and reasonably straightforward to show that the lifting operation preserves norms. That is

$$\|y\|_2 = \|\mathfrak{L}y\|_2 = \|\hat{y}\|_2$$

The space L_2 is the space of signals with finite 2-norm.

$$L_2 = \{y : \ \|y\|_2 < \infty\}$$

A useful interpretation of the 2-norm and space L_2 is that $\|y\|_2$ is the amount of (rms) energy (or power) contained in y and that L_2 contains those signals with finite energy.

Frequency Domain

Using Parseval's relationship [39], it can be shown that the 2-norm of a signal is also related to the 'area' under the magnitude of the Fourier transform of the signal which is also a measure of the (rms) energy in the signal.

$$\|y\|_2 = \left\{ \frac{1}{2\pi} \int_{-\pi}^{\pi} \|y(e^{j\omega})\|^2 \, d\omega \right\}^{\frac{1}{2}}$$

Here again, $y(e^{j\omega})$ can be either a lifted or lowered signal.

Since this integral must exist, convergence requires that all of the poles of $y(e^{j\omega})$ must lie within the unit circle, $|z| < 1$.

2.1.3 Lifting Sinusoids

Consider a scalar signal $y[k] = e^{j\omega k}$, its lift is

$$\hat{y}_l[k] = e^{j\omega(km+l)} = e^{j\omega l} e^{jm\omega k}$$

If we define the vector

$$\hat{\phi}_i = \begin{bmatrix} 1 \\ e^{j(\omega+i\Omega)} \\ \cdots \\ e^{j(\omega+i\Omega)(m-1)} \end{bmatrix}$$

where $\Omega = 2\pi/m$ is the plant-periodic frequency, then we see that $\hat{y}$ becomes

$$\hat{y}[k] = \hat{\phi}_0 \; e^{jm\omega k}$$

Thus, a sinusoid at frequency ω upon lifting becomes a vector valued sinusoid with frequency $m\omega$, and its 'direction' is defined by the vector $\hat{\phi}_i$.

Consider now a lifted signal $\hat{y}[k] = \hat{\alpha} \; e^{jm\omega k}$, and its direction is defined by the vector $\hat{\alpha}$. We can define an orthogonal basis by the matrix

$$\mathbf{\Phi}_\omega = \begin{bmatrix} \hat{\phi}_0 & \hat{\phi}_1 & \cdots & \hat{\phi}_{(m-1)} \end{bmatrix}$$

The vector $\hat{\alpha}$, can be written as a linear combination of these basis vectors

$$\hat{\alpha} = \mathbf{\Phi}_\omega \tilde{\alpha}$$

yielding

$$\hat{y}[k] = \sum_{i=0}^{m-1} \tilde{\alpha}_i \hat{\phi}_i \, e^{jm\omega k}$$

and the ith entry in $\tilde{\alpha}$ is the complex amplitude of the ith sinusoid $\hat{\phi}_i \, e^{jm\omega k}$. In real time, we see that the lowered signal $y[k]$ is described by m tones

$$y[k] = \sum_{i=0}^{m-1} \tilde{\alpha}_i e^{j(\omega + i\Omega)k}$$

where the ith tone is $e^{j\omega k}$ modulated by a sinusoid at an integer multiple of the plant-periodic frequency, $e^{j(i\Omega)k}$. Thus, *a sinusoidal signal in the lifted domain represents m tones in real time centered about ω and spaced by the lifting frequency Ω.*

2.2 Systems

2.2.1 Lifted System

Let $\mathbf{G} : \mathcal{S}^q \to \mathcal{S}^p$ represent a m-periodic system with p-outputs and q-inputs, and define the input-output map $\hat{\mathbf{G}} : \mathcal{S}^{mq} \to \mathcal{S}^{mp}$

$$\hat{\mathbf{G}} = \mathfrak{L}_m \mathbf{G} \mathfrak{L}_m^{-1}$$

The *lifted system* $\hat{\mathbf{G}}$ has mp-outputs, and mq-inputs as determined by the lifting operator.

Some authors [24, 18] refer to the lifted system as an *ω-stacked system*, where ω is the system period. In addition, they consider ω such systems by defining time zero to be a different point in the cycle; each of these stacked systems can be shown to be structurally equivalent.

Time Invariance

Define the delay operator

$$\mathbf{\Lambda} : \{y[0], y[1], \dots\} \longrightarrow \{0, y[0], y[1], \dots\}$$

Observe that delaying a lifted signal is the same as lifting a signal delayed m time-steps, so,

$$\mathbf{\Lambda}\mathfrak{L}_m = \mathfrak{L}_m\mathbf{\Lambda}^m$$

A system $\mathbf{G}$ is m-periodic if and only if it commutes with the mth power of the delay operator

$$\mathbf{G}\mathbf{\Lambda}^m = \mathbf{\Lambda}^m\mathbf{G}$$

Of course, a system that is 1-periodic is time invariant, and it is well established that an output waveform is independent of the time the input signal is applied, that is time $k = 0$ is arbitrary. For periodic systems this is only true so long as the input signal is applied at the same point in time relative to the start of a cycle, requiring the m delays in the above definition.

Premultiplying by $\mathfrak{L}_m$ and postmultiplying by $\mathfrak{L}_m^{-1}$ gives

$$\begin{aligned}
\mathfrak{L}_m\left[\mathbf{\Lambda}^m\mathbf{G} = \mathfrak{L}_m\mathbf{G}\mathbf{\Lambda}^m\right]\mathfrak{L}_m^{-1} \\
\mathbf{\Lambda}\mathfrak{L}_m\mathbf{G}\mathfrak{L}_m^{-1} = \mathfrak{L}_m\mathbf{G}\mathfrak{L}_m^{-1}\Lambda \\
\mathbf{\Lambda}\hat{\mathbf{G}} = \hat{\mathbf{G}}\mathbf{\Lambda}
\end{aligned}$$

which shows $\hat{\mathbf{G}}$ is time-invariant. This fact allows us to use the well established LTI modern and robust control theory to analyse periodic systems and is a cornerstone of this research.

Similarly, given a time-invariant $\hat{\mathbf{G}}$ system we can identify a corresponding periodic system $\mathbf{G}$ by

$$\mathbf{G} = \mathfrak{L}_m^{-1}\hat{\mathbf{G}}\mathfrak{L}_m$$

and $\mathbf{G}$ will be m-periodic. The proof is similar to the previous; however, not all time-invariant systems can be associated with causal periodic systems.

Causality

Define the kth truncation operator

$$\mathbf{\Pi}^k : \{y[0], y[1], \dots\} \longrightarrow \{y[0], \dots, y[k], 0, 0, \dots\}$$

Observe the following relationship between the truncation and lifting operators.

$$\mathbf{\Pi}^k \mathfrak{L}_m = \mathfrak{L}_m \mathbf{\Pi}^{km+(m-1)}$$

Truncating a lifted signal at the kth timestep is equivalent to truncating the lowered signal at the $km + (m-1)$ timestep and then lifting. Time $km + (m-1)$ is the $(m-1)$th (last) entry at timestep k in the lifted signal.

A system $\mathbf{G}$ is causal only if the output at time k does not depend upon future inputs. We can write this using the truncation operator as

$$\mathbf{\Pi}^k \mathbf{G} = \mathbf{\Pi}^k \mathbf{G} \mathbf{\Pi}^k \qquad k = 0, 1, \dots$$

If $\mathbf{G}$ is causal then

$$\begin{aligned}
\mathbf{\Pi}^{lm+(m-1)} \mathbf{G} &= \mathbf{\Pi}^{lm+(m-1)} \mathbf{G} \mathbf{\Pi}^{lm+(m-1)} \qquad l = 0, 1, \dots \\
\mathfrak{L}_m \left[\mathbf{\Pi}^{lm+(m-1)} \mathbf{G} \right. &= \left. \mathbf{\Pi}^{lm+(m-1)} \mathbf{G} \mathbf{\Pi}^{lm+(m-1)} \right] \mathfrak{L}_m^{-1} \\
\mathbf{\Pi}^l \mathfrak{L}_m \mathbf{G} \mathfrak{L}_m^{-1} &= \mathbf{\Pi}^l \mathfrak{L}_m \mathbf{G} \mathfrak{L}_m^{-1} \mathbf{\Pi}^l \\
\mathbf{\Pi}^l \hat{\mathbf{G}} &= \mathbf{\Pi}^l \hat{\mathbf{G}} \mathbf{\Pi}^l
\end{aligned}$$

and the lifted system, $\hat{\mathbf{G}}$, is also causal. However, if $\hat{\mathbf{G}}$ is causal we are not guaranteed that $\mathbf{G}$ will also be causal. In order to ensure $\mathbf{G}$ will be causal for all k we must impose the constraint on $\hat{\mathbf{G}}$ that there be no direct effect of $u(km + j)$ on $y(km + i)$ for $i < j$.

2.2.2 System Norms

We will be interested in ways of describing the size or gain of LTP systems. A useful technique is to base the size of a system upon the magnitude of its output signals, but this is still open for considerable interpretation since different inputs, even with equal norms, can result in output signals of varying size. We define two system norms: 2-norm which measures the rms energy output for white noise inputs; and, ∞-norm which is the output signal norm

normalized by the input signal energy, where the input signal is chosen to maximize the size of the output signal, that is it is a worst case gain on signal energy.

Most importantly, we will be demonstrating that the system norms for a periodic system are equivalent to their lifted counterparts. This is important since the future developments for controller design and analysis will depend upon this fact.

∞-norm

Here we are going to define the system size by considering the output signal norm normalized by input signal norm, but in a worst case sense.

$$\|\mathbf{G}\|_\infty = \sup_{u \in L_2} \frac{\|y\|_2}{\|u\|_2}$$

By this definition we know that the ouptut signal energy is always less that the input signal energy multiplied by some gain, where this gain is the system ∞-norm.

$$\|y\|_2 \leq \|\mathbf{G}\|_\infty \, \|u\|_2$$

And there is a worst input signal which results in equality.

The usefulness of this definition is that it depends only upon the signals entering and leaving the system, and not upon the structure of the system itself; that is, it holds for either periodic or time-invariant system. This means that the ∞-norm of a periodic system is equal to its lift.

$$\|\mathbf{G}\|_\infty = \|\hat{\mathbf{G}}\|_\infty$$

For time-invariant systems we can write an equivalent definition of the system ∞-norm. If $\hat{\mathbf{G}}$ is a time-invariant system, obtained by lifting for example, then we can show without proof, starting from the above definition, using Parseval's relationship, the fact that $\|Ax\| \leq \overline{\sigma}(A)\|x\|$, and the triangle inequality, that

$$\|\mathbf{G}\|_\infty = \max_{\omega \in (-\pi, \pi]} \overline{\sigma}\left(\hat{\mathbf{G}}(e^{j\omega})\right)$$

where $\overline{\sigma}$ is the maximum singular value of a matrix and $\hat{\mathbf{G}}(e^{j\omega})$ is the systems transfer function matrix evaluated on the unit circle. In the sequel, we will discuss transfer function matrices and representations for lifted systems. Now we can interpret the system ∞-norm as the peak magnitude on maximum singular value plot for $\hat{\mathbf{G}}$.

2-norm

The system 2-norm results from stochastic considerations of the system response. For white noise inputs with zero mean, $\mathcal{E}\{u\} = 0$ ($\mathcal{E}$ is the expectation operator), and unity variance, $\mathcal{E}\{uu'\} = I$, we will equate the systen 2-norm to the expectation of output signal energy.

$$\|\mathbf{G}\|_2 = \mathcal{E}\left\{\|y\|_2\right\} : \quad u = \text{white noise}$$

Here, again this definition is useful for time-invariant and periodic system, and the 2-norm is equal for a periodic system and its lift.

$$\|\mathbf{G}\|_2 = \|\hat{\mathbf{G}}\|_2$$

When we consider at time-invariant system, $\hat{\mathbf{G}}$, we can show the system 2-norm is related to the systems transfer function matrix by

$$\|\hat{\mathbf{G}}\|_2 = \left\{ \frac{1}{2\pi} \int_{-\pi}^{\pi} \text{tr}\left[\hat{\mathbf{G}}'(e^{j\omega})\hat{\mathbf{G}}(e^{j\omega})\right]\, d\omega \right\}^{\frac{1}{2}}$$

realizing that $\text{tr}\left[\hat{\mathbf{G}}'\hat{\mathbf{G}}\right] = \sum \sigma_i^2\left(\hat{\mathbf{G}}\right)$ shows that the system 2-norm can be interpreted as the 'area' under the singular value plots of $\hat{\mathbf{G}}$.

$$\|\hat{\mathbf{G}}\|_2 = \left\{ \sum_i \frac{1}{2\pi} \int_{-\pi}^{\pi} \sigma_i^2\left(\hat{\mathbf{G}}(e^{j\omega})\right) d\omega \right\}^{\frac{1}{2}}$$

The interpretations for the ∞-norm and 2-norm are familiar from discussions of classical system which are typically SISO and the singular value plot is in fact the magnitude portion of a Bode diagram.

2.2.3 Representations

Given that we can associate a time-invariant system with a periodic system, it will be useful to be able to find a representation for the lifted system. In this section, we will develop a state-space model for the lifted system from a state-space model of the periodic system. Similar descriptions using difference equations and convolution sums can be made for the

lifted system, however, for the sake of brevity the interested reader is refered again to Meyer and Burruss [38].

Starting with a state-space represenation for a m-periodic LTP system

$$\begin{aligned} x[k+1] &= A_k x[k] + B_k u[k] \\ y[k] &= C_k x[k] + D_k u[k] \end{aligned}$$

where the system matrices are periodic

$$\begin{aligned} A_k &= A_{k+m} \qquad & B_k &= B_{k+m} \\ C_k &= C_{k+m} \qquad & D_k &= D_{k+m} \end{aligned}$$

we can determine the state at the start of the $(k+1)$th cycle from the state at the begining of the previous cycle and the input u during that cycle.

$$\begin{aligned} x[(k+1)m] = {} & A_{m-1}A_{m-2}\cdots A_0\, x[km] \\ & + A_{m-1}A_{m-2}\cdots A_1 B_0 u[km] \\ & + A_{m-1}A_{m-2}\cdots A_2 B_1 u[km+1] \\ & \vdots \\ & + B_{m-1} u[(k+1)m-1] \end{aligned}$$

Similarly for the output equation, we can describe the output y during the kth cycle from the state at the begining of the cycle and inputs during the cycle.

$$\begin{array}{rcrcrcrcr} y[km] & = & C_0 x[km] & + & D_0 u[km] & & & & \\ y[km+1] & = & C_1 A_0 x[km] & + & C_1 B_0 u[km] & + & D_1 u[km+1] & & \\ y[km+2] & = & C_2 A_1 A_0 x[km] & + & C_2 A_1 B_0 u[km] & + & C_2 B_1 u[km+1] & + & D_2 u[km+2] \\ & \vdots & & & & & & & \end{array}$$

$$\begin{array}{rcrcrcl} y[(km+(m-1)] & = & C_{m-1}A_{m-2}\cdots A_0 x[km] & + & C_{m-1}A_{m-2}\cdots A_1 B_0 u[km] & & \\ & & & + \quad \cdots & + & C_{m-1}A_1 B_0 u[km+(m-3)] & \\ & & & & + & C_{m-1}B_1 u[km+(m-2)] & \\ & & & & + & D_m u[km+(m-1)] & \end{array}$$

Defining the lifted signals $\hat{y}$ and $\hat{u}$ in the usual way, and realizing that the above equations are time-invariant with respect to the lifted signal and the (per cycle) sampled state $\hat{x}[k] =$

$x[km]$, we arrive at the following LTI state-space representation:

$$\begin{aligned}\hat{x}[k+1] &= \hat{A}\hat{x}[k] + \hat{B}\hat{u}[k] \\ \hat{y}[k] &= \hat{C}\hat{x}[k] + \hat{D}\hat{u}[k]\end{aligned}$$

Here we have used the $\hat{}$ notation to identify the per cycle sampled state $x[km]$. It must be pointed out that this is not a lifted signal like $\hat{y}$ and $\hat{u}$, and its dimension remains that of the unlifted system. This is important because although lifting does increase the size of the system from an input-output perspective it does not increase the order of the system.

The system matrices in the above equations are

$$\hat{A} = A_{m-1}A_{m-2}\cdots A_0$$

$$\hat{B} = \begin{bmatrix} A_{m-1}\cdots A_1 B_0 & | & \cdots & | & A_{m-1}B_{m-2} & | & B_{m-1} \end{bmatrix}$$

$$\hat{C} = \begin{bmatrix} C_0 \\ C_1A_0 \\ \vdots \\ C_{m-1}A_{m-2}\cdots A_0 \end{bmatrix}$$

$$\hat{D}_{(k,l)} = \begin{cases} 0 & k < l & \text{above the diagonal} \\ D_l & k = l & \text{on the diagonal} \\ C_kB_l & k = l+1 & \text{1st subdiagonal} \\ C_{k-1}A_{k-2}\cdots A_lB_{l-1} & k > l+1 & \text{below 1st subdiagonal} \end{cases}$$

The feedthrough matrix $\hat{D}$ relates the effect of inputs at cycle k to outputs in the same cycle, while the dynamic portion relates the effect of inputs over past cycles on the current cycle outputs. In order for the lifted model to represent a causal periodic system, there can be no effect of the input signal on previous outputs. This is achieved by requiring the portion of the lifted feedthrough matrix above the diagonal, which maps future inputs to past outputs within a cycle, to be zero. We notice that lifting a causal periodic system achieves this objective. If we wish to associate a time-invariant system with a causal periodic system, the time-inavariant system must be causal and its feedthrough matrix must be lower triangular.

2.2.4 Stability and Floquet Theory

The state-space for periodic system $\mathbf{G}$ is equivalent to that for lifted system $\hat{\mathbf{G}}$. This fact is a consequence of the sampling which occurs in the representation of the lifted system. Thus characteristics, such as stability, controllability and observability, which are concerned with the system's motion through the state-space, are equivalent for a periodic system and its lift.

This section discusses these characteristics. The properties bounded-input, bounded-output (BIBO) stability and asymptotic stability are discussed, and related to the well known results of Floquet theory.

BIBO Stability

It should be apparent that if any signal u is bounded

$$\|u[k]\| \leq M_1 < \infty \qquad \text{for all } k$$

then its lift is also bounded

$$\|\hat{u}[k]\| \leq \sqrt{m} M_1 < \infty \qquad \text{for all } k$$

and it is also true that any bounded lifted signal must come from a bounded lowered signal.

A relaxed system $\mathbf{G}$ is termed bounded-input, bounded-output stable if any bounded-input, $\|u[k]\| \leq M_1$, the output is also bounded, $\|y[k]\| \leq M_2$. Thus, if an m-periodic system $\mathbf{G}$ is BIBO stable we can determine M_1 and M_2, and, in addition the lifted system will be stable with bounds $\sqrt{m}M_1$ and $\sqrt{m}M_2$ on the inputs and outputs respectively. Similar logic follows to show that a BIBO stable lift results in a stable periodic system. Finally, it should be pointed out that for the lifted system, which is time-invariant, that a sufficient condition for BIBO stability is asymptotic stability.

Asymptotic Stability

A periodic system is asymptotically stable, by definition, if and only if for $u[k] = 0$ (zero-input) there exists $M < \infty$ and $a < 1$ such that

$$\|x[k]\| \leq M a^k$$

The sampled state of the lifted system is also asymptotically stable.

$$\|\hat{x}[k]\| = \|x[km]\| \leq M(a^m)^k = M\hat{a}^k$$

where $\hat{a} = a^m < 1$, and it is straighforward to show that if the lifted system is asymptotically stable so is the periodic system.

An equivalent statement of asymptotic stability for time-invariant systems is that the eigenvalues of the dynamics matrix $\hat{A}$ must be less that unity magnitude.

$$|\lambda(\hat{A})| < 1 \Leftrightarrow \text{asymptotic stability}$$

And when $\hat{A}$ comes from a lifted system, this is the standard test for stability of periodic systems. This is a familiar result from Floquet theory.

Floquet Theory

The theory of Floquet states that given a periodic system

$$x[k+1] = A_k x[k]$$

with the dynamics matrix m-periodic, $A_k = A_{k+m}$, there exist a change of basis $x[k] = T_k \bar{x}[k]$ such that

$$\bar{x}[k+1] = \bar{A}\bar{x}[k]$$

Furthermore, T_k is m-periodic and nonsingular for all k. The stability of the barred system is determined by the eigenvalues of $\bar{A}$ which must be less that one.

If $T_0 = T_m = I$, which may be done without loss of generality, then we see a familiar result in that

$$\hat{A} = \bar{A}^m$$

and $\hat{A}$ is stable if and only if $\bar{A}$ is also stable, and

$$\lambda(\hat{A}) = \lambda(\bar{A})^m$$

2.2.5 Controllability and Observability

Formal definitions of controllability and observability are quite involved and require mathematical detail which we wish to avoid. A reader who is interested in a more detailed discussion is refered to articles by Bittanti [4, 3] and Halanay [27].

In the following discussion, the periodic system is represented by $\mathbf{G} = [A_k, B_k, C_k, D_k]$ with lifted representation $\hat{\mathbf{G}} = [\hat{A}, \hat{B}, \hat{C}, \hat{D}]$. We will make the assumption that A_k is nonsingular for all k which means $\hat{A}$ is also nonsingular.

Controllability

An m-periodic system is controllable if the origin can be reached from any initial state $x[0]$ in finite time. Since $\mathbf{G}$ is a time-varying system we might expect a requirement of controllability at time k. However, it can be shown that if a periodic system is controllable at one point in time, then it is controllable at any time point.

If we suppose a periodic system $\mathbf{G}$ is controllable then there exists a sequence $u[k]$ which steers the state trajectory from $x[0]$ to the origin in finite time, $\tilde{k}m + \tilde{l}$. Necessarily, the control signal u must be zero for $k \geq \tilde{k}m + \tilde{l}$. Since the state equations of the lifted system are equivalent to the periodic system, we see the lifted signal $\hat{u}[k]$ will steer the lifted signal to the origin and will reach this objective at the start of the $(\tilde{k}+1)$th cycle. The lifted signal $\hat{u}[k]$ will be identically zero at the end of the $\tilde{k}$th cycle, $\hat{u}_{l \geq \tilde{l}}[\tilde{k}]$, and for all $k > \tilde{k}$. Since the lifted signal reaches the origin in finite time, $\tilde{k} + 1$, from an arbitrary intitial state it too is controllable.

If the lifted system $\hat{\mathbf{G}}$ is controllable then there is a lifted control signal $\hat{u}[k]$ which directs the state trajectory to the origin for arbitrary intitial conditions, in finite time. It should be apparent that the lowered signal $u[k]$ must control the state trajectory of the corresponding periodic system. Thus, we see that controllability of a periodic system is equivalent to controllability of its lift.

Observability

A m-periodic system is observable if the initial condition $x[0]$ can be determined from a finite duration output sequence $y[k]$. Without loss of generality we can assume u is identically zero. Again, since $\mathbf{G}$ is a time-varying system we might expect a requirement of observability at time k. However, it can be shown that if a periodic system is observable at one point in time, then it is observable at any time point.

If we suppose a periodic system $\mathbf{G}$ is observable then there exists a finite duration sequence $y[k]$ from which we can determine the initial state $x[0]$. Because the system equations for the lifted system are equivalent to the periodic system the lift of $y[k]$ suffices to determine the initial condition $\hat{x}[0] \equiv x[0]$. If the output sequence $y[k]$ is $\tilde{k}m + \tilde{l}$ long then $\hat{y}[k]$ is $\tilde{k}$ long and $\hat{y}_{l>\tilde{l}}[\tilde{k}]$ are arbitrary.

Similarly, if the lifted system is observable then there is a finite duration signal $\hat{y}[k]$ which determines the initial condition $\hat{x}[0]$. Again because of the equivalence of systems the lowered signal $y[k]$ determines the initial condition $x[0]$. Thus, we see that observability of a periodic system is equivalent to observability of its lift.

2.2.6 Frequency Response

The previous sections have established the equivalence between periodic and time-invariant systems, with some constraints on the lifted system relating to causality. Now we will extend the tools of classical and multivariable theory to periodic systems, with particular attention on the fundamental concepts of transfer functions, poles, zeros, and frequency response.

Transfer Function Matrix

Given a $p \times q$ m-periodic system with lift $\hat{\mathbf{G}}$ and state-space representation $[\hat{A}, \hat{B}, \hat{C}, \hat{D}]$, we can construct the $mp \times mq$ transfer function matrix

$$\hat{\mathbf{G}}(\hat{z}) = \hat{D} + \hat{C}(\hat{z}I - \hat{A})^{-1}\hat{B}$$

The argument $\hat{z}$ represents the per cycle delay from input $\hat{u}(\hat{z})$ to $\hat{y}(\hat{z})$, and the (k,l)th element relates the input at time l during a cycle to the output at time k in a cycle, although each may not occur within the same cycle. Since the feedthrough matrix D is lower triangular

those transfer functions above the diagonal, $(k,l) : k < l$, are all strictly proper emphasizing causality.

In general the transfer function matrix $\hat{\mathbf{G}}(\hat{z})$ will be full rank, except at a finite number of locations. We call this the normal rank, $\hat{r}$, and

$$\operatorname{nrank} \hat{\mathbf{G}}(\hat{z}) = \min\{mp, mq\} = \hat{r}$$

In general this is the case; when it is not there are inputs or outputs which are not linearly independent and which can be discarded.

In the lifted $\mathcal{Z}$-domain, the periodic system has the following zero-state, input-output relationship.

$$\hat{y}(\hat{z}) = \hat{\mathbf{G}}(\hat{z})\hat{u}(\hat{z})$$

and except at certain values of $\omega \in (-\pi, \pi]$ the input

$$\hat{u}[k] = \hat{\alpha}\ e^{j\omega k} \qquad \hat{\alpha} \in \mathbb{C}^{mq}$$

results in a steady-state response of

$$\hat{y}[k] = \hat{\beta}\ e^{j\omega k} = \hat{\mathbf{G}}(e^{j\omega k})\hat{\alpha}\ e^{j\omega k} \qquad \hat{\beta} \in \mathbb{C}^{mp}$$

An additional representation of transfer function matrix is made by considering its singular value decomposition (SVD) [16, 36] at each complex frequency $\hat{z}$.

$$\hat{\mathbf{G}}(\hat{z}) = \mathbf{U}(\hat{z})\mathbf{\Sigma}(\hat{z})\mathbf{V}(\hat{z})'$$

The matrices $\mathbf{U}$ and $\mathbf{V}$ are unitary and $\mathbf{\Sigma}$ is

$$\mathbf{\Sigma}(\hat{z}) = \operatorname{diag}\{\sigma_1(\hat{z}), \sigma_2(\hat{z}), \ldots, \sigma_{\hat{r}}(\hat{z})\} \in \mathbb{R}^{mp \times mq}$$

where

$$\overline{\sigma} = \sigma_1 \geq \sigma_2 \geq \cdots \geq \sigma_{\hat{r}} = \underline{\sigma} \geq 0$$

and are termed the singular values. The columns of the unitary matrices

$$\mathbf{U}(\hat{z}) = \begin{bmatrix} u_1 & \ldots & u_{mp} \end{bmatrix} \in \mathbb{C}^{mp \times mp}$$
$$\mathbf{V}(\hat{z}) = \begin{bmatrix} v_1 & \ldots & v_{mq} \end{bmatrix} \in \mathbb{C}^{mq \times mq}$$

are the left and right singular vectors respectively.

The analytic calculation of a SVD is extremely complicated and would provide little information with respect to effort required. However, the real advantage of the SVD lies in its numerical qualities. Within matrix analysis, it has been established as the primary tool for numerically calculating rank, range and null spaces of matrices; it will find similar application here.

The transfer function and singular value decompositions relate how the periodic system appears to its environment through u and y, and are *external* descriptions of a periodic system $\mathbf{G}$. They represent only the controllable and observable modes of the system and describe how energy and information passes through the system, from u to y, without specific concern for energy which is internal to the system.

The evaluation of $\hat{\mathbf{G}}(\hat{z})$ on the unit circle, $\hat{z} = e^{j\omega}$ is the system Fourier transform, and a singular value plot of $\hat{\mathbf{G}}$ is the multivariable extension of the Bode magnitude plot. However, multivariable systems have multiple gains which describe the 'amplification' of signals from input to output. The maximum and minimum singular values of the system bracket the gain of any signal $\hat{u}$ at frequency ω.

$$\underline{\sigma}\left(\hat{\mathbf{G}}(e^{j\omega})\right) \leq \frac{\|\hat{\mathbf{G}}(e^{j\omega})\hat{u}(e^{j\omega})\|}{\|\hat{u}(e^{j\omega})\|} \leq \overline{\sigma}\left(\hat{\mathbf{G}}(e^{j\omega})\right)$$

Poles

As alluded to regarding stability, the poles of the periodic system $\mathbf{G}$ are the eigenvalues of the dynamics matrix of the lifted system, $\hat{A}$, and the magnitude of the poles must be less than unity for the system to be stable.

The poles of a periodic system describe the characteristic frequencies of the dynamical system, and if $a^m e^{jm\omega}$ is an eigenvalue of $\hat{A}$ then we can say that the system decays as $(a^m)^k$ and oscillates with frequency $m\omega$ from cycle to cycle.

If we consider system evolution in real time, the characteristic frequencies are the mth-root of the lifted values as implied by Floquet theory. The decay constant becomes a and the system oscillates at the m frequencies $\omega + i\Omega$, where multiples of the plant-periodic frequency are a result of the mth-root and describe the effect of the system period m on the

characteristic frequencies of the periodic system.

This seemingly paradoxical result suggests that a lifted system with n poles describes a periodic system with mn poles. However, this is not the case. An nth order periodic system remains so upon lifting and has n poles. The $m-1$ extra characteristic frequencies arise purely from the periodicity of the system, and describe how sinusoids of frequency $\Omega = 2\pi/m$ which are constant from cycle to cycle are manifested in the response of the system. This is a similar result to that found in lifting $e^{j\omega k}$.

Zeros

While the poles describe the characteristic frequencies of the periodic system, zeros describe how the system is coupled to the environment and are associated with frequencies at which the transmission of energy and information from the input to the output is blocked.

Consider the system $\mathbf{G}$ to be both controllable and observable. A point $z_0 \in \mathbb{C}$ is a *transmission zero* of the periodic system if the transfer function matrix $\hat{\mathbf{G}}(\hat{z})$ loses rank at $\hat{z} = z_0$.

$$\operatorname{rank} \hat{\mathbf{G}}(z_0) = r < \hat{r}$$

If there are more outputs than inputs $p \geq q$ then a zero z_0 yields the *transmission blocking* property. In this case, there exists a vector $\hat{\alpha} \in \operatorname{null}(\hat{\mathbf{G}}(z_0))$ such that for an input $\hat{u}[k] = \hat{\alpha}\ z_0^k$ the output is identically zero.

$$\hat{y}[k] = \hat{\mathbf{G}}(z_0)\hat{\alpha}\ z_0^k = 0 \cdot z_0^k = 0$$

The vector α is termed a *zero direction*.

For lifted periodic systems the zero directions relate to signals in the time domain which both oscillate and decay. If $z_0 = a^m e^{jm\omega}$ is a zero of a periodic system with direction $\hat{\alpha}$, the lifted input $\hat{u}[k] = \hat{\alpha}\ z_0^k$ represents, in real time, a linear combination of m decaying tones modulated by multiples of the plant-periodic frequency

$$u[k] = \sum_{i=0}^{m-1} \tilde{\alpha}_i a^k e^{j(\omega + i\Omega)k}$$

Here again we see that single tones in the lifted domain result in m tones in the time domain.

This discussion relates zeros to the rank of certain matrices. A more rigorous development considers zeros and poles of a system with regard to the transfer function matrix's Smith-MacMillan form and invariant factors. Defining zeros by those frequencies at which $\hat{\mathbf{G}}(\hat{z})$ loses rank identifies the same complex frequencies as zeros but does not take into account multiplicity. For this research, it is enough to equate zeros with loss of rank and zero directions with the null space of the transfer function matrix. For a more complete treatment of zeros of multivariable systems, the interested reader is refered to [32, 33, 35, 47]. Also, this development, which relies on the lifted system, is consistent with other discussions of zeros for periodic systems [23].

2.2.7 Harmonic-lifted System

Another useful description of a periodic system can be achieved if we perform a change of basis on the input and output spaces so that the resulting system maps the m harmonics described by complex amplitude $\tilde{u}$ to the harmonic output described by $\tilde{y}$. Let $\mathbf{G}$ be an m-periodic SISO system and $\hat{\mathbf{G}}$ its $m \times m$ lift. At lifted frequency $m\omega$ this can be achieved by post-multiplying $\hat{\mathbf{G}}$ by $\mathbf{\Phi}_\omega$ and pre-multiplying by its inverse $\mathbf{\Phi}^{-1} = \frac{1}{m}\mathbf{\Phi}'_\omega$. The resulting *harmonic-lifted system*, $\tilde{\mathbf{G}}$ is

$$\tilde{\mathbf{G}}(e^{jm\omega}) = \frac{1}{m}\mathbf{\Phi}'_\omega \hat{\mathbf{G}}(e^{jm\omega})\mathbf{\Phi}_\omega$$
$$\tilde{\mathbf{G}}(e^{jm\omega}) : \ \tilde{u}\, e^{jm\omega k} \longrightarrow \tilde{y}\, e^{jm\omega k}$$

The usefulness of this description is that at a particular frequency the entries in the matrix $\tilde{\mathbf{G}}$ describe the gain-phase relationship between m-input and m-output sinusoids at frequencies $\omega + i\Omega$. In other words, an input (lowered) sinusoid $e^{j(\omega+i\Omega)k}$ results in m (lowered) sinusoid $\tilde{\mathbf{G}}_{li}e^{j(\omega+i\Omega)k}, i = 0, \ldots, m-1$.

The singular values of the harmonic-lifted system, $\tilde{\mathbf{G}}$ are equivalent to the lifted system, $\hat{\mathbf{G}}$, since we are, in effect, multiplying by unitary matrices, $\frac{1}{\sqrt{m}}\mathbf{\Phi}_\omega$ and it transpose.

$$\overline{\sigma}\left(\hat{\mathbf{G}}(e^{jm\omega_0})\right) = \overline{\sigma}\left(\tilde{\mathbf{G}}(e^{jm\omega_0})\right)$$

2.2.8 Lifting a Time-invariant System

Consider a SISO time-invariant system, in real time, with transfer function $\mathbf{H}(z)$. Using the relationships between lifted and lowered signals in the frequency domain, the (k,l)th entry of the lifted transfer function matrix becomes.

$$\hat{\mathbf{H}}_{kl}(z^m) = \frac{1}{m}\sum_{i=0}^{m-1}(ze^{j(i\Omega)})^{k-l}\mathbf{H}(ze^{j(i\Omega)})$$

Evaluating $\hat{\mathbf{H}}(\hat{z})$ on the unit circle, and noticing the (k,l)th entry in

$$\left\{\hat{\phi}_i\hat{\phi}_i'\right\}_{kl} = e^{j(\omega+i\Omega)(k-l)}$$

we can write the lifted transfer function matrix as

$$\begin{aligned}\hat{\mathbf{H}}(e^{jm\omega}) &= \frac{1}{m}\sum_{i=0}^{m-1}\hat{\phi}_i\hat{\phi}_i'\mathbf{H}(e^{j(\omega+i\Omega)}) \\ &= \frac{1}{m}\mathbf{\Phi}_\omega \operatorname{diag}\left\{\mathbf{H}(e^{j(\omega+i\Omega)})\right\}\mathbf{\Phi}_\omega'\end{aligned}$$

Thus we can see that the maximum and minimum singular values of $\hat{\mathbf{H}}$ are

$$\begin{aligned}\overline{\sigma}(e^{jm\omega}) &= \max_i\left|\mathbf{H}(e^{j(\omega+i\Omega)})\right| \\ \underline{\sigma}(e^{jm\omega}) &= \min_i\left|\mathbf{H}(e^{j(\omega+i\Omega)})\right|\end{aligned}$$

The harmonic lifted system, $\tilde{\mathbf{H}}$, is a diagonal matrix

$$\tilde{\mathbf{H}}(e^{jm\omega}) = \operatorname{diag}\left\{\mathbf{H}(e^{j(\omega+i\Omega)})\right\}$$

and a sinusoidal input signal, e.g., $e_1\, e^{jm\omega k}$ results only in a sinusoidal output signal at the same frequency multiplied by complex gain $\mathbf{K}(e^{j(\omega+i\Omega)})$, which is what we expect from LTI system theory.

2.3 Real-time Implementation

We would like to be able to perform filtering operations given a lifted representation of a periodic system. Given a lifted model of a periodic system, a corresponding periodic state-space model is not unique since we know nothing about the intra-cycle state structure from

the lifted representation. This makes the process of lowering systems extremely difficult. However for filtering, knowing only the lifted representation is sufficient.

The following algorithm implements a periodic filter using its lifted representation, $[\hat{A}, \hat{B}, \hat{C}, \hat{D}]$. In the algorithm presented below the matrix indices are temporal; that is, $\hat{C}_l$ is the $(l+1)$th row of matrix $\hat{C}$ but corresponds to time l in the cycle.

$\hat{x}[0] = x_0$
for $k = 0, 1, 2, \ldots$
    for $l = 0 : m-1$
        input $u[km+l]$
        $\hat{u}_l[k] = u[km+l]$
        $y[km+l] = \hat{C}_l\hat{x}[k] + \hat{D}_l\hat{u}[k]$
        output $y[km+l]$
    next l
    $\hat{x}[k+1] = \hat{A}\hat{x}[k] + \hat{B}\hat{u}[k]$
next k

Using the lifted system the state update need only be executed once per cycle, and happens at the end of the outer loop after all inputs in that cycle have been lifted. If the intra-cycle state of the filter must be known then a periodic representation must be found, however this is unnecessary since we are primarily interested in the input-output relationship of the filter.

The system output, which happens at each step within a cycle, the inner loop, can be determined by stepping down each row of the lifted output equation. Here we use the fiter state, calculated at the end of the last cycle, and the lifted input signal which contains l correct values of the input signal u up to time $km+l$.

This approach is computationally more efficient too. Counting multiplies in a $p \times q$ periodic representation we find we must execute $n^2+(p+q)n+pq$ operations each time-step for m time-steps. The using the lifted representation and the algorithm presented above we must execute $n^2 + m(p+q) + m(m-1)pq/2$ operations each cycle. Thus there is a savings

on the order of $(m-1)n^2$ operations each cycle if we implement a periodic filter using its lifted representation.

Chapter 3

Feedback Disturbance Rejection

Having developed analytical tools in the last chapter, most significant being the equivalence between time-periodic and certain time-invariant systems, we now turn to the problem of disturbance rejection. Given the rich tonal response of periodic systems, where the system response to even a single tone at frequency ω_0 contains m discrete tones centered at the disturbance frequency spaced by the plant-periodic frequency, Ω, we see immediately that disturbance rejection for periodic systems is more difficult than similar time-invariant problems. When a disturbance pollutes the system output with a single harmonic and the control path is periodic results in a disturbance rejection problem which must consider the effect controllers have not only on the target frequency, but also the potential introduction of additional tones in the output due to modulation by the periodic system. This multivariable problem must be posed carefully in order to achieve desired results.

This chapter investigates the narrowband disturbance rejection problem using the common fixed-gain feedback architectures. Such fixed-gain controllers are time-periodic but otherwise the controller parameters do not change and are in contrast to adaptive controllers which will be studied in a later chapter.

One of the original and fundamental applications of control theory, in particular feedback control theory, was to the problem of rejecting disturbances. These disturbances are unknown, that is their time response cannot be measured directly but some knowledge of their power spectrum may be available for purposes of design. For the narrowband case it is usually known that the disturbance frequency is within a narrow frequency range centered at a frequency ω_0.

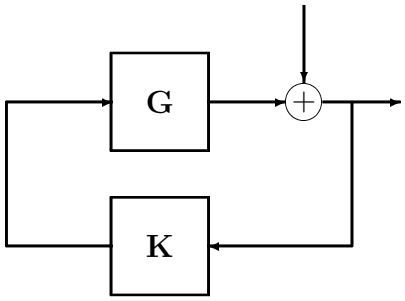

Figure 3.1: A disturbance compensation feedback loop

Classical LTI-SISO techniques place a narrow bandpass filter in the feedback path.

$$\mathbf{K}(z) = -\bar{k}\,\frac{\cos(\omega_0 - \varphi)z - \cos\varphi}{z^2 - 2\cos\omega_0 z + 1} \qquad \text{(NBF)}$$

The two poles on the unit circle, at $z = e^{\pm j\omega_0}$, result in a large loop-gain in the bandwidth about the disturbance frequency ω_0 and attenuation elsewhere, and the closed-loop system will be stable provided the in-bandwidth phase is near zero; thus, the system is gain stabilized out-of-bandwidth and phase stabilized in-bandwith. The system phase φ determines the placement of the controller's zero, and the normalized gain $\bar{k}$ determines the controller bandwidth. Figure 3.2 shows a typical design.

The high loop-gain makes the sensitivity, $\mathbf{S} = 1/(1 - \mathbf{GK})$, zero at the disturbance frequency while the loop-gain's out-of-bandwidth attenuation ensures the sensitivity will be near unity; thus, disturbances at frequencies away from the target frequency will not be amplified.

Similarly, the complimentary sensitivity, $\mathbf{T} = \mathbf{GK}/(1 - \mathbf{GK}) = \mathbf{GKS}$, will be unity magnitude at the disturbance frequency and small elsewhere, guaranteeing a unity *complex margin*

$$\beta_{\min} = ||\mathbf{T}||_\infty^{-1}$$

with a resulting lower bound of 6 dB for the *gain margin*

$$\mathrm{GM} \geq 1 + \beta_{\min}$$

and 60 degrees for the *phase margin*

$$\mathrm{PM} \geq 2\sin^{-1}\frac{\beta_{\min}}{2}$$

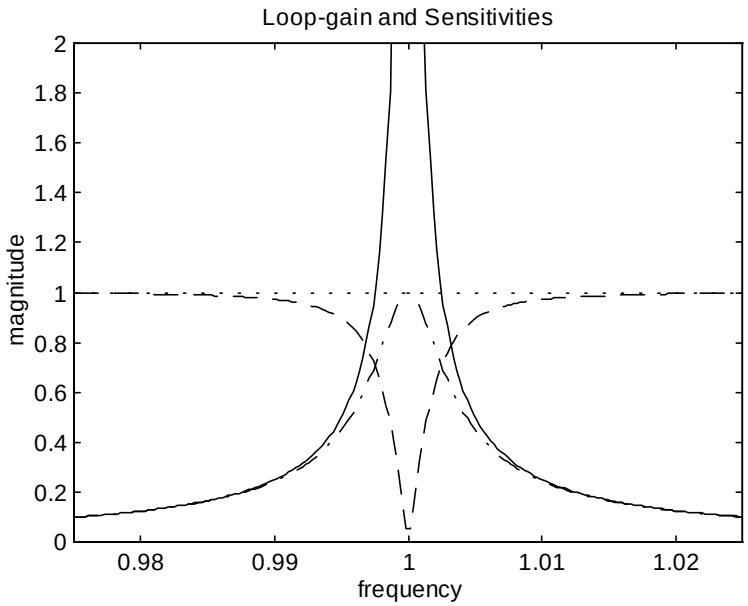

Figure 3.2: LTI-SISO loop-gain (solid), sensitivity (dash) and complimentary sensitivity (dot-dash) $k = \frac{1}{2}\%$, $\omega_0 = 1$, $\phi = 0$.

It can be shown that the phase margin is actually 90 degrees, and the gain margin is considerably larger than 6 dB (as much as 30 or 40 dB depending upon the bandwidth) [50]. In fact, our lower bound estimate of the gain margin can be improved by considering inverse multiplicative uncertainties and evaluating the gain margin using $\mathbf{S}$.

The conservative margins discussed above are a result of a multiplicative uncertainty model on the nominal plant $\mathbf{G}$

$$\mathbf{G}_t = (1 + \beta\mathbf{\Delta})\mathbf{G} \qquad \|\mathbf{\Delta}\|_\infty \leq 1$$

and stability can be guaranteed provided

$$|\mathbf{T}| \leq \frac{1}{\beta} \qquad \text{for all } \omega$$

Greater uncertainty in the plant can be allowed at frequencies away from ω_0 as $\mathbf{T}$ gets small. The tightest bound is at the center frequency, where $|\mathbf{T}| = 1/\beta$, which results in the 6 dB lower bound on the gain margin.

Unfortunately, our problem is not SISO. However, the following design objectives, which correspond to characteristics of the LTI-SISO design, will be used in our multivariable problem.

- **Nominal Performance:** Zero placement at the disturbance frequency in the lifted sensitivity, $\hat{\mathbf{S}}$, achieves narrowband disturbance rejection. For the multivariable case, this is also achieved by placing complex conjugate pole pairs at $e^{j\omega_0}$ in the loop-gain. Attention must be paid, however, to not only the location of the zero, but also to its direction. Since a particular zero direction relates to a particular harmonic signal in real-time, we must be sure that this direction corresponds to the disturbance.
- **Robust stability:** To ensure robust stability we will require the magnitude of the complimentary sensitivity to be suitably small. This is equivalent to requiring $\|\beta\hat{\mathbf{T}}\|_\infty < 1$.

In the remainder of this section we will discuss various design approaches for designing controllers to achieve the desired objectives. First, we will discuss the application of classical controllers (HHC) to the periodic problem and explain why such controllers often lack performance. Secondly, we will discuss multivariable design objectives and approaches to the problem. We will cast the nominal performance criteria as a weighted sensitivity problem. The technique of output weighting, also called frequency shaped cost functional, and input weighting or disturbance modelling will be discussed. The disadvantages and merits of both techniques will be mentioned.

In the sequel we will be concerned with SISO m-periodic plants and their $m \times m$ lifts. Also, the disturbance will be a single sinusoid.

$$\begin{aligned} \text{disturbance} \qquad & d[k] = e^{j\omega_0 k} \\ \text{lifted dist.} \qquad & \hat{d}[k] = \hat{\phi}_0\, e^{jm\omega_0 k} \\ \text{harmonic-lifted dist.} \qquad & \tilde{d}[k] = e_1\, e^{jm\omega_0 k} \end{aligned}$$

This can be done without loss of generality, and can be considered the most probable engineering scenario. The discussion that follows can be applied, in the logical fashion, to situations where the disturbance contains multiple tones. Note that the desired zero direction is defined by $\hat{\phi}_0$.

3.1 Classical Designs

Classical design approaches require a suitable model of the plant at the disturbance frequency. Some approaches have represented the periodic system's dynamics by a constant coefficient

matrix, which can equivalently be described by a complex gain, that relates the Fourier coefficients of harmonics in the input to harmonics at the same frequency in the output [50]. For our problem, this complex gain is described by the $(0,0)$th entry in harmonic-lifted system, $\tilde{\mathbf{G}}(e^{jm\omega_0})$.

$$\tilde{\mathbf{G}}_{00} = \frac{1}{m}\hat{\phi}_0'\hat{\mathbf{G}}(e^{jm\omega_0})\hat{\phi}_0$$

The magnitue $|\tilde{\mathbf{G}}_{00}|$ and phase $\varphi = \arg(\tilde{\mathbf{G}}_{00})$ of this complex gain are then used in the controller shown in Eq. (NBF) on page 34 where the normalized controller gain is $\bar{k} = k/|\tilde{\mathbf{G}}_{00}|$ and k becomes the design parameter.

The lifted transfer function matrix for the controller, $\mathbf{K}$, becomes

$$\hat{\mathbf{K}}(e^{jm\omega}) = \frac{1}{m}\mathbf{\Phi}_\omega' \operatorname{diag}\left\{\mathbf{K}(e^{j(\omega+i\Omega)})\right\}\mathbf{\Phi}_\omega$$

which makes the loop-gain, $\hat{\mathbf{L}} = \hat{\mathbf{G}}\hat{\mathbf{K}}$,

$$\begin{aligned}
\text{lifted:} \qquad \hat{\mathbf{L}}(e^{jm\omega}) &= \hat{\mathbf{G}}(e^{jm\omega})\hat{\mathbf{K}}(e^{jm\omega}) \\
&= \frac{1}{m}\mathbf{\Phi}_\omega'\tilde{\mathbf{G}}(e^{jm\omega}) \operatorname{diag}\left\{\mathbf{K}(e^{j(\omega+i\Omega)})\right\}\mathbf{\Phi}_\omega \\
\text{harmonic-lifted:} \qquad \tilde{\mathbf{L}}(e^{jm\omega}) &= \tilde{\mathbf{G}}(e^{jm\omega}) \operatorname{diag}\left\{\mathbf{K}(e^{j(\omega+i\Omega)})\right\}
\end{aligned}$$

Since the lowered controller $\mathbf{K}$ has a pole pair at $e^{\pm j\omega_0}$, the lifted loop-gain has a pole pair at $e^{\pm jm\omega_0}$ with necessary high loop-gain at the disturbance frequency, $\overline{\sigma}(\hat{\mathbf{L}}(e^{jm\omega_0})) \gg 1$, and seemingly good nominal performance.

$$\underline{\sigma}(\hat{\mathbf{S}}(e^{jm\omega_0})) \leq \frac{1}{|1 - \overline{\sigma}(\hat{\mathbf{L}}(e^{jm\omega_0})|} \ll 1$$

While this controller places a zero in the sensitivity as seen by the small $\underline{\sigma}(\hat{\mathbf{S}})$, the null space of $\hat{\mathbf{S}}$ does not correspond to ϕ_0—pure tones with frequency ω_0. That is, even though this choice of controller places a zero at the disturbance frequency, which yields the transmission blocking property, it does not orient the zero direction with the disturbance. Sinusoidal disturbances at frequency ω_0 are *not* blocked and, in fact, result in additional tones at the $m-1$ higher harmonics.

Evaluating the harmonic-lifted loop-gain at the disturbance frequency, $m\omega_0$ we get

$$\begin{aligned}
\tilde{\mathbf{L}}(e^{jm\omega_0}) &= \tilde{\mathbf{G}}(e^{jm\omega_0}) \operatorname{diag}\left\{\mathbf{K}(e^{j(\omega_0+i\Omega)})\right\} \\
&= \begin{bmatrix} \mathbf{K}(e^{j\omega_0})\tilde{\mathbf{G}}_0 & \mathbf{K}(e^{j(\omega_0+\Omega)})\tilde{\mathbf{G}}_1 & \cdots & \mathbf{K}(e^{j(\omega_0+(m-1)\Omega)})\tilde{\mathbf{G}}_{m-1} \end{bmatrix}
\end{aligned}$$

where $\tilde{\mathbf{G}}_i$ is the ith column of the harmonic-lifted system $\tilde{\mathbf{G}}(e^{jm\omega_0})$. If the controller bandwidth is less than the plant-periodic frequency Ω, $\mathbf{K}(e^{j\omega_0})$ will be large (infinite) and the remaining $m-1$ gains will be less than unity.

$$\begin{aligned} \mathbf{K}(e^{j\omega_0}) &\gg 1 \\ \mathbf{K}(e^{j(\omega_0+i\Omega)}) &\ll 1 \qquad i = 1, \ldots, m-1 \end{aligned}$$

Since the first column of $\tilde{\mathbf{L}}(e^{jm\omega_0})$ is larger, in a norm sense, than the other columns, the range of the loop-gain and return difference are in this direction,

$$\begin{aligned} \operatorname{range}\left(I - \tilde{\mathbf{L}}(e^{jm\omega_0})\right) &\simeq \operatorname{range}\tilde{\mathbf{L}}(e^{jm\omega_0}) \\ &\simeq \operatorname{span}\left\{\mathbf{K}(e^{j\omega_0})\tilde{\mathbf{G}}_0\right\} \end{aligned}$$

and the null space of the sensitivity is equal to the range of the return difference.

$$\operatorname{null}\tilde{\mathbf{S}}(e^{jm\omega_0}) \simeq \operatorname{range}\left(I - \tilde{\mathbf{L}}(e^{jm\omega_0})\right)$$

Thus we see that the zero direction of $\tilde{\mathbf{S}}(e^{jm\omega_0})$ does not correspond to the disturbance direction e_1 and we will not achieve good disturbance rejection in the desired direction.

The primary disadvantage of classical designs is that they do not take into account the plant periodicity. That would require accounting for each entry in the transfer function matrix, $\hat{\mathbf{G}}(\hat{z})$, during design. There are extensions of the SISO classical design methodology which can be used on multivariable systems, the most common being sequential loop closure. Controllers are designed independently for each path with a narrow bandpass filter in the feedback loop. At each step of the design process the filter gain and phase is chosen appropriately and is included in the plant; this ensures stability of the final design. This design method has several drawbacks [50].

First, sequential loop closure is extremely work intensive. For a SISO m-periodic system there are m^2 controllers to design. For even a system with relatively low order the labor involved could be prohibitive. Second, we do not necessarily have any guarantees on the orientation of the zero direction. As in the SISO case certain combinations of harmonics may receive good attenuation, while harmonics in the disturbance would not. Also, although nominal stability is achieved, there is not necessarily any guarantee on robust stability. Finally, the resulting controller is considerably more complex than required. Controllers designed by sequential loop closure will in general have $2m^2$ states. This excess of poles is

a liability from a robustness standpoint—the more poles added, the more likely the system could become unstable. Our performance objective is to place a zero at the disturbance frequency and orient the zero direction with the lifted disturbance signal. This can be done with only one conjugate pole pair at the disturbance frequency provided attention is paid to the periodic structure of the plant.

Multivariable design methods based on optimal control theory offer the most promising tools for designing periodic controllers for narrowband disturbance rejection. In the next section, we will investigate $\mathcal{H}_\infty$ techniques to design controllers which meet the nominal performance and robust stability objectives. Each objective will be cast as the solution to a weighted sensitivity problem and will be combined in a mixed sensitivity optimization.

3.2 Periodic Designs

3.2.1 Nominal Performance

$\mathcal{H}_\infty$ design methods provide the most useful tools for designing multvariable controllers. These methods identify disturbance rejection with making the maximum disturbance path gain small.

$$\begin{gathered}\overline{\sigma}\left(\hat{\mathbf{S}}(e^{jm\omega_0})\right) \leq \gamma \\ \Updownarrow \\ \|\hat{y}(e^{jm\omega_0})\| \leq \gamma \|\hat{d}(e^{jm\omega_0})\|\end{gathered}$$

and the requirement that $\overline{\sigma}(\hat{\mathbf{S}}) \leq \gamma$ is ensured if the loop-gain is large

$$\underline{\sigma}\left(\hat{\mathbf{L}}(e^{jm\omega_0})\right) \geq \frac{1+\gamma}{\gamma}$$

For general multivariable systems, the multiple disturbances may be uncorrelated signals in which case the specific direction of the disturbance vector d is unknown and suitable designs must account for the worst by attenuating in all directions. However, in the periodic case, the 'multiple' disturbances result from the lift of a periodic disturbance and, therefore, are correlated. Thus, given any particular periodic disturbance signal we do in fact know the disturbance direction, and worst case designs over-engineer the solution and are unnecessary.

Consider the harmonic-lifted sensitivity at the disturbance frequency

$$\tilde{\mathbf{S}}(e^{jm\omega_0}) = \begin{bmatrix} \tilde{\mathbf{S}}_0 & \tilde{\mathbf{S}}_1 & \cdots & \tilde{\mathbf{S}}_{m-1} \end{bmatrix}$$

where $\tilde{\mathbf{S}}_i$ is the ith column. We see that the response of the plant to harmonic-lifted disturbance $\tilde{d}[k] = e_1\, e^{jm\omega_0 k}$ is $\tilde{y}[k] = \tilde{\mathbf{S}}_0\, e^{jm\omega_0 k}$ and we can consider the nominal performace objective to be making $\|\tilde{\mathbf{S}}_0(e^{jm\omega})\|$ small.

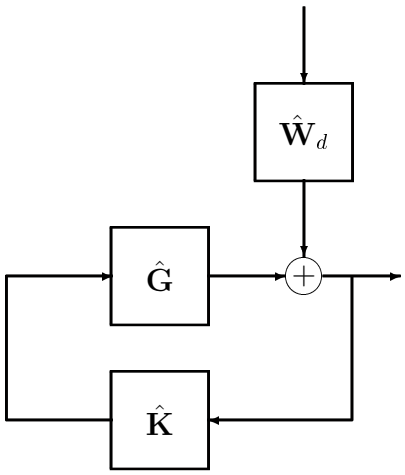

Figure 3.3: A block diagram of sensitivity input weighting.

The nominal performance critera can be cast as a weighted sensitivity problem.

$$\|\hat{\mathbf{S}}\hat{\mathbf{W}}_d\|_\infty < 1$$

where the weight $\hat{\mathbf{W}}_d$ is a narrowband filter which emphasizes the disturbance direction $\hat{\phi}_0$. A suitable choice is

$$\hat{\mathbf{W}}_d(\hat{z}) = \hat{\phi}_0 \left(k\, \frac{\hat{z}}{\hat{z} - e^{jm\omega_0}} \right)$$

If the nominal performance specification is met then

$$\underline{\sigma}(\hat{\mathbf{S}}) \leq \frac{1}{\overline{\sigma}(\hat{\mathbf{W}}_d)}$$

and the controller places a zero in the sensitivity where $\hat{\mathbf{W}}_d$ is large (infinite). In addtion, the zero direction is oriented with the disturbance since

$$\tilde{\mathbf{S}}(e^{jm\omega_0})e_1 = \tilde{\mathbf{S}}_0$$

Input weighting of the sensitivity function is equivalent to the technique known as disturbance modelling. As shown in Fig. 3.3, the weighting function $\hat{\mathbf{W}}_d$ can be considered a model of the disturbance. Using this interpretation an alternate choice for the weight $\hat{\mathbf{W}}_d$ can be made. If we model the disturbance in real time as

$$\mathbf{W}_d(z) = k\frac{z}{z - e^{j\omega_0}}$$

the lifted disturbance model becomes

$$\hat{\mathbf{W}}_d(e^{jm\omega}) = \frac{1}{m}\mathbf{\Phi}'_\omega \,\mathrm{diag}\left\{\mathbf{W}(e^{j(\omega+i\Omega)})\right\}\mathbf{\Phi}_\omega$$

and the weighted sensitivity becomes

$$\overline{\sigma}\left(\hat{\mathbf{S}}\hat{\mathbf{W}}_d(e^{jm\omega_0})\right) = \overline{\sigma}\left(\tilde{\mathbf{S}}\tilde{\mathbf{W}}_d(e^{jm\omega_0})\right) \simeq \|\tilde{\mathbf{S}}_0\mathbf{W}_d(e^{j\omega_0})\|$$

Thus, we see that the nominal peformance specification will be satisfied. Currently, there is no apparent technical advantage to using one disturbance model or the other. Our first choice is simpler, and based on that could be considered more attractive. However, it does not account for changes in the disturbance direction with changes in frequency. As long as rejection bandwidth is small these changes are insignificant; however, if the rejection bandwidth is large then a more accurate description of the disturbance, as suggested above, might be more appropriate. Of course, disturbance rejection over large bandwidths gets away from the narrowband topic discussed here.

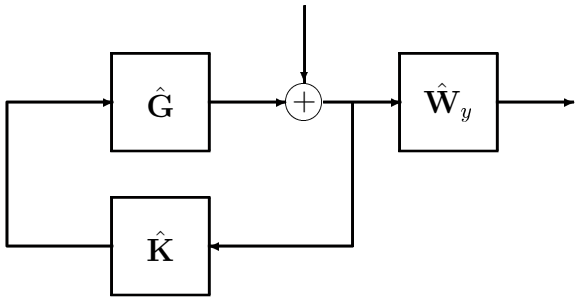

Figure 3.4: A block diagram of sensitivity output weighting.

At this point we should discuss the dual methodology to disturbance modelling and input weighting—frequency shaped cost functional or output weighting. This method is shown in block diagram form in Fig. 3.4. Here the weighted sensitivity criteria is

$$\|\hat{\mathbf{W}}_y\hat{\mathbf{S}}\|_\infty < 1$$

and $\hat{\mathbf{W}}_y$ is a narrowband filter with direction selected appropriately. At first glance a suitable choice for $\hat{\mathbf{W}}_y$ would be

$$\hat{\mathbf{W}}_y(\hat{z}) = \hat{\phi}_0' \left(k \frac{\hat{z}}{\hat{z} - e^{jm\omega_0}} \right)'$$

which is a $1 \times m$ weighting function. Output weighting is equivalent to input weighting as far as the singular value math is concerned since

$$\sigma(\hat{\mathbf{W}}_y \hat{\mathbf{S}}) = \sigma(\hat{\mathbf{S}}' \hat{\mathbf{W}}_y')$$

Thus, this choice for a weighting function would place a zero in the sensitivity

$$\underline{\sigma}(\hat{\mathbf{S}}) = \underline{\sigma}(\hat{\mathbf{S}}') \leq \frac{1}{\overline{\sigma}(\hat{\mathbf{W}}_y')}$$

However, the disturbance direction $\hat{\phi}_0$ is in the null space of $\hat{\mathbf{S}}'$ not $\hat{\mathbf{S}}$. Thus, $\hat{\phi}_0$ is eliminated from the range of $\hat{\mathbf{S}}$, but the disturbance may still excite the remaining $m - 1$ harmonics. This is similar to the result found for classical designs.

The output weight $\hat{\mathbf{W}}_y$ is often chosen, in other applications, to be a diagonal matrix whose entries are $\frac{\hat{z}}{\hat{z} - e^{jm\omega_0}}$. This choice will certainly place a zero in the sensitivity, and in fact places m of them and does so by placing m poles in the controller. This approach and result over engineers the problem, and the excess of poles (over what is needed) is considered a liability from a robustness standpoint.

3.2.2 Robust Stability

Before we get into robust stability, we will need the result of the Small Gain Theorem.

Small Gain Theorem: Let $\mathbf{\Delta}$ and $\mathbf{G}$ be two BIBO stable, m-periodic systems connected as shown.

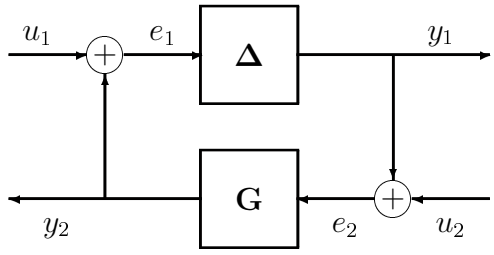

The closed-loop system will be stable for all $\|\mathbf{\Delta}\|_\infty \leq 1$ if and only if $\|\mathbf{G}\|_\infty < 1$. We can show this as follows:

(Sufficiency) If $u_2 = 0$ and $u_1 \in L_2$, then

$$\begin{aligned} e_1 &= u_2 + \mathbf{G\Delta} e_1 \\ \Rightarrow \quad \|e_1\|_2 &\leq \|u_1\|_2 + \|\mathbf{G\Delta}\|_\infty \|e_1\|_2 \end{aligned}$$

and

$$\|e_1\|_2 \leq \frac{1}{1 - \|\mathbf{G\Delta}\|_\infty} \|u_2\|_2$$

If $\|\mathbf{G}\|_\infty < 1$ then $\|\mathbf{G\Delta}\|_\infty \leq \|\mathbf{\Delta}\|_\infty \|\mathbf{G}\|_\infty < 1$ and the closed-loop gain is bounded which implies the closed-loop system is BIBO stable.

(Necessity)[56] We will show this by contradiction. If $\|\mathbf{G}\|_\infty = \|\hat{\mathbf{G}}\|_\infty \geq 1$ then $\|\frac{1}{\hat{z}}\hat{\mathbf{G}}\|_\infty \geq 1$. We can construct a proper rational matrix function $\hat{\mathbf{\Delta}}_1(\hat{z}) : \ \|\hat{\mathbf{\Delta}}_1\|_\infty \leq 1$ which will destabilize the closed-loop system with loop-gain $\frac{1}{\hat{z}}\hat{\mathbf{G}}\hat{\mathbf{\Delta}}_1$ (see for example Zhou [59]). Thus the loop-gain $\hat{\mathbf{G}}\hat{\mathbf{\Delta}}$ with $\hat{\mathbf{\Delta}} = \hat{z}\hat{\mathbf{\Delta}}_1$ also results in an unstable closed-loop system. In addition, $\hat{\mathbf{\Delta}}(\hat{z})$ is strictly proper and therefore a causal lift of an m-periodic system $\mathbf{\Delta}$ and $\|\mathbf{\Delta}\|_\infty = \|\hat{\mathbf{\Delta}}\|_\infty \leq 1$.

The concept of robustness comes from the fact that the true plant is unknown and different, whether relative or absolute, from the nominal model used for design. In many situations we can quantify this uncertainty with the result that the true plant, $\mathbf{G}_t$, belongs to a set of plant models, $\mathfrak{G}$.

$$\mathfrak{G} = \{\mathbf{G}_t = (I + \mathbf{\Delta})\mathbf{G} \quad : \quad \|\mathbf{\Delta}\|_\infty < 1\}$$

A controller, $\mathbf{K}$, is robust if it will stabilize every plant in $\mathfrak{G}$.

For SISO time-periodic systems the task of modelling the uncertainty is complicated, as compared to time-invariant counterparts, because they do not commute, illustrated best by the system algebra of their lifts. Therefore, similar to MIMO time-invariant systems, there is a difference between uncertainty at the inputs (actuators) and at the outputs (sensors). Here we are implictly refering to multiplicative uncertainties which have the advantage over additive uncertainties that they apply to the loop gain, $\mathbf{GK}$, as well as the plant model, $\mathbf{G}$. To simplify our discussion we will concern ourselves with multiplicative uncertainties at the output of the periodic system.

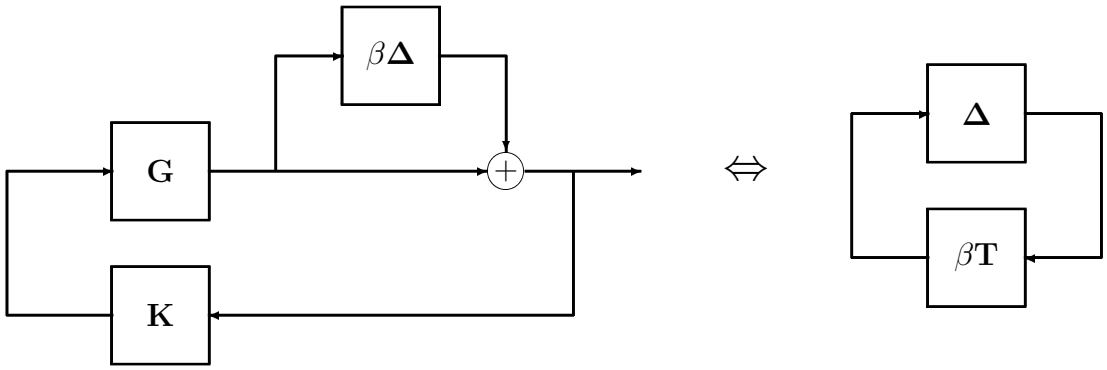

Figure 3.5: Equivalent block diagrams for output multiplicative uncertainty

Consider the true plant model to be

$$\mathbf{G}_t = (1 + \beta\mathbf{\Delta})\mathbf{G}$$

where $\mathbf{\Delta}$ is a stable m-periodic system with $\|\mathbf{\Delta}\|_\infty < 1$, and β is a scalar constant. Here, we are using operator notation and the above systems should not be considered to be equivalent to their lifts as yet, although that extension will be made shortly. Admittedly this model of uncertainty is simple—in more complicated situations β can be replaced by a dynamic weight—however, for our purposes this uncertainty model is sufficient and in fact our design will be able to handle uncertainties which exceed this bound, even though we do not design for them.

As shown in Fig. 3.5, the system connected to the input and output of $\mathbf{\Delta}$ is

$$\beta\mathbf{T} = \beta\mathbf{GK}(I - \mathbf{GK})^{-1}$$

which is the complementary sensitivity weighted by β. Thus if $\|\beta\mathbf{T}\|_\infty \leq 1$, by the small gain theorem, the closed-loop system will be stable. Because of the norm equivalence between periodic and lifted systems we have

$$\|\beta\hat{\mathbf{T}}\|_\infty \leq 1 \quad \Rightarrow \quad \text{robust stability}$$

We can alternatively interpret this robust stability criterion as a nominal performance criterion where $\beta\hat{\mathbf{T}}$ is the weighted closed-loop transfer function matrix from ficticious measurement noise, $\hat{n}$, to the system output, $\hat{y}$, see Fig. 3.6. Although the measurement noise

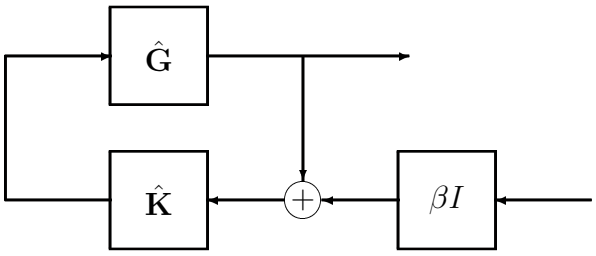

Figure 3.6: Block diagrams for measurement noise.

cannot destabilize the system, we see that from a norm objective point of view the robust stability criterion and this nominal performance criterion are equivalent. This will be useful when we combine the criteria in a mixed sensitivity setting.

3.2.3 Stability Margins

Now consider SISO time-periodic systems and the true m-periodic plant to be

$$\mathbf{G}_t = \mathbf{g}[k]\mathbf{G}$$

where $\mathbf{g}[k]$ is a scalar time periodic gain, $\mathbf{g}[k] = \mathbf{g}[k+m]$. Again we are considering multiplicative uncertainties at the output of the system. Real values of $\mathbf{g}$ correspond, of course, to changes in the gain at the output of the periodic system, while complex values on the unit circle, $\mathbf{g}[k] = e^{j\theta_k}$, correspond to changes in the phase of the periodic system.

We can now offer the following definitions of gain and phase margins for periodic system; these are consistent with similar definitions for MIMO systems [11].

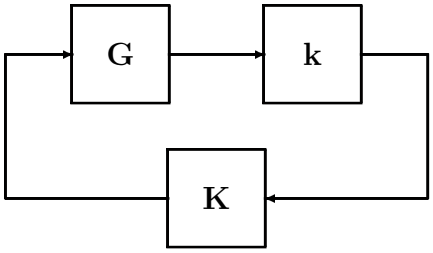

Figure 3.7: Block diagram of scalar multiplicative ouptut uncertainty.

Table 3.1: Lower bound estimates on periodic gain and phase margins using closed-loop sensitivities.

	Gain Margin (dB)	Phase Margin (deg)
Using	$G_L \quad , \quad G_U$	θ
$\|\hat{\mathbf{S}}\|_\infty = 1/\alpha$	$(1+\alpha)^{-1}\,, (1-\alpha)^{-1}$	$2\sin^{-1}(\alpha/2)$
$\|\hat{\mathbf{T}}\|_\infty = 1/\beta$	$1-\beta \quad , \quad 1+\beta$	$2\sin^{-1}(\beta/2)$

Periodic gain margin A periodic gain margin is a real interval $[G_L, G_U]$ such that

$$\mathbf{g}[k] \in [G_L, G_U] \qquad \forall\, k$$

and the closed-loop system remains stable. Notice again the periodic gain $\mathbf{g}$ is not necessarily constant, although it certainly can be, and, in fact, may at attenuate the system output at certain times in the cycle. The gain margin is not unique; that is, there does not necessarily exist only one interval which guarantees stability. For example, $[-\infty, 2]$ dB and $[-2, 60]$ dB may both be valid intervals.

Periodic phase margin A periodic phase margin is the largest real interval, $[-\theta, \theta]$, such that

$$\mathbf{g}[k] = e^{j\theta_k} \qquad \theta_k \in [-\theta, \theta] \quad \forall\, k$$

and the closed-loop system remains stable. The phase margin is unique since it is defined to be the largest symetric interval.

Calculation of the periodic gain and phase margin is most easily approached after lifting where the periodic gain, $\mathbf{g}[k]$, becomes a diagonal matrix

$$\hat{\mathbf{g}} = \text{diag}\{\mathbf{g}[k]\}$$

and the characteristic equation of the closed-loop system is

$$\det\left(I - \hat{\mathbf{g}}(\hat{\mathbf{G}}\hat{\mathbf{K}})\right) = 0$$

Real-μ analysis is required to exactly compute the gain and phase margins. However, suitable lower bounds can be found directly from singular value plots of the closed-loop sensitivities. A complete derivation is omitted for brevity, but the Table 3.1 gives the appropriate formulas.

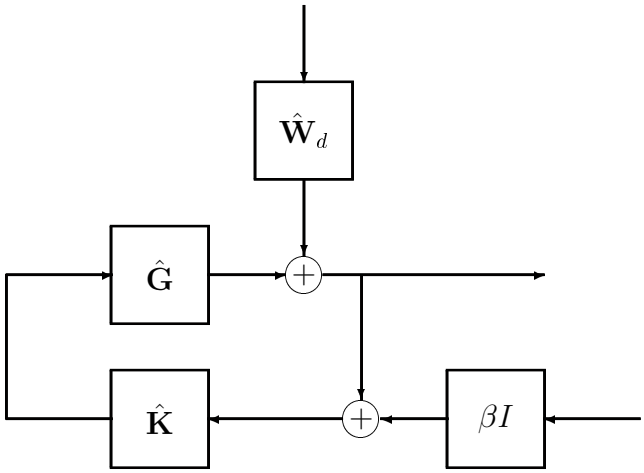

Figure 3.8: Block diagrams for mixed sensitivity problem.

3.2.4 Mixed Sensitivity

The combination of the nominal performance and robust stability requirements results in a mixed sensitivity problem [29, 34, 53]. In order to be able to solve the mixed sensitivity problem using the $\mathcal{H}_\infty$ machinery, we must pose the two objectives as a single norm criterion.

$$\left\| \begin{bmatrix} \hat{\mathbf{S}}\hat{\mathbf{W}}_d & \beta\hat{\mathbf{T}} \end{bmatrix} \right\|_\infty < 1$$

which, because the norm of a matrix bounds the norm of its submatrices, guarantees both the nominal performance and robust stability criteria. This problem can be cast as a generalized regulator problem, discussed in Chapter 5, where the generalized plant $\mathbf{P}$ is

$$\mathbf{P} = \begin{bmatrix} \mathbf{P}_{11} & \mathbf{P}_{12} \\ \mathbf{P}_{21} & \mathbf{P}_{22} \end{bmatrix} = \left[\begin{array}{cc|c} \hat{\mathbf{W}}_d & 0 & \hat{\mathbf{G}} \\ \hline \hat{\mathbf{W}}_d & \beta I & \hat{\mathbf{G}} \end{array}\right]$$

Given representations for the lifted plant transfer function matrix $\hat{\mathbf{G}}$ and weighting matrix $\hat{\mathbf{W}}_d$

$$\hat{\mathbf{G}} \sim \left[\begin{array}{c|c} \hat{A} & \hat{B} \\ \hline \hat{C} & \hat{D} \end{array}\right] \qquad \hat{\mathbf{W}}_d \sim \left[\begin{array}{c|c} \hat{A}_d & \hat{B}_d \\ \hline \hat{C}_d & \hat{D}_d \end{array}\right]$$

the generalized plant has the following representation.

$$\mathbf{P} \sim \left[\begin{array}{c|cc} A & B_1 & B_2 \\ \hline C_1 & D_{11} & D_{12} \\ C_2 & D_{21} & D_{22} \end{array}\right] = \left[\begin{array}{cc|cc|c} \begin{bmatrix} \hat{A} & 0 \\ 0 & \hat{A}_d \end{bmatrix} & & \begin{bmatrix} 0 & 0 \\ \hat{B}_d & 0 \end{bmatrix} & & \begin{bmatrix} \hat{B} \\ 0 \end{bmatrix} \\ \hline \begin{bmatrix} \hat{C} & \hat{C}_d \end{bmatrix} & & \begin{bmatrix} \hat{D}_d & 0 \end{bmatrix} & & \hat{D} \\ \begin{bmatrix} \hat{C} & \hat{C}_d \end{bmatrix} & & \begin{bmatrix} \hat{D}_d & \beta I \end{bmatrix} & & \hat{D} \end{array}\right]$$

A causal controller which stabilizes the closed-loop system and meets the norm bound can be found using the tools developed in Chapter 5.

Chapter 4

Feedforward Disturbance Rejection

4.1 Fixed-gain Feedforward

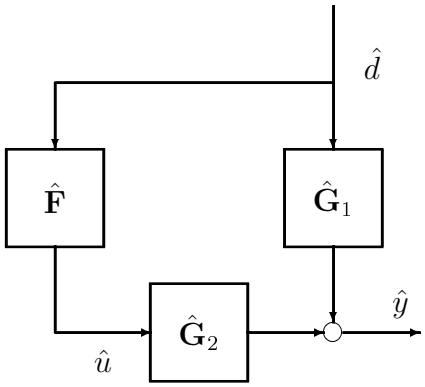

Figure 4.1: Block diagrams for feedforward control.

If a measurement of the disturbance or suitable correlated signal is available we can compensate for its effect using a feedforward compensator, see Fig. 4.1. Using this architecture we find that the transfer function matrix from $\hat{d}$ to $\hat{y}$ is

$$\hat{\mathbf{S}} = \hat{\mathbf{G}}_1 + \hat{\mathbf{G}}_2\hat{\mathbf{F}}$$

and we can eliminate all disturbances at frequency $m\omega_0$ by choosing

$$\hat{\mathbf{F}}(e^{jm\omega_0}) = -\hat{\mathbf{G}}_2(e^{jm\omega_0})^{-1}\hat{\mathbf{G}}_1(e^{jm\omega_0})$$

assuming the so called control-to-error transfer function matrix, $\hat{\mathbf{G}}_2$, is square, equal number of inputs and outputs, and invertible, no zero a the disturbance frequency. When $\hat{\mathbf{G}}_2$ either not square or invertible, the controller $\hat{\mathbf{F}}$ will be the best stable inverse, in a least-squares sense or in a sense to be described in the sequel, of the plant at the disturbance frequency. Unless specifically noted, we will assume $\hat{\mathbf{G}}_2$ is non-singular.

The remainder of this section describes several approaches for designing the controller $\hat{\mathbf{F}}$. First, we use $\mathcal{H}_\infty$ control theory to minimize the weighted norm of the controlled system. The second method implements a multivariable equivalent of the tapped-delay line. In our case, the delay will occur once per cycle, and the diagonal gain matrices represent periodic weights.

4.1.1 Periodic Designs

Similar to the feedback case, our objective is to make the weighted norm of the controlled system small.

$$\left\| \left(\hat{\mathbf{G}}_1 + \hat{\mathbf{G}}_2 \hat{\mathbf{F}} \right) \hat{\mathbf{W}}_d \right\|_\infty \leq 1$$

The input weight (disturbance model) $\hat{\mathbf{W}}_d$ can be chosen as before.

One of the advantages of the feedforward architecture is that the controlled system is guaranteed stable for all stable $\hat{\mathbf{F}}$. Thus, the requirement of robust stablility is not required; however, one of the advantages of the robust stability requirement for the feedback control problem was that it ensures low controller gains at frequencies without tight performance requirements. We would like to have a similar criterion for the feedforward case.

In addition to the nominal performance criteria, we include a criterion which limits the magnitude of the controller gain.

$$\left\| \beta \hat{\mathbf{F}} \right\|_\infty \leq 1$$

where β is a scalar gain.

Each of the single target objectives can be combined in a multi-target problem

$$\left\| \left[(\hat{\mathbf{G}}_1 + \hat{\mathbf{G}}_2 \hat{\mathbf{F}}) \hat{\mathbf{W}}_d \quad \beta \hat{\mathbf{F}} \right] \right\|_\infty < 1$$

which guarantees each criteria, since the norm of a matrix bounds the norm of the submatrices.

We can cast this multi-target problem in the $\mathcal{H}_\infty$ framework of the generalized regulator with the generalized plant $\mathbf{P}$ being

$$\mathbf{P} = \begin{bmatrix} \mathbf{P}_{11} & \mathbf{P}_{12} \\ \mathbf{P}_{21} & \mathbf{P}_{22} \end{bmatrix} = \left[\begin{array}{cc|c} \hat{\mathbf{G}}_1\hat{\mathbf{W}}_d & 0 & \hat{\mathbf{G}}_2 \\ \hat{\mathbf{W}}_d & \beta I & 0 \end{array}\right]$$

The generalized regulator can be represented as

$$\mathbf{P} \sim \left[\begin{array}{cc|cc|c} \begin{bmatrix} \hat{A} & \hat{B}_1\hat{C}_d \\ 0 & \hat{A}_d \end{bmatrix} & & \begin{bmatrix} \hat{B}_1\hat{D}_d & 0 \\ \hat{B}_d & 0 \end{bmatrix} & & \begin{bmatrix} \hat{B}_2 \\ 0 \end{bmatrix} \\ \hline \begin{bmatrix} \hat{C} & \hat{D}_1\hat{C}_d \end{bmatrix} & & \begin{bmatrix} \hat{D}_1\hat{D}_d & 0 \end{bmatrix} & & \begin{bmatrix} \hat{D}_2 \end{bmatrix} \\ \begin{bmatrix} 0 & \hat{C}_d \end{bmatrix} & & \begin{bmatrix} \hat{D}_d & \beta I \end{bmatrix} & & \begin{bmatrix} 0 \end{bmatrix} \end{array}\right]$$

where the plant $\hat{\mathbf{G}} = \begin{bmatrix} \hat{\mathbf{G}}_1 & \hat{\mathbf{G}}_2 \end{bmatrix}$ is represented by

$$\hat{\mathbf{G}} \sim \left[\begin{array}{c|cc} \hat{A} & \hat{B}_1 & \hat{B}_2 \\ \hline \hat{C} & \hat{D}_1 & \hat{D}_2 \end{array}\right]$$

A stable causal controller which meets the norm bound can be found using the tools developed in Chapter 5.

4.1.2 Periodic FIR Filters

Consider for now a SISO m-periodic system. The input-output relationship can be described as

$$y[n] = \sum_{l=0}^{n} h[n,t]u[t]$$

where $h[n,t]$ is the response of the system at time n to an impulse input at time t, and

$$h[n+m, t+m] = h[n,t]$$

due to periodicity; in addition, causality requires $h[n,t] = 0$ if $n < t$ or $t < 0$.

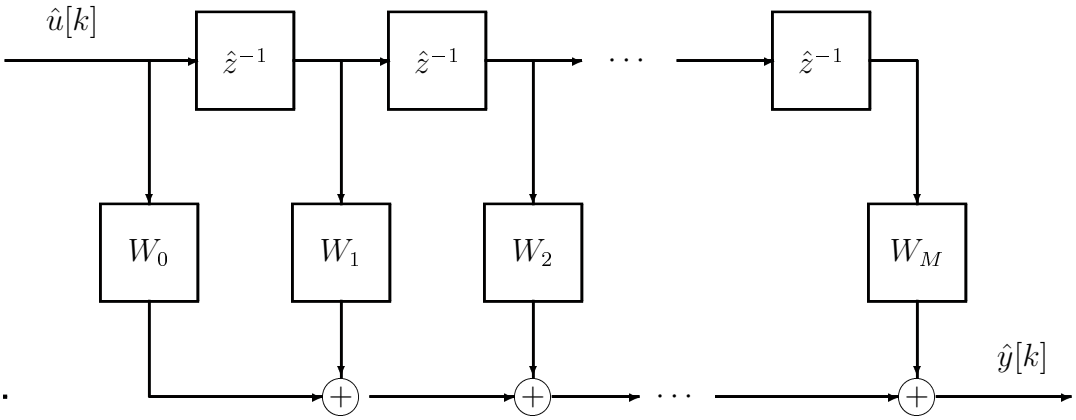

Figure 4.2: A Block diagram of an Mth order FIR filter.

If we let $n = km + l$ and $t = rm + s$ then

$$\begin{aligned} y[km+l] &= \sum_{r=0}^{k} \sum_{s=0}^{m-1} h[km+l, rm+s]u[rm+s] \\ &= \sum_{r=0}^{k} \sum_{s=0}^{m-1} h[(k-r)m+l, s]u[rm+s] \\ \hat{y}_l[k] &= \sum_{r=0}^{k} \mathbf{H}[k-r]\hat{u}[r] \end{aligned}$$

where $\mathbf{H}[n]$ is the impulse response matrix of the lifted system with

$$\{\mathbf{H}[n]\}_{ij} = h[nm+i, j]$$

We should notice now that $\mathbf{H}[0]$ is lower triangular (zero for $i < j$) by causality; this is consistent with previous results.

A periodic system has a finite impulse response (FIR) if the impulse response matrix of the lifted system is exactly zero after some finite time M; M is termed the order of the periodic FIR system.

$$\text{periodic FIR} \Leftrightarrow \mathbf{H}[n] \equiv 0 \quad n > M$$

We can of course construct a lifted periodic FIR filter with an M weight transversal filter, as shown in Fig. 4.2, where the delays are cycle delays, $\hat{z} = z^m$, and the tap weights

are $m \times m$ matrices. This gives the control system designer enormous flexibility, especially for our harmonic disturbance rejection problem.

An M weight FIR filter has $Mm^2 + m(m+1)/2$ parameters. The rejection of m tones requires at most $2m$ weights; thus, the control system designer has on the order of Mm^2 extra weights which can be chosen to meet additonal constraints such as bounded filter norm, bounded weight norms, or additional performance requirements.

Consider now a first-order FIR filter (two weights) with diagonal weighting matrices.

$$\hat{\mathbf{F}}(\hat{z}) = W_0 + W_1 \hat{z}^{-1} \qquad \begin{aligned} W_0 &= \text{diag}\{W_{0,i}\} \\ W_1 &= \text{diag}\{W_{1,i}\} \end{aligned}$$

Consider also a sinusoidal disturbance $\hat{d}[k] = \delta\, e^{jm\omega_0 k}$ and $\delta_i \neq 0 \quad i = 0 : m-1$. Our objective is to place a zero in the controlled system at $\hat{z} = e^{jm\omega_0}$ with its direction aligned with δ. Consequently the control direction, defined by the vector μ, is

$$\mu = \hat{\mathbf{F}}(e^{jm\omega_0})\delta$$

where

$$\mu = -\hat{\mathbf{G}}_2(e^{jm\omega_0})^{-1}\hat{\mathbf{G}}_1(e^{jm\omega_0})\delta$$

and the ith entry in the diagonal matrix $\hat{\mathbf{F}}(e^{jm\omega_0})$ is

$$\hat{\mathbf{F}}_i(e^{jm\omega_0}) = \frac{\mu_i}{\delta_i}$$

Evaluating $\hat{\mathbf{F}}(\hat{z})$ at $\hat{z} = e^{jm\omega_0}$ and equating real and imaginary parts, we find that

$$\begin{aligned} W_{0,i} &= \Re\left[\hat{\mathbf{F}}_i(e^{jm\omega_0})\right] - \cot(m\omega_0)\,\Im\left[\hat{\mathbf{F}}_i(e^{jm\omega_0})\right] \\ W_{1,i} &= -\csc(m\omega_0)\Im\left[\hat{\mathbf{F}}_i(e^{jm\omega_0})\right] \end{aligned}$$

Note that if the condition $\delta_i \neq 0 \quad i = 0 : m-1$ is not satisfied, then the diagonal controller must have an infinite gain at those times within the cycle. In this case, the FIR filter structure with diagonal weighting matrices will not achieve the objective, and another filter structure must be used. This is an area of continuing research.

4.2 Adaptive FIR Filters

The use of adaptive FIR filters, using the filtered-X LMS algorithm [57], for harmonic and narrowband disturbance rejection has been well documented [50]. Typical implementations of the filtered-X LMS algorithm are inadequate for controlling narrowband disturbance in conjunction with periodic plants. Reasons for this are often associated with the non-stationarity of the process statistics caused by plant periodicity. While this interpretation is certainly correct, a more useful interpretation arises when we consider the periodic system as a multivariable system as suggested by its lift.

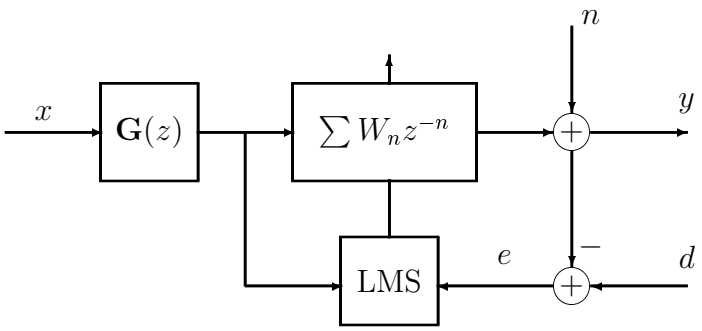

(a) Adaptive Inverse Control

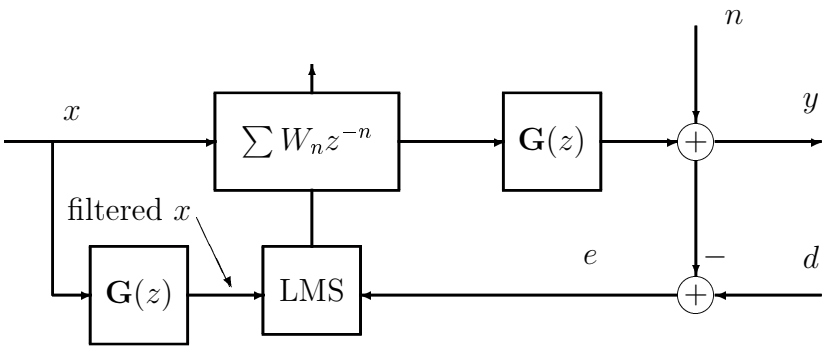

(b) Filtered-X LMS

Figure 4.3: Developement of the filtered-X LMS algorithm.

The filtered-X LMS algorithm [57] provides a method of Adaptive Inverse Control with the adaptive filter placed before the plant (see Fig. 4.3). An adjustment to the LMS algorithm

is required since the error is related to the plant output and not the output of the adaptive filter; thus, a suitable filtered version of the control signal x is required to be input to the LMS algorithm. Additionally, we must consider the effect commuting the adaptive filter with the plant may have on the system processes.

> For the same input, the same output results when the positions of the two cascaded filters are commuted provided that the filters are linear and time invariant. The adaptive filter, however, is neither linear nor time invariant. On the other hand, the adaptive filter and the plant would, to a good approximation, be commutable if the plant were linear and if the time variations fo the impulse responses of both the plant and the adaptive filter took place with time constants long compared to the combinded memory times of time constants of the adaptive filter and the plant. Thus, slow adaptation, the adaptive filter may be considered linear and commutable with $\mathbf{G}(z)$. [57]

A periodic plant is of course not strictly time-invariant although by lifting we can find a multivariable time-invariant system which corresponds to a periodic plant; however, MIMO system algebra does not allow the commutablity of multivariable systems making the commutablity arguements for the fitlered-X LMS algorithm invalid.

Some researchers have reformulated the LMS algorithm for multiple errors [12] where the cost function to be minimized is a vector norm of error signals. However, this algorithm is still not adequate for our purposes since they consider a scalar reference signal and the reference signal for our process is vector valued.

The remainder of this section considers an adaptive algorithm for use with MIMO system. We will consider Mth-order FIR filters of the last section

$$\hat{\mathbf{F}}(\hat{z}) = \sum_{n=0}^{M} W_n \hat{z}^{-n}$$

where W_n are diagonal matrices. The connection of this filter is shown in Fig. 4.4 where $\hat{x}$ and $\hat{u}$ are the unfiltered and filtered control signals respectively, $\hat{d}$ is the desired signal, $\hat{y}$ is the system output, and $\hat{e}$ is the system error. All are lifted signals. The cost function is the estimated value of the norm of the system error; note that this is a per cycle mean squared error.

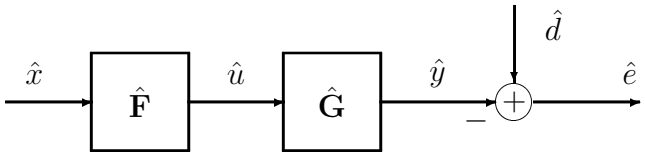

Figure 4.4: An adaptive filter block diagram

$$J = \frac{1}{2}\mathcal{E}\|\hat{e}\|^2 = \frac{1}{2}\mathcal{E}\left\{\sum_{l=0}^{m-1}|\hat{e}_l[k]|^2\right\}$$

and the error is

$$\begin{aligned}\hat{e}[k] &= \hat{d}[k] - \hat{\mathbf{G}}\hat{u}[k] \\ \hat{e}_l[k] &= \hat{d}_l[k] - \sum_{i=0}^{m-1}\hat{\mathbf{G}}_{li}\hat{u}_i[k] \\ &= \hat{d}_l[k] - \sum_{i=0}^{m-1}\sum_{n=0}^{M}\hat{\mathbf{G}}_{li}W_{n,i}\hat{x}_i[k-n]\end{aligned}$$

The plant (control-to-error path) is assumed to be quasi-static with its dynamics represented by the complex matrix $\hat{\mathbf{G}}$; this is suitable for the narrowband problem.

Using the method of steepest decent to control the adaptation of the filter, the gradient of the cost funtion is

$$\frac{\partial J}{\partial W_{n,i}} = \mathcal{E}\left\{\sum_{l=0}^{m-1}\hat{e}_l[k]\frac{\partial \hat{e}_l}{\partial W_{n,i}}[k]\right\}$$

and we can determine the instantaneous error gradient to be

$$\frac{\partial \hat{e}_l}{\partial W_{n,i}}[k] = -\hat{\mathbf{G}}_{li}\hat{x}_i[k-n]$$

We will use the instantaneous estimate of the cost gradient.

$$\frac{\partial J}{\partial W_{n,i}}[k] = -\hat{x}_i[k-n]\sum_{l=0}^{m-1}\hat{\mathbf{G}}_{li}\hat{e}_l[k]$$

The weight update equation, which adjusts the filter weights in a direction opposite of cost gradient is

$$\begin{aligned} W_{n,i}[k+1] &= W_{n,i}[k] - \rho \frac{\partial J}{\partial W_{n,i}}[k] \\ &= W_{n,i}[k] + \rho \hat{x}_i[k-n] \sum_{l=0}^{m-1} \hat{\mathbf{G}}_{li} \hat{e}_l[k] \end{aligned}$$

where ρ is chosen to control the size of each step of the adaptation routine.

It is interesting to note that the summation on the right hand side of the weight update equation is the error at time k filtered by the transpose of the lifted plant, $\hat{\mathbf{G}}^T$.

$$\left\{ \hat{\mathbf{G}}^T \hat{e} \right\}_i = \sum_{l=0}^{m-1} \hat{\mathbf{G}}_{li} \hat{e}_l[k]$$

This algorithm can be used to make adaptive the fixed-gain feedforward method described earlier in this chapter. Figure 4.5 shows a block diagram of the adaptive control scheme for narrowband disturbance rejection. A model of the control-to-error path, used to filter the error signal, is contained in $\hat{\mathbf{G}}_2^\star$ and can be constructed by a lifted periodic FIR filter

$$\hat{\mathbf{G}}_2^\star(\hat{z}) = G_1 \hat{z}^{-1} + G_2 \hat{z}^{-2}$$

This construction implicitly assumes there is no feedthrough response on the lifted system ($G_0 \equiv 0$). This typically is not the case; however, inclusion of a lowertriangular feedthrough term may over determine the problem and two weighting matrices are suitable to describe the complex gain of $\hat{\mathbf{G}}_2$ at the disturbance frequency. The weighting matrices, G_1 and G_2, are selected such that

$$\hat{\mathbf{G}}_2^\star(e^{jm\omega_0}) = \hat{\mathbf{G}}_2(e^{jm\omega_0})$$

The pre-filter $\hat{\mathbf{G}}_2^\star$ can be measured adaptively using the LMS algorithm on each entry. Care must be exercised that the system input is harmonic at the desired frequency, $m\omega_0$, and that the input signals span the space of $m \times 1$ lifted harmonic signals; that is, at least m independent harmonic signals must be used in the adaptation process so that the pre-fitler $\hat{\mathbf{G}}_2^\star$ contains suitable information about the control-to-error path at the disturbance frequency.

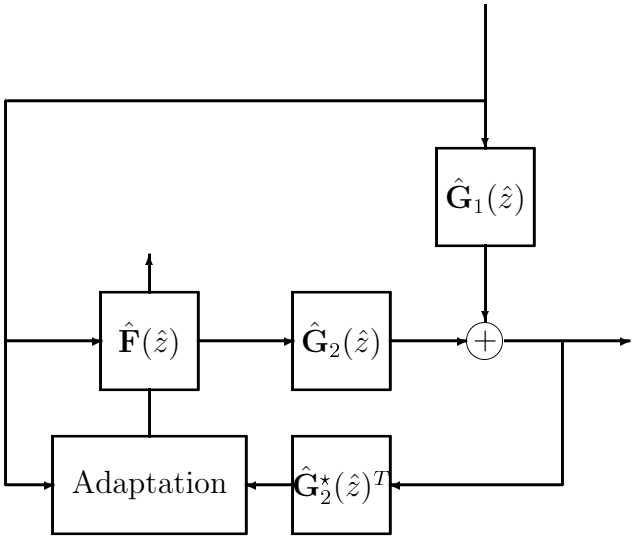

Figure 4.5: A block diagram of an adaptive control scheme for narrowband disturbance rejection.

Chapter 5

Periodic $\mathcal{H}_\infty$ Solutions

In the previous two chapters, control system objectives are posed as bounds on the ∞-norm of the closed-loop or controlled system. These types of analytical constraints have encouraged the development of $\mathcal{H}_\infty$ control theory in recent years. Due to the equivalence between a LTP system and its LTI lift, it appears conventional $\mathcal{H}_\infty$ control theory can be used to design periodic controllers which meet stated objectives; however, appropriate steps must be taken to ensure the resulting controller is causal, i.e., it is lower triangular at $\hat{z} = \infty$. This problem has been solved theoretically by Voulgaris and others [55, 56] by modifying the Nehari problem (a step in the $\mathcal{H}_\infty$ solution) to account for the additional causality constraint on the controller. In practice, this approach is complicated and difficult to implement.

In this chapter we present two techniques which can be used to solve the periodic $\mathcal{H}_\infty$ problem. Both methods can be used directly with state-space models of the generalized plant and can be added rather seamlessly into existing $\mathcal{H}_\infty$ solvers.

The $\mathcal{H}_\infty$ control theory has been considerably simplified by loopshifting methods which null and scale the feedthrough matrices of the generalized plant. The first approach accounts for controller causality in this loop-shifting process and is appropriate for explicit, discrete-time solutions to the $\mathcal{H}_\infty$ problem.

The second method uses Q-parameterization to make a causal controller. General parameterized controllers do not directly present themselves to causal solutions because of fully populated feedthrough matrices, e.g., controllers found using bilinear transformations and

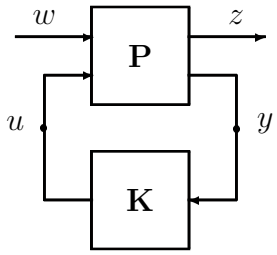

Figure 5.1: A generalized regulator block diagram.

continuous-time $\mathcal{H}_\infty$ solutions. Proper choice of the free-parameter can result in a causal lifted system.

5.1 Preliminaries

The $\mathcal{H}_\infty$ problem is typically cast as a generalized regulator problem. A generalized plant, whose specific components depend upon the particular problem being solved, is connected in a feedback setting with the controller as shown in Fig. 5.1. The generalized plant, $\mathbf{P}$, describes the input/output relationship between the q_1 exogenous inputs w, p_1 performance outputs z, q_2 control signals u, and p_2 measured outputs y.

$$\begin{bmatrix} z \\ y \end{bmatrix} = \begin{bmatrix} \mathbf{P}_{11} & \mathbf{P}_{12} \\ \mathbf{P}_{21} & \mathbf{P}_{22} \end{bmatrix} \begin{bmatrix} w \\ u \end{bmatrix}$$

The generalized plant $\mathbf{P}$ can be represented in state-space notation as

$$\mathbf{P} \sim \left[\begin{array}{c|cc} A & B_1 & B_2 \\ \hline C_1 & D_{11} & D_{12} \\ C_2 & D_{21} & D_{22} \end{array}\right]$$

We will require there be more costs than control signals, $p_1 \geq q_2$, and more exogenous inputs than measurements, $q_1 \geq p_2$. Thus, D_{12} is a tall matrix and D_{21} is a fat matrix. In addition, we will require D_{12} and D_{21} to be full column rank and full row rank respectively. The sub-system $\mathbf{P}_{22}$ which maps control signals to measurements must be a causal lifted transfer function matrix; therefore, D_{22} must be lower trianglular.

The other standard $\mathcal{H}_\infty$ assumptions apply (see for example [15, 26]) and are concerned with the existance of stabilizing controllers and finding these solutions by solving algebraic

Riccati equations. The details of these assumptions are not germane to this discussion and are omitted for simplicity. The interested reader is refered to appropriate citations.

The connection of the generalized plant with the controller via $u = \mathbf{K}y$ results in the closed-loop system which is described by the following linear fractional transformation (LFT)

$$\mathcal{F}_l(\mathbf{P}, \mathbf{K}) = \mathbf{P}_{11} + \mathbf{P}_{12}\mathbf{K}(I - \mathbf{P}_{22}\mathbf{K})^{-1}\mathbf{P}_{21}$$

Solutions to the $\mathcal{H}_\infty$ problem are in fact sub-optimal solutions and the objective is to find a controller, if one exists, which stabilizes the closed-loop system and meets the following norm bound for a given value of γ.

$$\|\mathcal{F}_l(\mathbf{P}, \mathbf{K})\|_\infty < \gamma$$

Without loss of generality, we can assume $\gamma = 1$ which can be achieved by scaling the generalized plant.

$$\left[\begin{array}{c|cc} A & \gamma^{\frac{1}{2}}B_1 & B_2 \\ \hline \gamma^{-\frac{1}{2}}C_1 & \gamma^{-1}D_{11} & \gamma^{-\frac{1}{2}}D_{12} \\ C_2 & \gamma^{-\frac{1}{2}}D_{21} & D_{22} \end{array}\right] \longrightarrow \left[\begin{array}{c|cc} A & B_1 & B_2 \\ \hline C_1 & D_{11} & D_{12} \\ C_2 & D_{21} & D_{22} \end{array}\right]$$

Optimal solutions are found by iterating on the norm bound γ in a process known as γ-iteration.

$\mathcal{H}_\infty$ solutions give all stabilizing controllers parameterized by

$$\mathbf{K} = \mathcal{F}_l(\mathbf{J}, \mathbf{Q})$$

which achieve the closed-loop norm bound

$$\|\mathcal{F}_l(\mathbf{P}, \mathbf{K})\|_\infty < 1$$

and the free parameter, $\mathbf{Q}$, is any stable system with $\|\mathbf{Q}\|_\infty < 1$. If $\mathbf{Q}$ is unstable or has ∞-norm greater than unity then the closed-loop system $\mathcal{F}_l(\mathbf{P}, \mathbf{K})$ will be either unstable, not meet the norm constraint, or both.

The fixed-parameter $\mathbf{J}$ is not unique, however the majority of the $\mathcal{H}_\infty$ solutions in the literature are related to the so-called central controller; this central controller has a state-estimator structure. Finding the central controller involves finding positive semi-definite

solutions to algebraic Riccati equations with addtional norm bounded coupling conditions. The Riccati solutions generate a state feedback matrix, an output injection matrix, and state estimate of the worst case disturbance.

In the remaining sections of this chapter we will discuss approaches to finding controllers which satisfy the causality constraint of a lifted system, i.e. make the feedthrough matrix of the controller, $\mathbf{K}$, is lower triangular. It is assumed the reader is familiar with developments for calculating $\mathcal{H}_\infty$ controllers for general LTI systems. For the sake of brevity much of these developments are omitted here. We will focus primarily on causality.

5.2 Satifying Causality by Loop-shifting

A considerable simplification of the generalized plant can be achieved by loop-shifting which nulls and scales the feedthrough matrix of the generalized plant. The loop-shifted plant, $\widehat{\mathbf{P}}$ is then used to compute the controller $\widehat{\mathbf{K}}$. The loop shifting process is then reversed to obtain a controller $\mathbf{K}$ which meets the objective for the original plant $\mathbf{P}$.

In general, the controller achieved by this process has a fully populated feedthrough matrix and, therefore, does not represent a causal periodic system. If certain modified problems are solved at various steps in the loop-shifting process then we can ensure the resulting controller is causal.

In the remainder of this section we will discuss the details of the loop-shifting and reverse loop-shifting processes and point out the necessary modified problems which must be solved. The formulation presented here follows closely the loop-shifting procedure presented in Green and Limebeer [26]. Appropriate changes have been made for our problem, and some issues have been highlighted which may have been unclear.

Step 1

The purpose of this step is to minimize $\|\bar{D}_{11}\|$. Here we are using the matrix induced 2-norm which is equivalent to its maximum singular value [16] and is consistent with our system definition of the ∞-norm. We need $\bar{D}_{11}$ small for technical reasons introduced in Step 2.

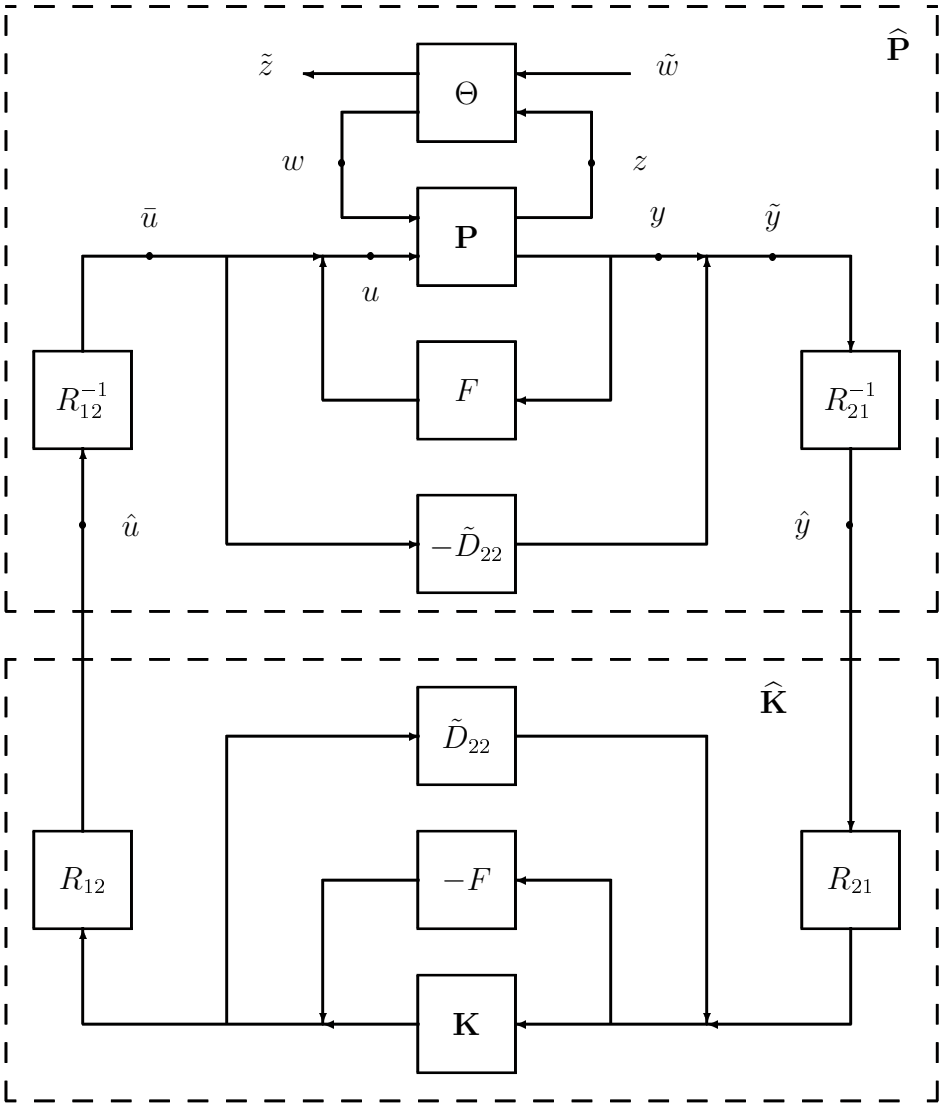

Figure 5.2: A block diagram of the loop-shifing procedure.

Given a generalized plant

$$\begin{bmatrix} z \\ y \end{bmatrix} = \begin{bmatrix} \mathbf{P}_{11} & \mathbf{P}_{12} \\ \mathbf{P}_{21} & \mathbf{P}_{22} \end{bmatrix} \begin{bmatrix} w \\ u \end{bmatrix}$$

and the following loop-shift

$$u = Fy + \bar{u}$$

the modified plant $\overline{\mathbf{P}}$ maps $\begin{bmatrix} w' & \bar{u}' \end{bmatrix}'$ to $\begin{bmatrix} z' & y' \end{bmatrix}'$ and has the following representation.

$$\overline{\mathbf{P}} \sim \left[\begin{array}{c|cc} \bar{A} & \bar{B}_1 & \bar{B}_2 \\ \hline \bar{C}_1 & \bar{D}_{11} & \bar{D}_{12} \\ \bar{C}_2 & \bar{D}_{21} & \bar{D}_{22} \end{array}\right]$$

$$= \left[\begin{array}{c|cc} A + B_2F(I - D_{22}F)^{-1}C_2 & B_1 + B_2F(I - D_{22}F)^{-1}D_{21} & B_2(I - FD_{22})^{-1} \\ \hline C_1 + D_{12}F(I - D_{22}F)^{-1}C_2 & D_{11} + D_{12}F(I - D_{22}F)^{-1}D_{21} & D_{12}(I - FD_{22})^{-1} \\ (I - D_{22}F)^{-1}C_2 & (I - D_{22}F)^{-1}D_{21} & (I - D_{22}F)^{1}D_{22} \end{array}\right]$$

We observe that

$$\bar{D}_{11} = \mathcal{F}_l(D, F) = D_{11} + D_{12}F(I - D_{22}F)^{-1}D_{21}$$

and we should select an F that minimizes $\|\mathcal{F}_l(D, F)\|$; such a result must make $\|\mathcal{F}(D, F)\| < 1$. If there is no such F then there is no solution to the $\mathcal{H}_\infty$ problem since we cannot guarantee norm bounds on Θ used in Step 2 and hence stability of the closed loop system. In addition, to maintain causality F must be lower triangular. To calculate such an F first we observe that

$$Q = F(I - D_{22}F)^{-1}$$

is lower triangular since both D_{22} and F are. Thus,

$$\|\mathcal{F}_l(D, F)\| = \|D_{11} + D_{12}QD_{21}\|$$

and we can consider the problem of picking a lower triangular Q instead. Once Q is found we can solve for F.

$$F = (I + QD_{22})^{-1}Q$$

Since D_{12} is full column rank (tall) and D_{21} is full row rank (fat), we can decompose each to

$$D_{12} = Q_{12}\begin{bmatrix} R_{12} \\ 0 \end{bmatrix} \qquad D_{21} = \begin{bmatrix} R_{21} & 0 \end{bmatrix} Q_{21}$$

where Q_{ij} are unitary matrices and R_{ij} are non-singular, lower triangular matrices. These decompositions are similar to a QR decompostion.

Considering the norm of the LFT, we can pre-multipy by Q'_{12} and post-multiply by Q'_{21} and not affect the norm since multiplication by unitary matrices does not change the norm. Thus, we get

$$\begin{aligned}\|D_{11} + D_{12}QD_{21}\| &= \|Q'_{12}(D_{11} + D_{12}QD_{21})Q'_{21}\| \\ &= \|Q'_{12}(D_{11} + D_{12}R_{12}^{-1}\hat{Q}R_{21}^{-1}D_{21})Q'_{21}\| \\ &= \left\| \hat{D}_{11} + \begin{bmatrix} \hat{Q} & 0 \\ 0 & 0 \end{bmatrix} \right\|\end{aligned}$$

where

$$\hat{D}_{11} = Q'_{12}D_{11}Q'_{21} \quad \text{and} \quad \hat{Q} = R_{12}QR_{21}$$

and again we have reduced the problem to finding a matrix $\hat{Q}$, which is still lower triangular, that minimizes the norm. Further, we partition $\hat{D}_{11}$ as

$$\hat{D}_{11} = \begin{bmatrix} \hat{D}_{1111} & \hat{D}_{1112} \\ \hat{D}_{1121} & \hat{D}_{1122} \end{bmatrix}$$

where $\hat{D}_{1111}$ is a $q_2 \times p_2$ matrix and is the same size as $\hat{Q}$. The problem is now

$$\min_{\hat{Q} \in \underline{\triangle}} \left\| \begin{bmatrix} \hat{D}_{1111} + \hat{Q} & \hat{D}_{1112} \\ \hat{D}_{1121} & \hat{D}_{1122} \end{bmatrix} \right\|$$

where $\underline{\triangle}$ is the set of lower trianglular matrices of appropriate size. Again, once $\hat{Q}$ is found we can calculate Q and F.

This problem should be contrasted with the general case, F is any $q_2 \times p_2$ matrix, which is discussed in Appendix A. Exact solutions to our problem have not been found and are an area of continuing research; however, we do point out a numerical approach [2].

The results of Overton [40] discuss minimizing the maximum eigenvalue of a symetric matrix. Our matrix

$$G(\hat{Q}) = \begin{bmatrix} \hat{D}_{1111} + \hat{Q} & \hat{D}_{1112} \\ \hat{D}_{1121} & \hat{D}_{1122} \end{bmatrix}$$

is a non-symetric, affine function of $\hat{Q}$. The problem of minimizing the maximum singular value of $G(\hat{Q})$ can be written in a form suitable to Overtons algorithm since the positive eigenvalues of

$$A(\hat{Q}) = \begin{bmatrix} 0 & G(\hat{Q}) \\ G(\hat{Q})' & 0 \end{bmatrix}$$

are the singular values of $G(\hat{Q})$. The difficulties in minimizing $\overline{\sigma}(G(\hat{Q}))$ or $\lambda_{\max}(A(\hat{Q}))$ is that the functions are not be differentiable at points where singular values or eigenvalues coalesce [40]. Loosely speaking, the algorithm offered by Overton involves iterations on quadratic programming problems with additional steps to account for possible multiple eigenvalues.

Step 2

In this step we force the $(1,1)$ term of the feedthrough matrix to be zero. Define

$$\Theta = \begin{bmatrix} -\bar{D}_{11} & (I - \bar{D}_{11}\bar{D}_{11}')^{\frac{1}{2}} \\ (I - \bar{D}_{11}'\bar{D}_{11})^{\frac{1}{2}} & \bar{D}_{11}' \end{bmatrix}$$

which is a unitary matrix, $\Theta\Theta' = I$. The matrix Θ is a map from $\begin{bmatrix} \tilde{w}' & z' \end{bmatrix}'$ to $\begin{bmatrix} \tilde{z}' & w' \end{bmatrix}'$. The composition[1] of Θ to $\overline{\mathbf{P}}$ yields the modified plant $\widetilde{\mathbf{P}}$.

$$\begin{aligned} \widetilde{\mathbf{P}} &\sim \left[\begin{array}{c|cc} \tilde{A} & \tilde{B}_1 & \tilde{B}_2 \\ \hline \tilde{C}_1 & 0 & \tilde{D}_{12} \\ \tilde{C}_2 & \tilde{D}_{21} & \tilde{D}_{22} \end{array}\right] \\ &= \left[\begin{array}{c|cc} \bar{A} + \bar{B}_1\Theta_{22}(I - \bar{D}_{11}\Theta_{22})^{-1}\bar{C}_1 & \bar{B}_1(I - \Theta_{22}\bar{D}_{11})^{-1}\Theta_{21} & \bar{B}_2 + \bar{B}_1\Theta_{22}(I - \bar{D}_{11}\Theta_{22})^{-1}\bar{D}_{12} \\ \hline \Theta_{12}(I - \bar{D}_{11}\Theta_{22})^{-1}\bar{C}_1 & 0 & \Theta_{12}(I - \bar{D}_{11}\Theta_{22})^{-1}\bar{D}_{12} \\ \bar{C}_2 + \bar{D}_{21}\Theta_{22}(I - \bar{D}_{11}\Theta_{22})^{-1}\bar{C}_1 & \bar{D}_{21}(I - \Theta_{22}\bar{D}_{11})^{-1}\Theta_{21} & \bar{D}_{22} + \bar{D}_{21}\Theta_{22}(I - \bar{D}_{11}\Theta_{22})^{-1}\bar{D}_{12} \end{array}\right] \end{aligned}$$

Because Θ is unitary we have

$$\|\tilde{z}\|^2 - \|\tilde{w}\|^2 = \|z\|^2 - \|w\|^2$$

If $\|\mathcal{F}_l(\widetilde{\mathbf{P}}, \mathbf{K})\|_\infty < 1$ then left hand side of this expression is negative; thus, the right hand side is also negative and we have $\|\mathcal{F}_l(\mathbf{P}, \mathbf{K})\|_\infty < 1$. Also, since Θ is a constant matrix with $\|\Theta_{22}\| = \|\bar{D}_{11}\| < 1$ then $\mathcal{F}_l(\mathbf{P}, \mathbf{K})$ is stable if and only if $\mathcal{F}_l(\widetilde{\mathbf{P}}, \mathbf{K})$ is; this can be shown using the small gain theorem.

[1] The composition operator is defined by the Redheffer star product

$$\mathcal{C}_l(\mathbf{P}, \mathbf{K}) = \mathbf{P} \star \mathbf{K} = \begin{bmatrix} \mathcal{F}_l(\mathbf{P}, \mathbf{K}_{11}) & \mathbf{P}_{12}(I - \mathbf{K}_{11}\mathbf{P}_{22})^{-1}\mathbf{K}_{12} \\ \mathbf{K}_{21}(I - \mathbf{P}_{22}\mathbf{K}_{11})^{-1}\mathbf{P}_{21} & \mathcal{F}_u(\mathbf{K}, \mathbf{P}_{22}) \end{bmatrix}$$

Step 3

We make the $(2,2)$ term zero by connecting $-\tilde{D}_{22}$ in parallel with $\widetilde{\mathbf{P}}$ as illustrated in Fig. 5.2.

$$\tilde{y} = y - \tilde{D}_{22}\bar{u}$$

The system $\widetilde{\mathbf{P}}$ maps $\begin{bmatrix}\tilde{w}' & \bar{u}'\end{bmatrix}'$ to $\begin{bmatrix}\tilde{z}' & \tilde{y}'\end{bmatrix}'$ and has zero $(1,1)$ and $(2,2)$ entries in the feedthrough matrix $\tilde{D}$.

Step 4

In this step we scale the $(1,2)$ and $(2,1)$ entries to satisfy $\hat{D}'_{12}\hat{D}_{12} = I_{q_2}$ and $\hat{D}_{21}\hat{D}'_{21} = I_{p_2}$.

Decompose $\tilde{D}_{12}$ and $\tilde{D}_{21}$ as

$$\tilde{D}_{12} = \tilde{Q}_{12}\begin{bmatrix}\tilde{R}_{12}\\ 0\end{bmatrix} \qquad \tilde{D}_{21} = \begin{bmatrix}\tilde{R}_{21} & 0\end{bmatrix}\tilde{Q}_{21}$$

where $\tilde{Q}_{ij}$ are unitary matrices and $\tilde{R}_{ij}$ are non-singular, lower triangular matrices. These decompositions are similar to a QR decompostion.

Now we make a causal change of basis to the measurement and control signals.

$$\bar{u} = \tilde{R}_{12}^{-1}\hat{u} \quad \text{and} \quad \hat{y} = \tilde{R}_{21}^{-1}\tilde{y}$$

The (finally!) modified generalized plant is

$$\widehat{\mathbf{P}} \sim \left[\begin{array}{c|cc}\hat{A} & \hat{B}_1 & \hat{B}_2\\ \hline \hat{C}_1 & 0 & \hat{D}_{12}\\ \hat{C}_2 & \hat{D}_{21} & 0\end{array}\right] = \left[\begin{array}{c|cc}\tilde{A} & \tilde{B}_1 & \tilde{B}_2\tilde{R}_{12}^{-1}\\ \hline \tilde{C}_1 & 0 & \tilde{D}_{12}\tilde{R}_{12}^{-1}\\ \tilde{R}_{21}^{-1}\tilde{C}_2 & \tilde{R}_{21}^{-1}\tilde{D}_{21} & 0\end{array}\right]$$

Build the Controller

In this step we compute the controller. This process involves finding positive semidefinite solutions to two algebraic Riccati equations which must also satisfy a coupling condition. In any event a controller can be found which meets the objectives and has a zero feedthrough matrix.

$$\widehat{\mathbf{K}} \sim \left[\begin{array}{c|c}\hat{A}_K & \hat{B}_K\\ \hline \hat{C}_K & 0\end{array}\right]$$

This controller maps measurements $\hat{y}$ to control signals $\hat{u}$.

Reverse Step 4

Here we undo Step 4 by applying the change of basis used there. The modified controller is

$$\widetilde{\mathbf{K}} \sim \left[\begin{array}{c|c} \tilde{A}_K & \tilde{B}_K \\ \hline \tilde{C}_K & 0 \end{array}\right] = \left[\begin{array}{c|c} \hat{A}_K & \hat{B}_K R_{21}^{-1} \\ \hline R_{12}^{-1}\hat{C}_K & 0 \end{array}\right]$$

This controller passes measurements $\tilde{y}$ to controls $\bar{u}$.

Reverse Step 3

Here we undo Step 3. The matrix $\tilde{D}_{22}$ is fedback from $\bar{u}$ to $\tilde{y}$ with the result that

$$\overline{\mathbf{K}} \sim \left[\begin{array}{c|c} \bar{A}_K & \bar{B}_K \\ \hline \bar{C}_K & 0 \end{array}\right] = \left[\begin{array}{c|c} \tilde{A}_K - \tilde{B}_K\tilde{D}_{22}\tilde{C}_K & \tilde{B}_K \\ \hline \tilde{C}_K & 0 \end{array}\right]$$

Reverse Step 1

Finally we reverse Step 1 by applying $u = Fy + \bar{u}$ used there. The final controller is

$$\mathbf{K} \sim \left[\begin{array}{c|c} A_K & B_K \\ \hline C_K & D_K \end{array}\right] = \left[\begin{array}{c|c} \bar{A}_K & \bar{B}_K \\ \hline \bar{C}_K & F \end{array}\right]$$

and since our selection of for F was lower triangular we see that the final controller is causal.

5.3 Satisfying Causality by Q-parameterization

In this section, we assume we have a parameterized $\mathcal{H}_\infty$ controller

$$\mathbf{K} = \mathcal{F}_l(\mathbf{J}, \mathbf{Q})$$

and $\mathbf{Q}$ is stable with $\|\mathbf{Q}\|_\infty < 1$. The fixed parameter $\mathbf{J}$ can be represented as

$$\mathbf{J} \sim \left[\begin{array}{c|cc} A & B_1 & B_2 \\ \hline C_1 & D_{11} & D_{12} \\ C_2 & D_{21} & D_{22} \end{array}\right]$$

Here we do not assume **J** represents a causal periodic system, i.e. none of the D_{ij}'s are necessarily lower triangular; however, we will assume D_{12} and D_{21} are square and invertible. This is a safe assumption. The structure of **J** requires they be square, and invertibility is equivalent to full column or row rank which is standard.

Typical 'central' solutions make $\mathbf{Q} = 0$ which results in

$$\mathbf{K} = \mathcal{F}_l(\mathbf{J}, 0) = \mathbf{J}_{11} \sim \left[\begin{array}{c|c} A & B_1 \\ \hline C_1 & D_{11} \end{array}\right]$$

which does not necessarily represent a causal periodic system.

Assume the free parameter is a constant matrix, $\mathbf{Q} = Q$, then the controller is represented by

$$\begin{aligned}\mathbf{K} = \mathcal{F}_l(\mathbf{J}, Q) &\sim \left[\begin{array}{c|c} A_K & B_K \\ \hline C_K & D_K \end{array}\right] \\ &= \left[\begin{array}{c|c} A + B_2Q(I - D_{22}Q)^{-1}C_2 & B_1 + B_2Q(I - D_{22}Q)^{-1}D_{21} \\ \hline C1 + D_{12}Q(I - D_{22}Q)^{-1}C_2 & D_{11} + D_{12}Q(I - D_{22}Q)^{-1}D_{21} \end{array}\right]\end{aligned}$$

We notice that

$$\mathcal{F}_l(D, Q) = D_{11} + D_{12}Q(I - D_{22}Q)^{-1}D_{21}$$

and we can make **K** causal by choosing Q such that $\mathcal{F}_l(D, Q)$ is lower triangular and $\|Q\| < 1$. Exact solutions to this problem have not been found and are an area of continuing research; however, we do provide the following analysis which is useful for making intelligent choices.

Let F be a lower triangular matrix and $F = \mathcal{F}_l(D, Q)$. Using the assumptions on D_{12} and D_{21} we can show

$$Q = \mathcal{F}_l(\hat{D}, F - D_{11}) = \mathcal{F}_l(\bar{D}, F)$$

where $\bar{D}$ is defined by the Redheffer star product (see Fig. 5.3).

$$\bar{D} = \hat{D} \star \tilde{D} = \begin{bmatrix} \mathcal{F}_l(\hat{D}, \tilde{D}_{11}) & \hat{D}_{12}(I - \tilde{D}_{11}\hat{D}_{22})^{-1}\tilde{D}_{12} \\ \tilde{D}_{21}(I - \hat{D}_{22}\tilde{D}_{11})^{-1}\hat{D}_{21} & \mathcal{F}_u(\tilde{D}, \hat{D}_{22}) \end{bmatrix}$$

and

$$\hat{D} = \begin{bmatrix} 0 & D_{12}^{-1} \\ D_{21}^{-1} & -D_{21}^{-1}D_{22}D_{12}^{-1} \end{bmatrix} \qquad \tilde{D} = \begin{bmatrix} -D_{11} & I \\ I & 0 \end{bmatrix}$$

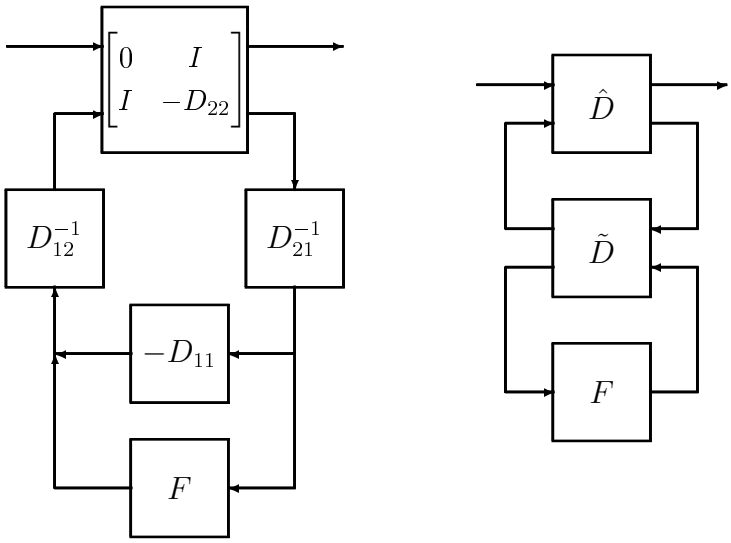

Figure 5.3: An LFT of Q in terms of D and F.

Our objective is to find a lower triangular F that makes $\|Q\| = \|\mathcal{F}_l(\bar{D}, F)\| < 1$. It would appear that we could use the machinery introduced in Step 2 of the last section to find such an F; however, $\bar{D}_{22}$ may not be lower triangular. Solutions to this problem are an area of continuing research.

We do notice that

$$Q = D_{12}^{-1}U(I - \hat{D}_{22}U)^{-1}D_{21}^{-1}$$

where $U = F - D_{11}$ and the bounded norm criteria gives us

$$\begin{aligned} & \|Q\| = \|D_{12}^{-1}U(I - \hat{D}_{22}U)^{-1}D_{21}^{-1}\| < 1 \\ \Leftrightarrow \qquad & \|D_{12}^{-1}U(I - \hat{D}_{22}U)^{-1}D_{21}^{-1}x\| < \|x\| \qquad \forall \quad x \end{aligned}$$

a change of basis gives

$$\Leftrightarrow \qquad \|D_{12}^{-1}Uy\| < \|D_{21}(I - \hat{D}_{22}U)y\| \qquad \forall \quad y$$

Choosing an F which minimizes $\|U\| = \|F - D_{11}\|$ would be an intelligent choice for an F which may satisfy the above expression and hence make $\|Q\| < 1$, especially if $\underline{\sigma}(D_{12})$ and $\underline{\sigma}(D_{21})$ are large. This problem can be solved using the machinery in Step 2 of the last

section, but this might be an aggressive approach for an approximate solution to our original problem. Another choice, which minimizes the Frobenius norm, is

$$F = \text{lower-triangular}(D_{11})$$

and bounds the matrix 2-norm.

$$\|F - D_{11}\| \leq \|F - D_{11}\|_F = \sqrt{\sum_{i=1}^{q_2} \sum_{j=i+1}^{p_2} |\{D_{11}\}_{ij}|^2}$$

This choice for F is simple to find and check if $\|Q\| < 1$.

Chapter 6

Case Study

The helicopter community has spent enormous effort on the control of helicopter vibrations, which arise from the forward motion of the aircraft, even through calm air. The most significant vibration suppression technique developed for this problem is higher harmonic control (HHC) where periodic vibrations are decomposed into in-phase and quadrature components, multiplied by an appropriate plant model (at the operating frequency), and reintroduced to the helicopter rotor. Such an approach has resulted in nearly 5–6 dB suppression, considered excellent results in the helicopter community [14, 28, 49, 48]. Two facts should be realized about higher-harmonic control:

1. HHC can be shown to be equivalent to time-invariant, high gain, narrowband feedback [50].

2. HHC assumes the plant is pseudo time-invariant at the operating frequency and can be described by a single complex gain.

Helicopters are, in fact, during forward flight, systems with time-periodic coefficients acted upon by a periodic disturbance, where the period for both the rotor plant and disturbance is determined by the blade passing frequency. Also, we have already shown that classical narrowband feedback does not necessarily achieve good disturbance for m-periodic discrete-time systems with similar deficiencies for sampled-data control.

This chapter presents a case study of the harmonic and narrowband disturbance rejection techniques developed in this research applied to the helicopter vibration problem. A

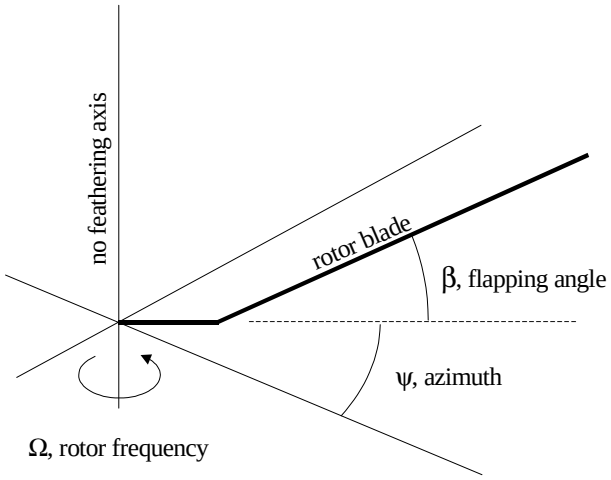

Figure 6.1: Rotor blade schematic showing flapping angle and azimuth.

simplified helicopter rotor blade, modelling flapping motion only, is used in the development of the discrete-time controllers.

6.1 Model

A simplified helicopter rotor blade can be described by the following equation of motion [6] (see Appendix B):

$$\beta'' + \frac{\gamma}{8}\beta' + \left\{1 + \epsilon + \frac{\gamma}{8}\left(\frac{4\sqrt{2}}{3}\mu\sin(\varphi + \frac{\pi}{4}) + \mu^2\sin 2\varphi\right)\right\}\beta = \frac{\gamma}{8}\left(1 + \mu^2 + \frac{8}{3}\mu\sin\varphi + 2\mu^2\cos 2\varphi\right)\theta + \frac{\gamma}{8}\left(\frac{4}{3}\hat{\lambda} + 2\mu\hat{\lambda}\sin\varphi\right)$$

where we have normalized time by the blade passing frequency so that $'$ denotes $d/d\varphi$, β is the blade flapping angle, and θ is the blade cyclic pitch and is used to control the rotor.

The parameters ϵ, γ, μ, and $\hat{\lambda}$ are the offset ratio, Lock inertia number, advance ratio, and inflow ratio respectively and depend upon atmospheric properties, helicopter geometry, aerodynamics, and flight conditions. In this study, these parameter have the following values: $\gamma = 6$, $\epsilon = 0.06$, $\mu = 0.3$, $\hat{\lambda} = 0.2$; these numbers are typical.

This system is obviously periodic. All periodic terms result from the rotor lift which oscillates as the blade advances and retreats, and is a function not only of azimuth, but also, flapping position and velocity. It is interesting to note that when the helicopter is hovering, $\mu = 0$, all periodic terms vanish, and the system natural frequency becomes $\sqrt{1+\epsilon}$.

The second term on the right is the continuous-time disturbance signal and is proportional to the inflow ratio. At steady state, the response of the rotor to the disturbance is periodic with period 2π, and the Fourier expansion of the rotor flapping angle includes a DC component and harmonics at multiples of the blade-passing frequency.

$$\beta(\varphi) = a_0 + \sum_{n=1}^{\infty} a_n \sin(n\varphi + \phi_n)$$

The characteristics of this response are consistent with our observations of discrete-time m-periodic system which exhibit at most m tones in their response.

The rotor equation-of-motion can be written in state-space form as

$$\begin{bmatrix} \beta' \\ \beta'' \end{bmatrix} = \overbrace{\begin{bmatrix} 0 & 1 \\ -\left\{1 + \epsilon + \frac{\gamma}{8}\left(\frac{4\sqrt{2}}{3}\mu\sin(\varphi + \frac{\pi}{4}) + \mu^2 \sin 2\varphi\right)\right\} & -\frac{\gamma}{8} \end{bmatrix}}^{A(\varphi)} \begin{bmatrix} \beta \\ \beta' \end{bmatrix} + \underbrace{\begin{bmatrix} 0 \\ \frac{\gamma}{8}\left(\frac{4}{3}\hat{\lambda} + 2\mu\hat{\lambda}\sin\varphi\right) \end{bmatrix}}_{B_1(\varphi)} \mathbf{1}(\varphi) + \underbrace{\begin{bmatrix} 0 \\ \frac{\gamma}{8}\left(1 + \mu^2 + \frac{8}{3}\mu\sin\varphi + 2\mu^2\cos 2\varphi\right) \end{bmatrix}}_{B_2(\varphi)} \theta(\varphi)$$

The control signal is the blade incidence with respect to the no-feathering plane, $\theta(\varphi)$, and the disturbance is now represented as a unit-step function, $\mathbf{1}(\varphi)$.

Including the continuous-time disturbance as part of the plant matrices, and posing the disturbance as a unit-step may seem misleading. However, the response of the system to the unit-step disturbance remains exact, even in a sampled-data context where the continuous-time unit-step is constructed using a zero-order hold on a discrete-time unit-step.

$$\mathbf{1}(\varphi) = \text{zoh}\{\mathbf{1}[k]\}$$

Accordingly, the disturbance frequency is zero, and the lifted disturbance is represented as

$$\hat{d}[k] = \phi_0 \mathbf{1}[k]$$
$$\hat{d}(\hat{z}) = \phi_0 \frac{\hat{z}}{\hat{z} - 1}$$

where the disturbance direction is $\hat{\phi}_0 = \begin{bmatrix} 1 & \cdots & 1 \end{bmatrix}'$. For problems where a disturbance excites the plant at a frequency other than a multiple of plant period, or where it is not known, one must explicitly account for the disturbance, and other suitable techniques for approximating the disturbance's action on the sample-data system must be used.

The system output is the blade flapping angle, β, with the output matrices of

$$C(\varphi) = \begin{bmatrix} 1 & 0 \end{bmatrix} \qquad D_1(\varphi) = D_2(\varphi) = 0$$

and the following continuous-time periodic systems are the disturbance and control paths respectively.

$$\mathbf{G}_{c,1} = \left[\begin{array}{c|c} A(\varphi) & B_1(\varphi) \\ \hline C(\varphi) & D_1(\varphi) \end{array}\right] \qquad \mathbf{G}_{c,2} = \left[\begin{array}{c|c} A(\varphi) & B_2(\varphi) \\ \hline C(\varphi) & D_2(\varphi) \end{array}\right]$$

Figure 6.1 shows a block diagram of the resulting system and includes the zero-order hold and sampler of the sampled-data system.

A sampled-data representation of the continuous-time system is made using the approach discussed in Appendix C. There are m samples per cycle resulting in an m-periodic discrete-time system. The number of samples per cycle is chosen to be

$$m = 16$$

and provides a suitable compromise between signal reconstruction and the computational demands imposed by sampling too fast. Both the disturbance and control signals are assumed to be zero-order held signals. The discrete-time system is then lifted to make a time-invariant system used in controller design.

Open-loop performance The system's steady-state, open-loop response is shown in Fig. 6.3, and can be calculated from the lifted system.

$$\hat{\beta}_{\text{ss}} = \hat{\mathbf{G}}_1(1)\hat{\phi}_0$$

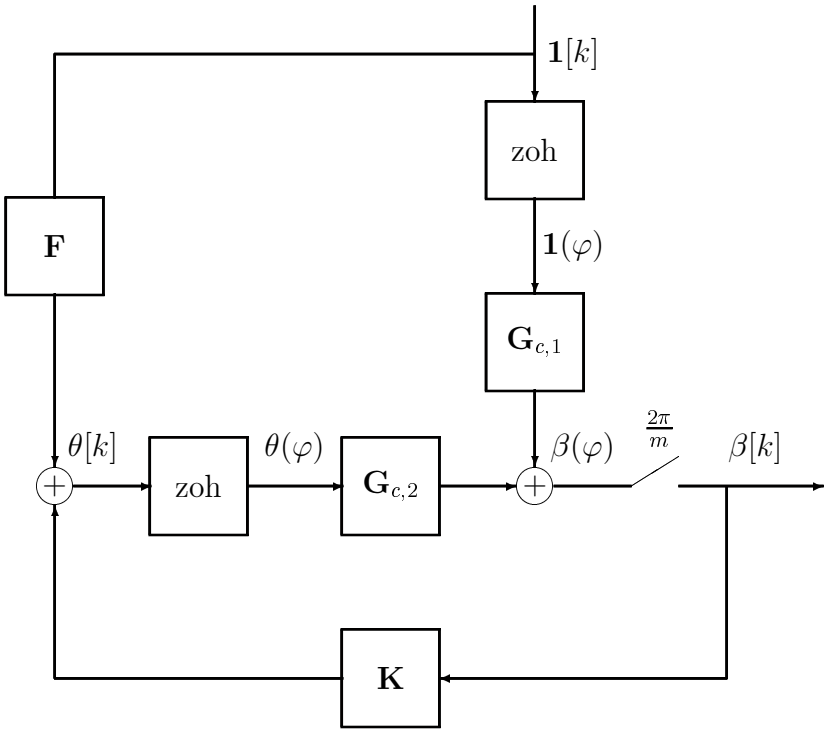

Figure 6.2: A block diagram of the sampled-data rotor system.

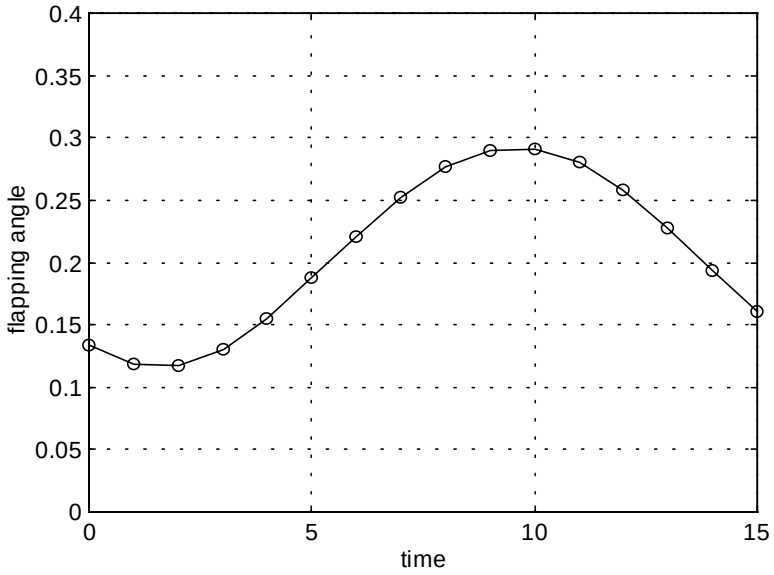

Figure 6.3: Rotor flapping angle open-loop response.

The RMS energy in the output signal is defined by the norm of the lifted system output over one cycle.

$$\beta_{\text{rms}} = \sqrt{\frac{1}{m}\sum_{k=0}^{m-1}(\beta[k])^2} = \frac{\|\hat{\beta}_{\text{ss}}\|}{\sqrt{m}} = 0.2151$$

The magnitude of the first four Fourier coefficients of the discrete-time response are

$$a_0 = 0.2058 \qquad a_1 = 0.0441$$
$$a_2 = 0.9311 \times 10^{-3} \qquad a_3 = 0.2039 \times 10^{-4}$$

We should notice that the DC component, a_0, dominates the response of the system.

Open-loop stability The lifted system has eigenvalues (Floquet multipliers) at

$$\lambda(\hat{A}) = \left\{0.0943e^{\pm j0.3720}\right\}$$

A time constant for the rotor system is determined by

$$\tau = \frac{-1}{\ln|\lambda|} = 0.4235 \text{ cycles}$$

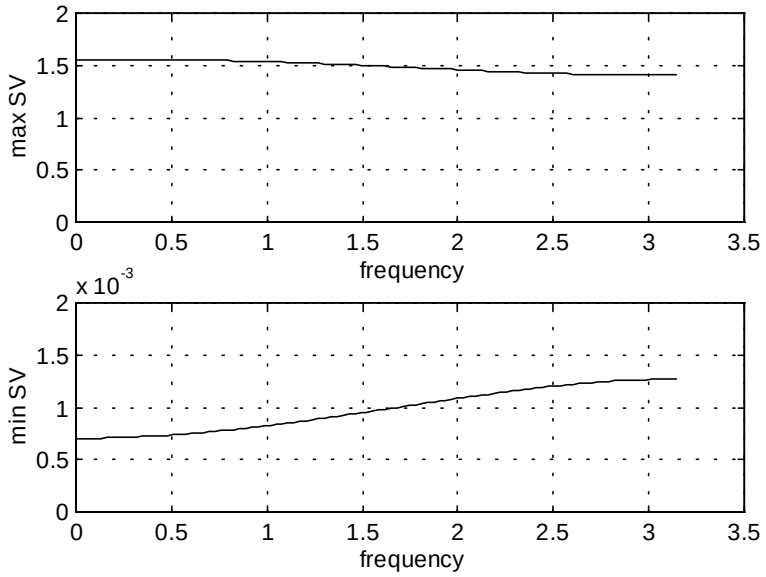

Figure 6.4: Maximum and minimum singular values of $\hat{\mathbf{G}}_2$, the control path.

and the natural frequency is

$$\omega_n = 1.059$$

which is approximately the hovering (time-invariant) natural frequency of $\sqrt{1+\epsilon} = 1.030$.

Open-loop gain and SVs Singular value plots of the control path are shown in Fig. 6.4 with ∞-norm

$$\|\hat{\mathbf{G}}_2\|_\infty = 1.558 \quad \text{at} \quad \omega = 0$$

6.2 About the controllers

The disturbance, control and measurement are each scalar signals; hence, the controller, whether feedback or feedforward, is a sixteen-periodic SISO filter, and its lift is a sixteen-input, sixteen-output LTI filter. Because the lift is a complete representation of a periodic filter, it will not be necessary to construct periodic representations of any of the filters in this case study. Given the lifted representation of a controller, a corresponding periodic state-space model is not unique since we know nothing about the intra-cycle state structure from the lifted representation. This makes the process of lowering systems extremely difficult.

However for filtering, knowing only the lifted representation is sufficient. Each filter can be implemented using its lifted representation using the real-time implementation algorithm discussed here and in Section 2.3.

The periodic feedback and feedforward controllers, designed using $\mathcal{H}_\infty$ methods, are filters which can be represented in state-space form by

$$\begin{aligned}\hat{x}[k+1] &= \hat{A}\hat{x}[k] + \hat{B}\hat{u}[k] \\ \hat{y}[k] &= \hat{C}\hat{x}[k] + \hat{D}\hat{u}[k]\end{aligned}$$

and the feedthrough matrix, $\hat{D}$, is lower-triangular. After all inputs, u, to the filter have been lifted, forming $\hat{u}$, the state is updated; this happens at the end of a cycle. The system output, which happens at each step within a cycle, can be determined by stepping down each row of the lifted output equation. Here we use the fiter state, $\hat{x}[k]$, calculated at the end of the last cycle, and the lifted input signal, $\hat{u}$, which contains l correct values of the input signal u up to time $km + 1$.

In this chapter, we build three feedback controllers and three feedforward compensators. The first two feedback controllers are variations on classical control (HHC) designs: Classical-I targets the apparent disturbance frequency $\omega_0 = 0$, eliminating the DC response of the rotor flapping angle; Classical-II goes after the harmonic response of system by targeting the disturbance frequency $\omega_0 = 2\pi/m$. The third feedback controller, a periodic controller designed to specified nominal performance and robust stability criteria, achieves near perfect (on the order of machine epsilon) disturbance rejection, while the classical controllers can only eliminate the target frequency from the system output. This is as expected from the analysis in Section 3.1. In addition, the periodic controller exhibits improved stabilty margins, compared with the classical designs.

For each of the classical designs, we show the closed-loop amplification of the Fourier coefficients in the rotor system response. Also, we point out that in some cases these components are amplified. This fact is not critical in this specific case, since those harmonics which are amplified are several orders of magnitude less than the dominant tones, but this fact is noted as a potential liability of using classical controllers for narrowband disturbance rejection.

Among the three feedforward controllers, the first is a periodic design which minimizes a specified nominal performance criteria. This controller is special in that it achieves perfect

disturbance rejection across the bandwidth. This is possible since it is able to invert the control path; in general, however, this does not represent practial expectations for performance. The second feedforward controller is a fixed-gain periodic FIR filter. This controller achieves near perfect disturbance rejection, and can be realized by a scalar periodic gain. The third feedforward controller uses an adaptation algorithm to make the periodic FIR filter adaptive. This controller achieves an acceptable level of performance within a reasonable time span, nearly 25 dB within 100 cycles.

6.3 Feedback controllers

6.3.1 Classical Designs

Classical LTI-SISO designs place a narrow bandpass filter in the feedback path.

$$\mathbf{K}(z) = -\bar{k}\,\frac{\cos(\omega_0 - \varphi)z - \cos\varphi}{z^2 - 2\cos\omega_0 z + 1}$$

The parameter ω_0 is the disturbance frequency, φ is the system phase at the disturbance frequency, and the gain $\bar{k}$ determines the controller bandwidth. Implementation of such controllers with time-periodic systems assumes the system is pseudo time-invariant and can be represented by a single complex gain.

As shown in Section 3.1, LTI narrow bandpass controllers do not necessarily achieve good disturbance rejection for LTP plants. They do reject harmonics at the frequency ω_0 in the sense that these frequencies do not appear in the output; however, classical controllers do not reject the other $m-1$ tones which appear in the response of an m-periodic system, and may in fact amplify them.

In this section, two classical controllers are designed for the rotor system, and the performance, stability, and robustness of each is discussed. The first controller is intended to target the disturbance $\hat{d}[k] = \mathbf{1}[k]$ with the disturbance frequency being $\omega_0 = 0$. The second controller is an attempt to control the higher harmonics in the response; the disturbance frequency is $\omega_0 = 2\pi/16$. Both controllers perform as expected by removing their appropriate component. However, neither achieves 'perfect' disturbance rejection.

Classical-I

Classical-I is intended to target the disturbance $\hat{d}[k] = \mathbf{1}[k]$. Thus, the disturbance frequency is $\omega_0 = 0$ and $\varphi = 0$. As expected, this controller targets the DC response in the blade flapping angle.

$$\mathbf{K}(z) = -\frac{0.01}{z-1} \tag{CL1}$$

The RMS response of the closed-loop system is

$$\beta_{\text{rms}} = 0.0486$$

which is a reduction of 12.9 dB. This is expected since the DC component is such a large part of the open-loop system response. However, this controller does not affect the other harmonics and in some cases amplifies them, see Fig. 6.7.

Figure 6.5 shows the singular values of the sensitivity and complimentary sensitivity. The bandwidth, determined from the half power points of $\underline{\sigma}(\hat{\mathbf{S}})$, is

$$\text{BW} = 0.1609$$

The closed-loop eigenvalues are $\lambda(\hat{A}) = \{0.8635, 0.1009e^{\pm j0.4291}\}$ and estimates of the gain margin and phase margin are shown in Table 6.1.

Classical-II

Classical-II attempts to control the harmonics in the system response; accordingly, the disturbance frequency is chosen to be $\omega_0 = 2\pi/16$. As expected, this controller eliminates the harmonic at the disturbance frequency but does not reject higher harmonics or the DC response.

$$\mathbf{K}(z) = -0.01\frac{-0.9239z + 1}{z^2 - 1.8478z + 1} \tag{CL2}$$

The RMS response of the closed-loop system is

$$\beta_{\text{rms}} = 0.1742$$

which is a reduction of 1.8 dB. This is expected since this controller targets the first harmonic leaving the DC component relatively untouched and the DC component is such a large part of

Table 6.1: Lower bound estimates on the gain and phase margins for Classical-I.

		Gain Margin (dB)	Phase Margin (deg)
Using		low , high	low , high
$\|\hat{\mathbf{S}}\|_\infty$	1.120	-5.55 , 19.4	-53.0 , 53.0
$\|\hat{\mathbf{T}}\|_\infty$	1.102	-20.7 , 5.61	-54.0 , 54.0

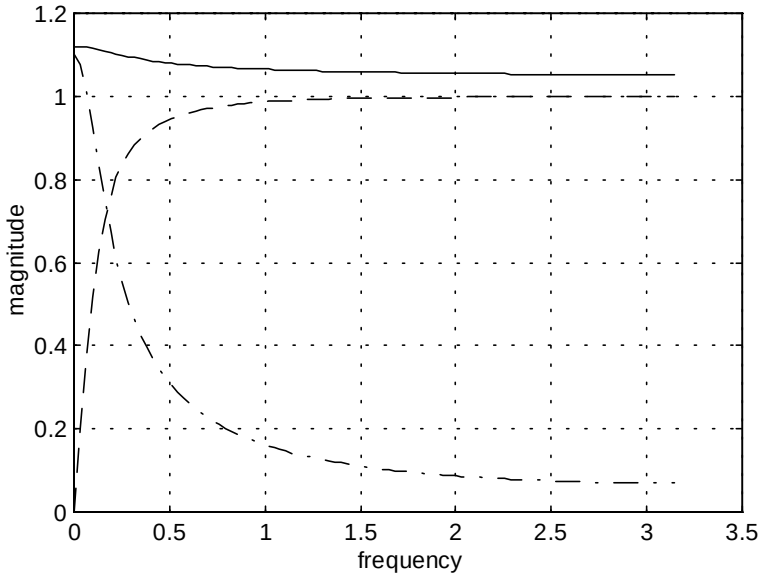

Figure 6.5: Singular value plots of the closed-loop sensitivities using Classical-I: $\overline{\sigma}(\hat{\mathbf{S}})$ (solid), $\underline{\sigma}(\hat{\mathbf{S}})$ (dashed), $\overline{\sigma}(\hat{\mathbf{T}})$ (dot-dash).

the open-loop system response. However, this controller does not affect the other harmonics and in some cases amplifies them, see Fig 6.7.

Figure 6.6 shows the singular value of the sensitivity function. The bandwidth is

$$\text{BW} = 0.2039$$

The closed-loop eigenvalues are $\lambda(\hat{A}) = \{0.9850e^{\pm j0.0820}, 0.0963e^{\pm j0.2606}\}$ and estimates of the gain margin and phase margin are shown in Table 6.2

The gain of the controllers was selected to give nearly the same bandwidth in the closed-

Table 6.2: Lower bound estimates on the gain and phase margins for Classical-II.

		Gain Margin (dB)	Phase Margin (deg)
Using		low , high	low , high
$\|\hat{\mathbf{S}}\|_\infty$	5.248	-1.51 , 1.83	-10.9 , 10.9
$\|\hat{\mathbf{T}}\|_\infty$	4.664	-2.09 , 1.68	-12.3 , 12.3

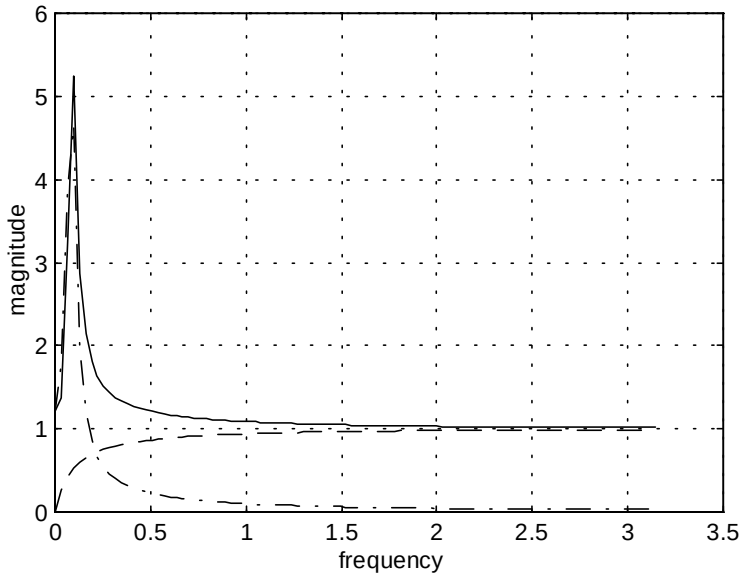

Figure 6.6: Singular value plots of the closed-loop sensitivities using Classical-II: $\overline{\sigma}(\hat{\mathbf{S}})$ (solid), $\underline{\sigma}(\hat{\mathbf{S}})$ (dashed), $\overline{\sigma}(\hat{\mathbf{T}})$ (dot-dash).

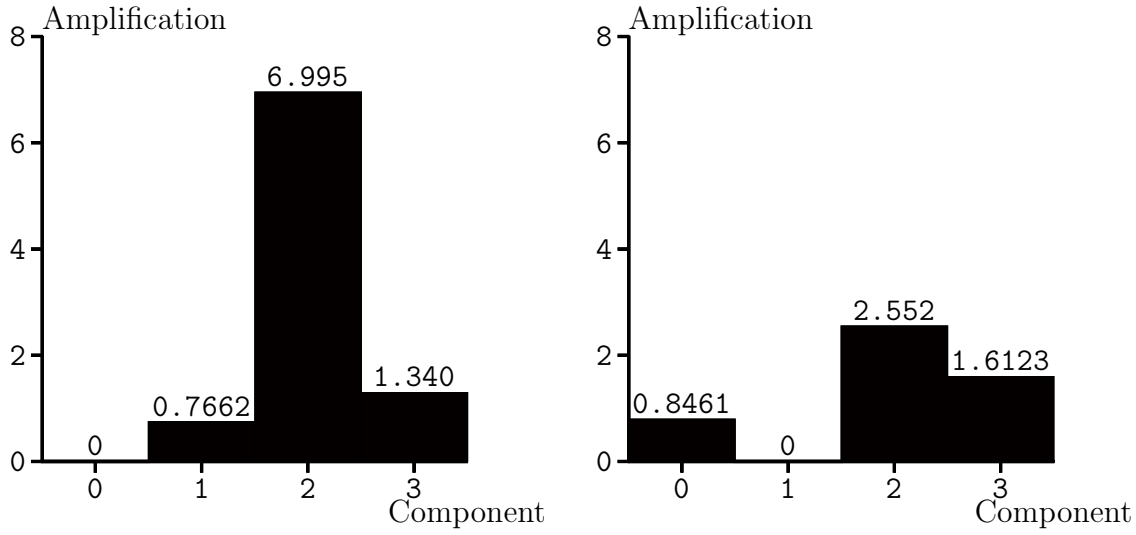

(a) Classical-I (b) Classical-II

Figure 6.7: Closed-loop amplification of Fourier coefficients in the rotor system response.

loop systems. It is interesting to note that the same gain $\bar{k} = 0.01$ achieves this objective. However, it is clear from looking at the singular value plots and margins of each system that Classical-II has the potential not only to amplify broadband disturbances, e.g., in the rotor problem this may be caused by turbulence or gusts, but is also not robust to changes in the plant. Lower gains would restore robustness to the system at the sacrifice of controller bandwidth and potentially lower performance.

6.3.2 Periodic Designs

Periodic designs are found using a modified mixed sensitivity problem from that outlined in Chapter 3.

$$\left\| \begin{bmatrix} \hat{\mathbf{S}}\hat{\mathbf{G}}_1\hat{\mathbf{W}}_d & \alpha\hat{\mathbf{T}} \\ \rho\mathbf{K}\hat{\mathbf{S}}\hat{\mathbf{G}}_1\hat{\mathbf{W}}_d & \rho\alpha\mathbf{K}\hat{\mathbf{S}} \end{bmatrix} \right\|_\infty < 1$$

resulting from the open-loop generalized plant is

$$\mathbf{P} = \left[\begin{array}{cc|c} \hat{\mathbf{G}}_1\hat{\mathbf{W}}_d & 0 & \hat{\mathbf{G}}_2 \\ 0 & 0 & \rho I \\ \hline \hat{\mathbf{G}}_1\hat{\mathbf{W}}_d & \beta I & \hat{\mathbf{G}}_2 \end{array}\right]$$

The modified generalized plant accounts for the disturbance path, $\hat{\mathbf{G}}_1$, and includes the control signal, weighted by ρ, in the system cost. This is necessary since the control path has zero feedthrough before lifting, $D_2 = 0$, and the resulting feedthrough term, $\hat{D}_2$, in the lifted system is rank deficient; hence $\mathbf{P}_{12}(\infty)$ would not be not full column rank. The addition of the control signal to the cost restores this condition. The control weight is made small, $\rho = 10^{-8}$, so that the addition of the control to the cost has little effect on our primary objective of nominal performance and robust stability.

The plant transfer function matrices $\hat{\mathbf{G}}_1$ and $\hat{\mathbf{G}}_2$ are as before and the input weight is

$$\mathbf{W}_d(\hat{z}) = \hat{\phi}_0 \left(k \frac{\hat{z}}{\hat{z} - 0.99999} \right)$$

where $\hat{\phi}_0$ is the disturbance direction discussed previously. The pole of the frequency weight, defined by the disturbance frequency $\omega_0 = 0$ therefore a $\hat{z} = 1$, is placed inside the unit-circle due to requirements for solvability of the Riccati equations in the $\mathcal{H}_\infty$ solution. An appropriate bandwidth is chosen by adjusting the gain; the final choice is $k = 0.003$. The complimentary sensitivity weight is $\alpha = 1$.

The generalized plant is realized in state-space form, and an optimal $\mathcal{H}_\infty$ solution is found by γ-iteration. This optimal value is

$$\gamma^* = 1.000$$

Causal controllers are found using the method of Q-parameterization discussed in Section 5.3 with norm

$$\|Q\| = 0.2837$$

The RMS response of the closed-loop system is

$$\beta_{\text{rms}} = 4.163 \times 10^{-6}$$

Table 6.3: Lower bound estimates of the gain and phase margins for an $\mathcal{H}_\infty$ optimal periodic controller.

		Gain Margin (dB)	Phase Margin (deg)
Using		low , high	low , high
$\|\hat{\mathbf{S}}\|_\infty$	1.018	-5.94 , 35.1	-58.8 , 58.8
$\|\hat{\mathbf{T}}\|_\infty$	1.000	$-\infty$, 6.02	-60.0 , 60.0

a reduction of 94 dB and rejection of all tones. Figure 6.8 shows the singular value of the sensitivity function. The bandwidth is

$$\text{BW} = 0.5071$$

The closed-loop eigenvalues are $\lambda(\hat{A}) = \{0, 0.2043, 0.5069, 0.09432e^{\pm j0.3723}\}$. It is interesting to note that the closed-loop system has a pole at the origin which corresponds to a lifted delay of one cycle. Lower bound estimates of the gain and phase margins are shown in Table 6.3.

Both the nominal performance and robust stability specifications are achieved by this controller. This might be expected since the specifications are accounted for during controller synthesis.

6.3.3 Discussion

The periodic controller, designed using $\mathcal{H}_\infty$ methods, achieves improved performance over and exhibits larger robustness margins than the classical designs. While the classical designs reject only harmonics at the target frequency, the periodic controller realizes perfect disturbance rejection over a wider bandwidth—nearly two and a half times as wide. Also, because robustness is considered directly during design, this controller has considerably larger robustness margins. Our case study demonstrates an improvement in the lower bound estimates of the gain margin from $[-1.51, 1.83]$ dB to $[-5.94, 35.1]$ dB and the phase margin from ± 10.9 degrees to ± 58.8 degrees (both using $\hat{\mathbf{S}}$).

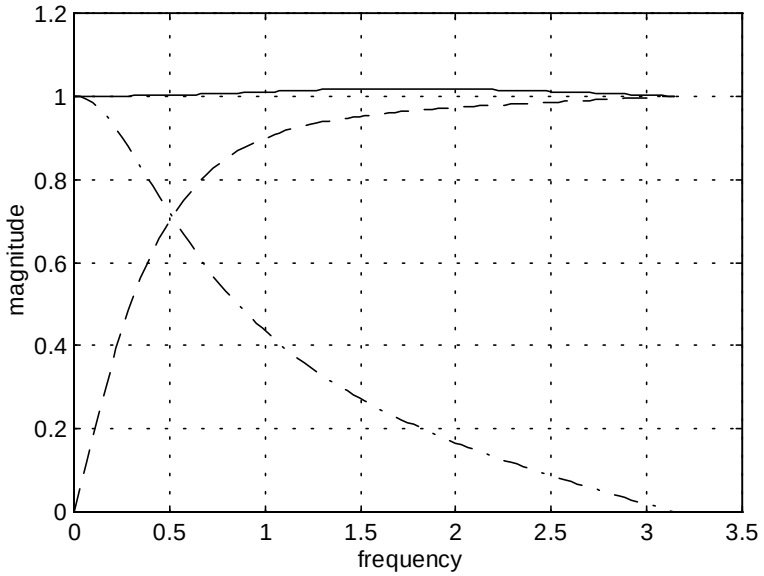

Figure 6.8: Singular value plots of the closed-loop sensitivities using a periodic controller: $\overline{\sigma}(\hat{\mathbf{S}})$ (solid), $\underline{\sigma}(\hat{\mathbf{S}})$ (dashed), $\overline{\sigma}(\hat{\mathbf{T}})$ (dot-dash).

6.4 Feedforward Designs

6.4.1 Periodic Designs

Periodic designs for feedforward disturbance rejection are found using the mixed sensitivity problem covered in Section 4.1.1.

$$\left\| \begin{bmatrix} (\hat{\mathbf{G}}_1 + \hat{\mathbf{G}}_2\hat{\mathbf{F}})\hat{\mathbf{W}}_d \\ \rho\hat{\mathbf{F}}\hat{\mathbf{W}}_d \end{bmatrix} \right\|_\infty < 1$$

The generalized plant is

$$\mathbf{P} = \left[\begin{array}{c|c} \hat{\mathbf{G}}_1\hat{\mathbf{W}}_d & \hat{\mathbf{G}}_2 \\ 0 & \rho I \\ \hline \hat{\mathbf{W}}_d & 0 \end{array}\right]$$

Because of zero feedthrough in the lowered systems, $D_1 = D_2 = 0$, both $\hat{\mathbf{G}}_1$ and $\hat{\mathbf{G}}_2$ are strictly proper and in particular $\hat{\mathbf{G}}_2^{-1}$ is improper and we cannot construct $\hat{\mathbf{F}} = -\hat{\mathbf{G}}_2^{-1}\hat{\mathbf{G}}_1$ directly. However, if we choose the disturbance weight to be

$$\hat{\mathbf{W}}_d = I$$

then the minimizing the norm of the controlled system

$$\min_{\hat{\mathbf{F}}} \left\| \hat{\mathbf{G}}_1 + \hat{\mathbf{G}}_2 \hat{\mathbf{F}} \right\|_\infty = \gamma^*$$

will result in the best stable inverse of $\hat{\mathbf{G}}_2$ weighted by the disturbance path $\hat{\mathbf{G}}_1$.

In our case, because

$$\text{range}^\perp(\hat{\mathbf{G}}_1(\infty)) = \text{range}^\perp(\hat{\mathbf{G}}_2(\infty))$$

the optimal solution yields

$$\hat{\mathbf{G}}_1 + \hat{\mathbf{G}}_2 \hat{\mathbf{F}}^* = 0$$

where $\hat{\mathbf{F}}^*$ is the optimal controller, and we can achieve perfect disturbance rejection at all frequencies in all directions. The optimal filter, $\hat{\mathbf{F}}^*$, is realizable because the equivalence of $\text{range}^\perp(\hat{\mathbf{G}}_1(\infty))$ and $\text{range}^\perp(\hat{\mathbf{G}}_2(\infty))$ allows for pole-zero cancelation at infinity.

With the control included in the cost we cannot achieve $\gamma^* = 0$ since the controller gain will be non-zero. However, we must continue to include the control signal; this is again related to the loss of rank in $\hat{\mathbf{G}}_2(\infty)$. Without the control included in the cost, $\mathbf{P}_{12}(\infty)$ would not be full column rank. The addition of the control to the cost restores this condition. We can approach the best disturbance rejection controller since as $\rho \to 0$

$$\left\| \begin{bmatrix} \hat{\mathbf{G}}_1 + \hat{\mathbf{G}}_2 \hat{\mathbf{F}} \\ \rho \hat{\mathbf{F}} \end{bmatrix} \right\|_\infty \longrightarrow \left\| \hat{\mathbf{G}}_1 + \hat{\mathbf{G}}_2 \hat{\mathbf{F}} \right\|_\infty$$

The control weight is made small, $\rho = 10^{-8}$, and the achieved norm is $\gamma^* = 0.05732$. Figure 6.9 shows the singular values of the controller.

The controller has poles at $\lambda(\hat{A}_K) = \{0, 0.2402\}$, and the RMS response of the controlled-system is functionally zero

$$\beta_{\text{rms}} = 10^{-14}$$

A solution to the narrowband problem which yields perfect disturbance rejection at all frequencies and all disturbances is certainly fortunate, however, it is very difficult if not impossible to achieve in practice. Perturbations in both the disturbance and control paths

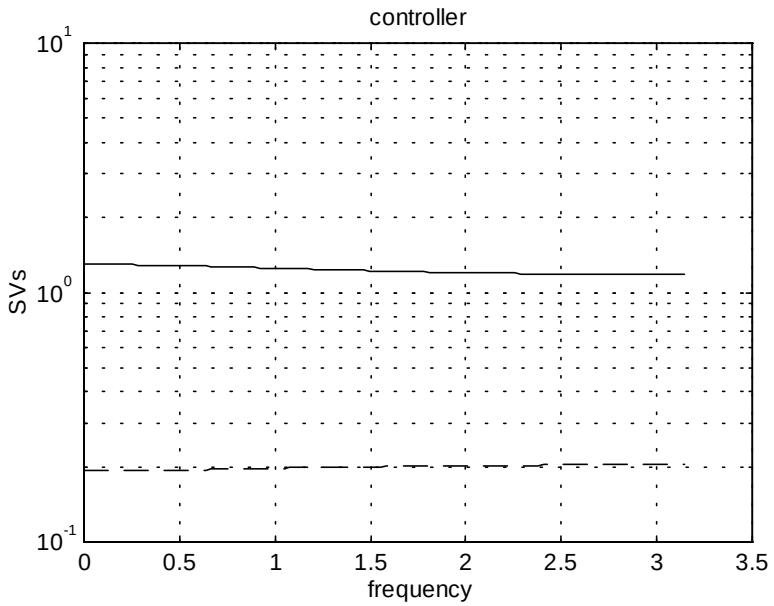

Figure 6.9: Singular values of a feedforward periodic controller.

results directly loss of performance. For the narrowband case, only the response of the controlled system at the disturbance frequency in the disturbance direction is important. Section 4.1.2 discussed the use of periodic FIR filters for narrowband disturbance rejection; this is the subject of the next section.

6.4.2 Periodic FIR Filter

At any frequency which is a multiple of the plant-periodic frequency, the system transfer function matrices are real valued.

$$\omega_0 = \tfrac{2\pi n}{m} \quad n = 0 : m-1 \quad \Rightarrow \quad \hat{z} = 1$$
$$\hat{\mathbf{G}}_1(1), \quad \hat{\mathbf{G}}_2(1) \quad \in \mathbb{R}^{mp \times mq}$$

At steady-state, the control signal is definied by the vector

$$\mu = -\hat{\mathbf{G}}_2^{-1}(1)\hat{\mathbf{G}}_1(1)\ \delta$$

where $\delta = \hat{\phi}_0$ is the disturbance direction and is real. Hence the controller gains are real and we can construct a controller using a single diagonal gain matrix

$$\hat{\mathbf{F}} = F = \text{diag}\{\mu_i\}$$

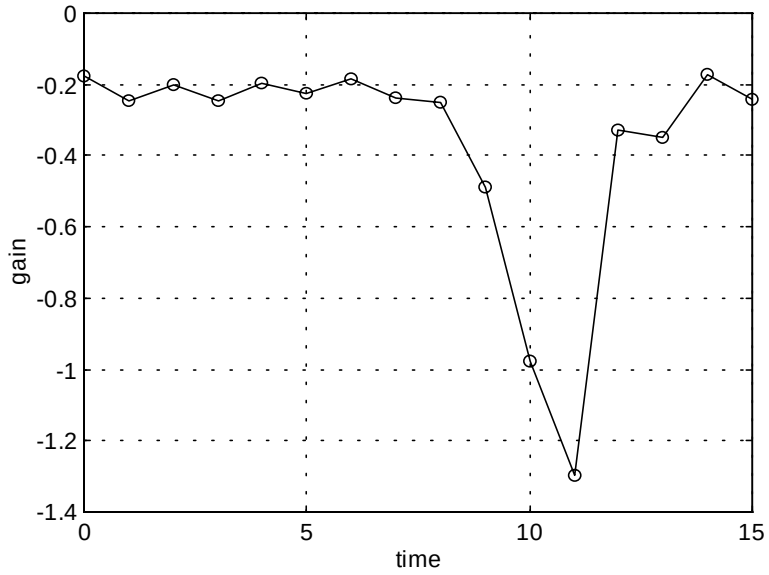

Figure 6.10: Periodic gain for narrowband disturbance rejection as a function of time.

This diagonal gain matrix is a periodic gain in real time. For our case study, Fig. 6.10 shows the periodic gain as a function of time. Figure 6.11 shows the singular values of the controlled system.

The RMS response of the controlled system is functionally zero.

$$\beta_{\text{rms}} = 10^{-17}$$

The primary difficult even with this method, which provides a fairly simple controller, is that some explicit knowledge of the disturbance path must be known. In many situations, only a coherent reference to the disturbance is available. In such situations, adaptive schemes, covered in Section 4.2, provide an attractive means for find controller gains without the requirement of explicitly knowing the disturbance path. This is the subject of the next section.

6.4.3 Adaptive FIR Filter

We can adapt the periodic gain, realized by the diagonal matrix F in the last section, using adaptive FIR filters developed in Section 4.2.

The adaptation gain is made as large as possible without letting the adaptation process

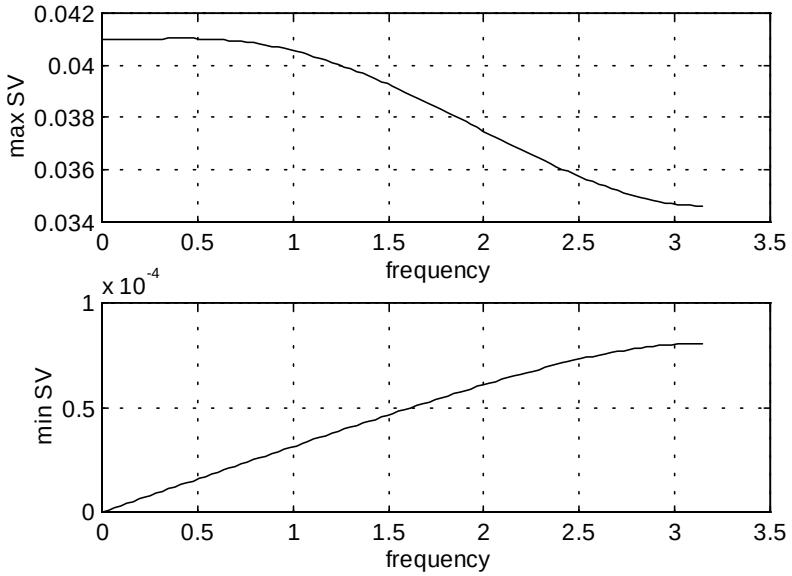

Figure 6.11: Maximum and minimum singular values of the controlled system using a periodic FIR filter: $\hat{\mathbf{G}}_1 + \hat{\mathbf{G}}_2\hat{\mathbf{F}}$.

be unstable.

$$\rho = 1$$

The estimate of the control-to-error path is

$$\hat{\mathbf{G}}_2^\star = \hat{\mathbf{G}}_2(1)$$

and is real valued since $\hat{\mathbf{G}}_2(1)$ is real.

Figure 6.12 shows the RMS response of the system using the adaptive periodic gain. In this instance the RMS response is defined by the norm of the system response over that period.

$$\beta_{\text{rms}}[k] = \frac{\|\hat{\beta}[k]\|}{\sqrt{m}}$$

It is interesting to note that there are multiple time constants in the adaptation process, and that the controller adapts fairly rapidly at the start of the process. We would expect 10 dB of suppression associated with the DC response should come fairly easily. The adaptation achieves approximately 25 dB in the first 100 cycles, 10 seconds for a rotor turning at 10 Hz,

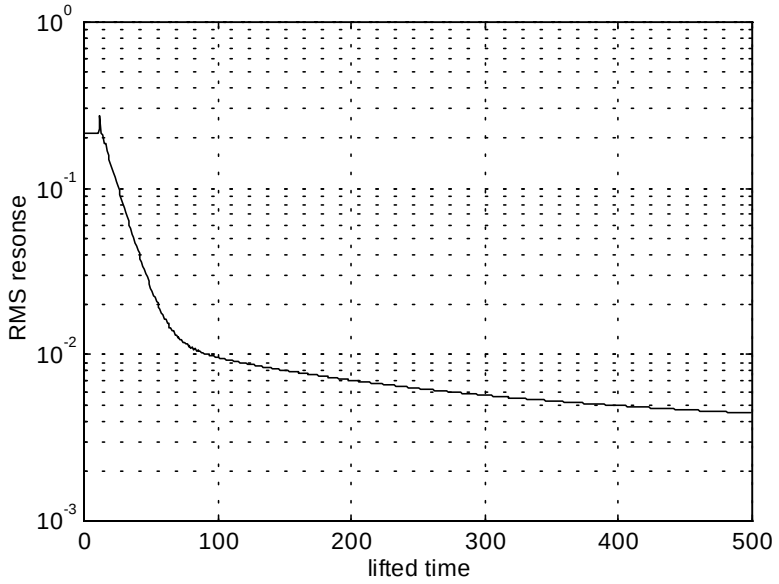

Figure 6.12: RMS response of the controlled system using an adaptive periodic gain. The controller was turned on at time $k = 10$.

so there is additional rejection of the other tones as well. After 100 cycles the adaptation process proceeds at a slower rate.

Figure 6.13 shows the adpative periodic gains at cycle 500 in comparison with the calculated values of the last section. As adaptation proceeds the obvious error in the gains near time step 10 will become smaller, however this happens slowly since it is dominated by the long time constant seen in the RMS response.

Interestingly, the normalized weight error in the adaptive periodic gains, defined by

$$\text{error} = \frac{\|F[k] - F^*\|}{\|F^*\|}$$

where F^* is the exact value calculated in the last section, does not become small quicly, approaching only 72% after 500 cycles, while the system achieves good performance quickly. This might be expected since the weight error depends upon the maximum difference within a period between the weight $F[k]$ and the ideal value, while the ability to reject tones at the lower frequencies, which dominate our uncontrolled response, depends upon the relative value of all of the gains across the period. The weights achieve good rejection of the lower frequencies since they are nominally correct across the period, and the weight error is large

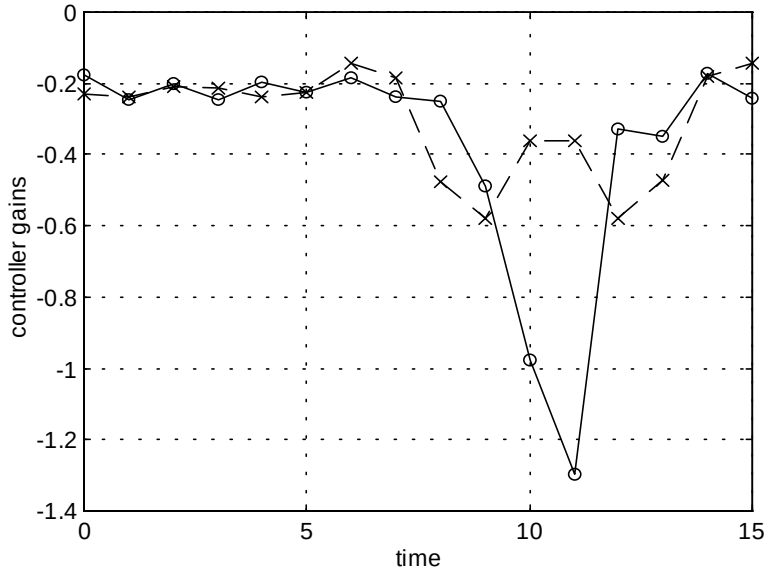

Figure 6.13: The adaptive periodic controller gains (×, dashed) after 500 cycles compared with calculated values (∘, solid).

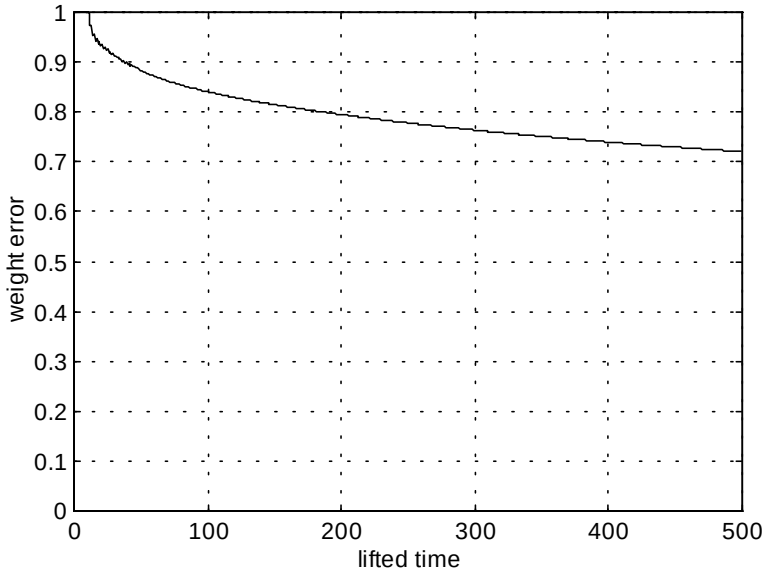

Figure 6.14: Normalized error in the adaptive periodic gains.

because only a few gains do not adapt quickly. Undoubtedly, there may be an appropriate scaling and change of basis of the signals which allows for multiple adaptation rates and a more uniform error in the gains across a period.

6.4.4 Discussion

Near perfect disturbance rejection is achieved using the feedforward disturbance rejection architecture. This is expected. The disturbance, or at least a coherent reference to it, is available for measurement, and the controller alters the magnitude and direction of the disturbance so that when reintroduced via the control path there is cancelation in the system output.

The periodic feedforward controller meets a norm objective which minimize the weighted ∞-norm of the controlled system; an optimal controllers is found using γ-iteration. This feedforward controllers achieves perfect disturbance rejection across the entire frequency range. Spectacular results, such as this, should not be considered the rule however.

A multivariable equivalent of the tapped-delay line is used in the description of periodic FIR filters, which is in fact a periodic gain. Perfect rejection is demonstrated. The periodic FIR filters is made adaptive using an algorithm similar to filtered-X LMS but modified for the multivariable problem.

Althought perfect rejection is, in theory, attainable using adaptive FIR filters, since it will eventually converge to the fixed-gain solution, the achieved level of performance depends largely upon the time-constants which govern adaptation. The case study demonstrates nearly 25 dB rejection in 100 cycles; this performance exceeds the classical feedback design.

Chapter 7

Conclusion

This research relies heavily upon the linear system theory made available by the development of the lifted representation by Meyer and Burrus [38]. In the past, the mathematical complexity of periodic systems has largely limited their study. However, the machinery of multivariable control theory can be applied directly to periodic systems for both analysis and synthesis. Thus, we can describe periodic systems using tools such as system norms, transfer function matrices, and Bode diagrams; in like manner, we can take advantage of the computational capabilites of state-variable representations for controller synthesis, and much of current, linear, system theory can be directly applied to linear periodic systems without modification. The simplification of much of periodic system theory is the lifted representation's greatest benefit. However, the causality constraint, embodied in a lower triangular feedthrough matrix, is its greatest difficulty.

In this research, constraints on controlled system ∞-norms specify nominal performance and robust stability objectives. Causal periodic controllers, which meet appropriate control objectives, can be found easily using existing LTI $\mathcal{H}_\infty$ control theory with slight modifications. Satisfying causality by loop-shifting and by Q-parameterization are introduced as two techniques to be added to $\mathcal{H}_\infty$ solvers and to make causal controllers. In both cases, the additional step involves the minimization of a constant LFT over a set of lower triangular matrices. Thus, the fabrication of periodic controllers which meet appropriate objective is, at least, brought within the realm of practicality. The lifted representation allows for simplified system expression, simplified periodic system theory, and simplified controller development.

The narrowband disturbance rejection problem for LTP systems is considerably more

complicated than its LTI counterpart. The modulation of an input signal with the plant-periodic frequency of a periodic system results in a system response which includes harmonics at the input signal's frequency and additional harmonic at frequencies spaced by the plant-periodic frequency. The thesis of this research inquires whether we can achieve improved disturbance rejection results by accounting for system periodicity during controller design. The answer to this question is, most certainly, yes. Periodic controllers are able to take better advantage of system structure than classical narrowband controllers. In this research, harmonic and narrowband disturbance rejection is investigated for linear time-periodic plants. The various architectures are classical and periodic feedback controllers, periodic feedforward controllers, fixed-gain FIR filters, and adaptive feedforward controllers.

Zero placement in the controlled system's disturbance path is the primary objective of periodic narrowband disturbance rejection. This is similar to the time-invariant problem. In the time-invariant feedback problem problem, this is achieved by placing a high-gain narrowband pass filter in the feedback path. Techniques for time-invariant feedforward control appropriately invert the control path while accounting for disturbance path dynamics. For the time-periodic problem, a zero is placed by using the same techniques as the time-invariant problem, but the zero direction, defined by the null space of the controlled system at the disturbance frequency, is made coincident with the disturbance.

Classical designs do not achieve the desired objectives of narrowband disturbance rejection when applied to time-periodic plants. Such controllers do place a zero in the periodic system's sensitivity; however, because of their structure, the disturbance, in general, does not lie in the closed-loop sensitivity's null space, resulting in transmission of the disturbance and poor performance. Classical controllers do eliminate the target frequency from the control system output. They also have the potential penalty of amplifying other harmonics, and, as demonstrated in the case study (Section 6.3.1), may be limited by reduced stability margins which restrict controller gains and achievable performance.

In this research, periodic feedback control objectives are cast as constraints on the ∞-norm of the system sensitivity and complimentary sensitivity. $\mathcal{H}_\infty$ design methods are used to fabricate periodic controllers, and the resulting controllers are high-gain, narrowband-pass, periodic filters. The closed-loop sensitivity has the requisite zero and the disturbance direction is oriented with the disturbance.

Periodic controllers achieve improved performance over and exhibit larger robustness margins than the classical designs discussed previously. $\mathcal{H}_\infty$ controllers realize disturbance rejection over a wider bandwidth—nearly two and a half times as wide in our case study. Such controllers have considerably larger robustness margins because robustness can be considered directly during design. For example, our case study demonstrates an improvement in the lower bound estimates of the gain margin from $[-1.51, 1.83]$ dB to $[-5.94, 35.1]$ dB and the phase margin from ± 10.9 degrees to ± 58.8 degrees (both using the sensitivity).

Using the feedforward disturbance rejection architecture, the disturbance, or at least a coherent reference to it, is available for measurement. A feedforward controller alters the magnitude and direction of the disturbance so that when reintroduced via the control path there is cancelation in the system output. Nominal performance results, similar to periodic feedback, can be achieved.

Nominal performance is cast as objective on the ∞-norm of the controlled system's disturbance path; optimal controllers are found using γ-iteration. Such feedforward controllers achieve perfect disturbance rejection. A multivariable equivalent of the tapped-delay line is used to describe periodic FIR filters. Such filters allow controllers to be implemented using simplified structures, and allow the designer to focus on system performance at target frequencies. Perfect rejection is also possible using periodic FIR filters. In addition, using an algorithm similar to filtered-X LMS but modified for the multivariable problem, periodic FIR filters can be made adaptive. The case study demonstrates nearly 25 dB rejection in 100 cycles; this performance exceeds classical feedback design, and adaptation happens quickly.

It does not seem surprising that effective control of periodic systems requires periodic controllers. Given the apparent complexity of periodic systems, the fact that previous control engineers have approximated, out of necessity, periodic systems using pseudo-time-invariant and quasi-static models is understandable. The development of the lifted system by Meyer and Burrus [38] in 1975 has opened possibilities for periodic system theory, permitting periodic system analysis using existing LTI system theory, even though many researchers have failed to take advantage of this connection. In this research, the principal insight is that the study of periodic systems and the construction of periodic controllers is no more complicated than similar tasks for MIMO-LTI systems, an area of control theory with many theorists and practitioners.

Contributions

The following is a list of the contributions of this research to the area of periodic system theory and control.

- Lifting of sinusoidal signals.
- Harmonic-lifted system.
- Structure of lifted LTI systems.
- An algorithm for real-time implementation using lifted systems.
- Analysis of the disadvantages of LTI controllers for periodic system narrowband disturbance rejection.
- The implications of output and input weighting on disturbance rejection results for periodic systems.
- Definition and structure of periodic FIR filters.
- Adaptation algorithm for periodic a class of FIR filters.
- Satisfying causality of periodic $\mathcal{H}_\infty$ solutions using loop-shifting.
- Satisfying causality of periodic $\mathcal{H}_\infty$ solutions using Q-parameterization.

Many of the contributions of this research are related, necessarily, to the description of lifted sinusoidal signals and the response of lifted systems to those signals in the form of the harmonic-lifted system. The investigation of feedback and feedforward disturbance rejection is not new from a linear system theory perspective, but its application to periodic systems is. Included in this is analysis of the effect LTI controllers have for narrowband disturbance rejection and techniques for designing periodic controllers. Also, the extension of not only FIR filters to periodic systems but also adaptive FIR filters is a new technology. Finally, the use of loop-shifting and Q-parameterization to meet causality requirements in periodic $\mathcal{H}_\infty$ solutions is an improvement over previous methods.

Bibliography

[1] Dirk Aeyels and Jaques L. Willems. Pole assignment for linear periodic systems by memoryless output feedback. *IEEE Trans. on Automatic Control*, 40(4), April 1995.

[2] Christopher Beattie. personal conversations, 1998.

[3] S. Bittanti. *Time Series and Linear Systems*, volume 86 of *Lecture Notes in Contol and Information Sciences*, chapter Deterministic and Stochastic Linear Periodic Systems. Springer-Verlag, Berlin, 1986.

[4] Sergio Bittanti and Paolo Bolzern. Discrete-time linear periodic systems: Gramian and modal criteria for reachability and controllability. *Int. J. of Control*, 41(4):909–928, 1985.

[5] Sergio Bittanti and Paolo Bolzern. Stabilizability and detectability of linear periodic systems. *Systems and Control Letters*, 6:141–145, 1985.

[6] A. R. S. Bramwell. *Helicopter Dynamics*. Edward Arnold, London, 1976.

[7] Patrizio Colaneri. Output stabilization via pole placement of discrete-time linear periodic systems. *IEEE Transactions on Automatic Control*, 36(6):739–742, June 1991.

[8] Munther A. Dahleh and J. Boyd Pearson Jr. Optimal rejection of persistent disturbances, robust stability, and mixed sensitivity minimization. *IEEE Transactions on Automatic Control*, 33(8):722–731, August 1988.

[9] Munther A. Dahleh, Petros Voulgaris, and Lena S. Valavani. Optimal rejection of bounded persistent disturbances in periodic systems. *Proceedings of the 29th Conference on Decision and Control*, pages 2300–2305, December 1990.

[10] Munther A. Dahleh, Petros Voulgaris, and Lena S. Valavani. Optimal and robust controllers for periodic and multirate systems. *IEEE Transactions on Automatic Control*, 37(1):90–99, January 1992.

[11] R. Lane Dailey. Lecture notes for the workshop on $\mathcal{H}_\infty$ and μ methods for robust control, May 21–22 1990.

[12] Stephen J. Elliott, Ian M. Stothers, and Philip A. Nelson. A multiple error LMS algorithm and its applicaiton to the actiove cotnrol of sound and vibration. *IEEE Trans. on Acoustics, Speech and Signal Proc.*, ASSP-35(10):1423–1434, October 1987.

[13] L. P. Fowler, D. G. Cole, H. H. Robertshaw, and V. Giurgiutiu. Individual feedforward-feedback control of a flexible rotor blade: a comparison of approaches. *Proc. of SPIE Conf. on Smart Structures and Materials*, 1995.

[14] Peretz P. Friedmann and Thomas A. Millott. Vibration reduction in rotorcraft using active control: a comparison of various approaches. *J. of Guidance, Control and Dynamics*, 18(4):664–673, Jul.-Aug. 1995.

[15] Keith Glover and John C. Doyle. State-space formulae for all stabilizing controllers that satisfy and $\mathcal{H}_\infty$-norm bound and relations to risk sensitivity. *Systems and Control Letters*, 11:167–172, 1988.

[16] Gene H. Golub and Charles F. Van Load. *Matrix Computations*. The Johns Hopkins University Press, third edition, 1996.

[17] O. M. Grasselli and F. Lampariello. Dead-beat control of linear periodic discrete-time systems. *Int. J. of Control*, 33(6):1091–1106, 1981.

[18] Osvaldo M. Grasselli, Sauro Longhi, and Antonio Tornambe. System equivalence for periodic models and systems. *SIAM J. of Control and Optimization*, 33(2):455–468, March 1995.

[19] Osvaldo Maria Grasselli. A canonical decomposition of linear periodic discrete-time systems. *Int. J. of Control*, 40(1):201–214, 1984.

[20] Osvaldo Maria Grasselli and Sauro Longhi. Disturbance localization with dead-beat control for linear periodic discrete-time systems. *Int. J. of Control*, 44(5):1319–1347, 1986.

[21] Osvaldo Maria Grasselli and Sauro Longhi. Output dead-beat controllers and functional dead-bead observers for linear periodic discrete-time systems. *Int. J. of Control*, 43(2):517–537, 1986.

[22] Osvaldo Maria Grasselli and Sauro Longhi. Disturbance localization by measurement feedback for linear periodic discrete-time systems. *Automatica*, 24(3):375–385, 1988.

[23] Osvaldo Maria Grasselli and Sauro Longhi. Zeros and poles of linear periodic multivariable discrete-time systems. *Circuits, Systems and Signal Processing*, 7(3):361–380, 1988.

[24] Osvaldo Maria Grasselli and Sauro Longhi. Finite zero structure of linear periodic discrete-time systems. *International Journal of Systems Science*, 22(10):1785–1806, 1991.

[25] Osvaldo Maria Grasselli and Sauro Longhi. Pole placement for nonreachable periodic discrete-time systems. *Mathematics of Control, Signal, and Systems*, 4:439–455, 1991.

[26] Michael Green and David J. N. Limebeer. *Linear Robust Control*. Prentice Hall, Englewood Cliffs, New Jersey, 1995.

[27] Aristide Halanay and Vlad Ionescu. *Time-varying Discrete Linear Systems*. Birkhäuser Verlag, Basel, Switzerland, 1983.

[28] Seven R. Hall and Norman M. Werely. Linear control issues in the higher harmonic control of helicopter vibrations. In *Proc. of the 45th Annual Forum of the American Helicopter Society*, Boston, MA, May 1989.

[29] E. M. Kasenally and D. J. N. Limebeer. Closed formulae for a parametric mixed sensitivity problem. *Systems and Control Letters*, 12:1–7, 1989.

[30] Pramod P. Khargonekar, Kameshwar Poolla, and Allen Tannenbaum. Robust control of linear time-invariant plants using periodic compensation. *IEEE Transactions on Automatic Control*, AC-30(11):1088–1098, 1985.

[31] Michio Kono. Eigenvalue assignment in linear periodic discrete-time systems. *Int. J. of Control*, 32(1):149–158, 1980.

[32] B. Kouvaritakis and A. G. J. MacFarlane. Geometric approach to analysis and synthesis of system zeros: Part 1. square systems. *Int. J. of Control*, 23(2):149–166, 1976.

[33] B. Kouvaritakis and A. G. J. MacFarlane. Geometric approach to analysis and synthesis of system zeros: Part 2. non-square systems. *Int. J. of Control*, 23(2):167–181, 1976.

[34] H. Kwakernaak. Minimax frequency domain performance and robustness optimization of linear feedback systems. *IEEE Trans. on Automatic Control*, AC-30:994–1004, 1985.

[35] A. G. J. Macfarlane and N. Karcanias. Poles and zeros of linear multivariable systems: a survey of the algebraic, geometric and complex-variable theory. *Int. J. of Control*, 24(1):33–74, 1976.

[36] J. M. Maciejowski. *Multivariable Feedback Design*. Addison-Wesley, Reading, Massachusetts, 1989.

[37] David G. Meyer. A parametrization of stabilizing controllers for multirate sampled-data systems. *IEEE Transactions on Automatic Control*, 35(2):233–236, 1990.

[38] R. A. Meyer and C. S. Burrus. A unified analysis of multirate and periodically time-varying digital filters. *IEEE Transactions on Circuits and Systems*, 22(3):162–168, 1975.

[39] Alan V. Oppenheim and Ronald W. Schafer. *Discrete-time Signal Processing*. Prentice Hall, Englewood Cliffs, New Jersey, 1989.

[40] Michael L. Overton. On minimizing the maximum eigenvalue of a symetric matrix. *SIAM J. of Matrix Anal. Appl.*, 9(2):256–268, April 1988.

[41] R. Pandiyan and S. C. Sinha. Time-varying controller synthesis for structures subjected to parametric periodic loadings. *Proceedings of the 35th Structures, Structural Dynamics, and Materials Conference*, 5:2449–2459, 1994.

[42] B. Park and E. I. Verriest. Canonical forms on discrete linear periodically time-varying systems and a control application. *Proceedings of the 28th IEEE Conference on Decision and Control*, pages 1220–1225, December 1989.

[43] Stephen Parrott. On a quotient norm and the Sz.-Nagy-Foiaş lifting theorem. *Journal of Functional Analysis*, 30:311–328, 1978.

[44] Antonio Pastor and Vincente Hernandez. Differential periodic Ricatti equations: Existence and uniqueness of nonnegative definite solutions. *Mathematics of Control, Signals, and Systems*, 6:341–362, 1993.

[45] Jenny L. Rawson and Chin S. Hsu. Design of periodic output feedback for robust stability. *Proceedings of the American Controls Conference*, 2:1011–1012, 1992.

[46] J. A. Richards. *Analysis of Periodically Time-Varying Systems*. Springer-Verlag, Berlin, 1983.

[47] H. H. Rosenbrock. The zeros of a system. *Int. J. of Control*, 18(2):297–299, 1973.

[48] J. Shaw, N. Albion, E. J. Hanker, and R. S. Teal. Higher harmonic control: Wind tunnel demonstration of fully effective vibratory hub force suppression. *J. of the American Helicopter Society*, 34(1):14–25, 1989.

[49] John Shaw and Nichola Albion. Active control of the helicopter rotor for vibration reduction. *J. of the American Helicopter Society*, 26(3):32–39, 1981.

[50] Lisa A. Sievers and Andreas H. von Flotow. Comparison and extensions of control methods for narrowband disturbance rejection. *1990 ASME Winter Annual Meeting*, November 1990.

[51] S. C. Sinha and P. Joseph. Control of general dynamic systems with periodically varying parameters via liapunov-floquet transformation. *Journal of Dynamic Systems, Measurement, and Control*, 116:650–658, December 1994.

[52] J. Sreedhar and Paul Van Dooren. On finding stabilizing state feedback gains for a discrete-time periodic system. *Proceedings of the American Control Conference*, 1994.

[53] M. Verma and E. Jonckheere. L^∞-compensation with mixed sensitivity as a broadband matching problem. *Systems and Control Letters*, 4:125–129, 1984.

[54] Erik I. Verriest. The operational transfer function and parameterization of N-periodic systems. *Proceedings of the 27th IEEE Conference on Decision and Control*, pages 1994–1999, December 1988.

[55] Petros G. Voulgaris and Bassam Bamieh. Optimal $\mathcal{H}_\infty$ and $\mathcal{H}_2$ control of hybrid multirate systems. *Systems and Control Letters*, 20:249–261, 1993.

[56] Petros G. Voulgaris, Munther A. Dahleh, and Lena S. Valavani. $\mathcal{H}_\infty$ and $\mathcal{H}_2$ optimal controllers for periodic and multirate systems. *Automatica*, 30(2):251–263, 1994.

[57] B. Widrow and S. D. Stearns. *Adaptive Signal Processing*. Prentice-Hall, 1985.

[58] Lihua Xie and Carloz E. de Souza. $\mathcal{H}_\infty$ state estimation for linear periodic systems. *IEEE Transactions on Automatic Control*, 38(11):1704–1707, November 1993.

[59] Kemin Zhou. *Essentials of Robust Control*. Prentice Hall, 1998.

Appendix A

Minimizing constant LFTs

Consider the LFT

$$\mathcal{F}_l\left(\begin{bmatrix} D_{11} & D_{12} \\ D_{21} & D_{22} \end{bmatrix}, F\right) = D_{11} + D_{12}F(I - D_{22}F)^{-1}D_{21}$$

in which F and D_{ij}'s are constant matrices with the following dimensions

$$\begin{array}{cc} & \begin{matrix} q_1 & q_2 \end{matrix} \\ \begin{matrix} p_1 \\ p_2 \end{matrix} & \begin{bmatrix} D_{11} & D_{12} \\ D_{21} & D_{22} \end{bmatrix} \end{array}$$

and $p_1 \geq q_2$ and $p_2 \leq q_1$. Unless stated otherwise we assume $(I - D_{22}F)^{-1}$ exists.

The aim of this paper is to determine a matrix F which minimizes the norm of the LFT

$$\gamma_{opt} = \min_F \|\mathcal{F}_l(D, F)\|$$

where the norm is the induced norm $\|A\| = \overline{\sigma}(A)$.

First, we convert the problem into its equivalent model-matching expression by defining

$$Q = F(I - D_{22}F)^{-1}$$

Thus,

$$\|\mathcal{F}_l(D, F)\| = \|D_{11} + D_{12}QD_{21}\|$$

and we can consider the problem of picking Q instead. Once Q is found be can solve for F.

$$F = (I + QD_{22})^{-1}Q$$

Depending upon the size and rank of D_{12} and D_{21} we have the following cases.

1-block: D_{12} and D_{21} are non-singular (square and invertible).

2-block: D_{12} is non-singular and D_{21} is full row rank (fat), or
D_{21} is non-singular and D_{12} is full column rank (tall).

4-block: D_{12} is full column rank and D_{21} is full row rank.

1-block: If both D_{12} and D_{21} are non-singular (square and invertible), then we can solve for Q directly.

$$Q = -D_{12}^{-1}D_{11}D_{21}^{-1}$$

and $\mathcal{F}_l(D, F) = 0$, and $\gamma_{opt} = 0$.

The optimal feedback matrix F is given by

$$F = -(D_{12} - D_{11}D_{21}^{-1}D_{22})^{-1}D_{11}D_{21}^{-1}$$

2-block: We will consider the case that D_{12} is full row rank (tall) and D_{21} is non-singular first. Perform a singular value decomposition on D_{12}.

$$D_{12} = U_{12}\begin{bmatrix} 0 \\ \Sigma_{12} \end{bmatrix} V_{12}'$$

where U_{12} and V_{12} are unitary matrices.

Considering the norm of the LFT, we can premultiply by U_{12}' without affecting the norm since multiplication by unitary matrices does not change the norm. Thus, we get

$$\begin{aligned} \|D_{11} + D_{12}QD_{21}\| &= \|U_{12}'(D_{11} + D_{12}QD_{21})\| \\ &= \|U_{12}'(D_{11} + D_{12}V_{12}\Sigma_{12}^{-1}\hat{Q})\| \\ &= \left\| \hat{D}_{11} + \begin{bmatrix} 0 \\ \hat{Q} \end{bmatrix} \right\| \end{aligned}$$

where

$$\hat{D}_{11} = U'_{12} D_{11} \quad \text{and} \quad \hat{Q} = \Sigma_{12} V'_{12} Q D_{21}$$

and we have reduced the problem to finding a matrix $\hat{Q}$ which minimizes the norm.

Partition $\hat{D}_{11}$ as

$$\hat{D}_{11} = \begin{bmatrix} \hat{D}_{111} \\ \hat{D}_{112} \end{bmatrix}$$

where $\hat{D}_{112}$ is a $q_2 \times p_2$ matrix and is the same size as $\hat{Q}$. A suitable choice for $\hat{Q}$ which minimizes

$$\left\| \begin{bmatrix} \hat{D}_{111} \\ \hat{D}_{112} + \hat{Q} \end{bmatrix} \right\|$$

is

$$\hat{Q} = -\hat{D}_{1122}$$

and the minimum norm is determined by the submatrix.

$$\gamma_{opt} = \overline{\sigma}\left(\hat{D}_{111}\right)$$

Once $\hat{Q}$ is found we can calculate Q.

$$Q = V_{12} \Sigma_{12}^{-1} \hat{Q} D_{21}^{-1}$$

For the case that D_{21} is full column rank and D_{12} is non-singular we follow a similar procedure but perform the singular value decomposition on D_{21} and post-multiply by V_{21} instead. The matrix $\hat{D}_{11}$ is

$$\hat{D}_{11} = D_{11} V_{21} = \begin{bmatrix} \hat{D}_{111} & \hat{D}_{112} \end{bmatrix}$$

where $\hat{D}_{112}$ is a $q_2 \times p_2$ matrix and is the same size as $\hat{Q}$. The minimizing $\hat{Q}$ is

$$\hat{Q} = -\hat{D}_{112}$$

and the minimum norm is determined by the submatrix

$$\gamma_{opt} = \overline{\sigma}\left(\hat{D}_{111}\right)$$

Again, once $\hat{Q}$ is found we can calculate Q.

$$Q = D_{12}^{-1} \hat{Q} \Sigma_{21}^{-1} U'_{21}$$

4-block: Here D_{12} is full column rank (tall) and D_{21} is full row rank (fat). First, perform a singular value decompositon on D_{12} and D_{21}.

$$D_{12} = U_{12}\begin{bmatrix} 0 \\ \Sigma_{12} \end{bmatrix} V_{12}' \qquad D_{21} = U_{21}\begin{bmatrix} 0 & \Sigma_{21} \end{bmatrix} V_{21}'$$

where U_{ij} and V_{ij} are unitary matrices.

Considering the norm of the LFT, we can pre-multiply by U_{12}' and post-multiply by V_{21} and not affect the norm since multiplication by unitary matrices does not change the norm. Thus we get

$$\begin{aligned} \|D_{11} + D_{12}QD_{21}\| &= \|U_{12}'(D_{11} + D_{12}QD_{21})V_{21}\| \\ &= \|U_{12}'(D_{11} + D_{12}V_{12}\Sigma_{12}^{-1}\hat{Q}\Sigma_{21}^{-1}U_{21}'D_{21})V_{21}\| \\ &= \left\| \hat{D}_{11} + \begin{bmatrix} 0 & 0 \\ 0 & \hat{Q} \end{bmatrix} \right\| \end{aligned}$$

where

$$\hat{D}_{11} = U_{12}'D_{11}V_{21} \quad \text{and} \quad \hat{Q} = \Sigma_{12}V_{12}'QU_{21}\Sigma_{21}$$

and again we have reduced the problem to finding a matrix $\hat{Q}$ which minimizes the norm.

Partition $\hat{D}_{11}$ as

$$\hat{D}_{11} = \begin{bmatrix} \hat{D}_{1111} & \hat{D}_{1112} \\ \hat{D}_{1121} & \hat{D}_{1122} \end{bmatrix}$$

where $\hat{D}_{1122}$ is a $q_2 \times p_2$ matrix and is the same size as $\hat{Q}$. Using Parrott's theorem [43], a suitable choice for $\hat{Q}$ which minimizes

$$\left\| \begin{bmatrix} \hat{D}_{1111} & \hat{D}_{1112} \\ \hat{D}_{1121} & \hat{D}_{1122} + \hat{Q} \end{bmatrix} \right\|$$

is

$$\hat{Q} = -(\hat{D}_{1122} + \hat{D}_{1121}(I - \hat{D}_{1111}'\hat{D}_{1111})^{-1}\hat{D}_{1111}'\hat{D}_{1112}$$

Parrott's theorem also proves that the minimum norm is determined by the norm of submatrices.

$$\gamma_{opt} = \max\left\{ \overline{\sigma}\left(\begin{bmatrix} \hat{D}_{1111} & \hat{D}_{1112} \end{bmatrix} \right), \overline{\sigma}\left(\begin{bmatrix} \hat{D}_{1111}' & \hat{D}_{1121}' \end{bmatrix} \right) \right\}$$

Again, once $\hat{Q}$ is found we can calculate Q.

$$Q = V_{12}\Sigma_{12}^{-1}\hat{Q}\Sigma_{21}^{-1}U_{21}'$$

Appendix B

Helicopter Rotor Blade Equation of Motion

This section derives the periodic equation of motion for a helicopter rotor blade. The derivation follows directly that found in Bramwell [6]. The model is of a rigid helicopter rotor blade turning at a constant frequency Ω, and the model is presented in two parts: the equation of motion for blade flapping; and, the aerodynamic moment as a function of azimuth angle, and blade position and velocity.

$$\beta'' + (1+\epsilon)\beta = M_A/I\Omega^2$$

$$M_A = I\Omega^2\frac{\gamma}{8}\left[\left(1+\frac{8}{3}\mu\sin\psi+2\mu^2\sin^2\psi\right)\ \theta+\frac{4}{3}\lambda-\beta'-\frac{4}{3}\mu\beta\cos\psi \right. \\ \left. +\ 2\lambda\mu\sin\psi-\frac{4}{3}\mu\sin\psi\ \beta'-\frac{2}{\mu}^2\cos\psi\sin\psi\ \beta\right]$$

A simplifying assumption related to the induce velocity is made, not accounted for in the Bramwell derivation. Here, the induced velocity is assumed to be constant with respect to blade azimuth and radius. At higher forward speeds the induced velocity is small by comparison and this assumption may be justified. Our main purpose is to facilitate the modeling of the rotor blade to provide a testbed on which to compare controllers.

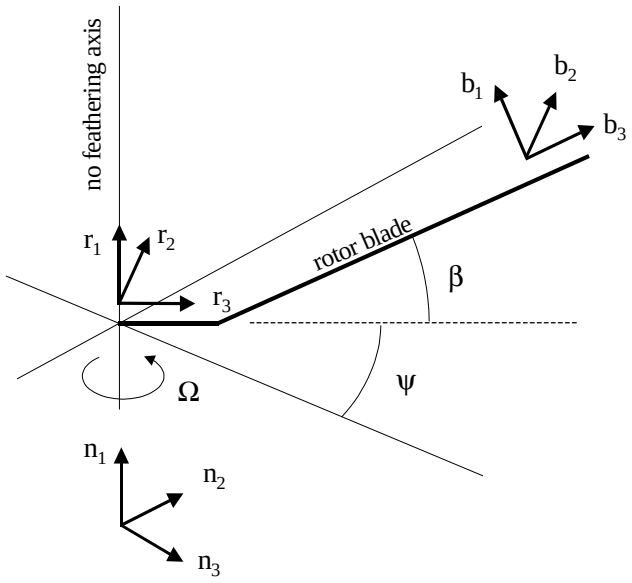

Figure B.1: Rotor coordinates.

B.1 Flapping Equation

Refer to figure B.1. The blade flapping hinge is offset a distance eR from the axis of rotation, and the blade rotates at a constant angluar velocity $\vec{\omega} = \Omega\,\hat{r}_3$. Locating the center of mass a distance $x_{cg}R$ along the blade

$$\vec{r}_{cg} = (eR + x_{cg}R\cos\beta)\,\hat{r}_1 + x_{cg}R\sin\beta\,\hat{r}_3$$

the velocity of the center of mass is

$$\begin{aligned}\vec{v}_{cg} &= \dot{\vec{r}}_{cg} + \vec{\omega}\times\vec{r}_{cg} \\ &= -x_{cg}R\sin\beta\dot{\beta}\,\hat{r}_1 + \Omega(eR + x_{cg}R\cos\beta)\,\hat{r}_2 + x_{cg}R\cos\beta\dot{\beta}\,\hat{r}_3\end{aligned}$$

The translational kinetic energy is

$$\begin{aligned}T_{tr} &= \frac{1}{2}m|\vec{v}_{cg}|^2 \\ &= \frac{1}{2}mx_{cg}^2R^2\dot{\beta}^2 + \frac{1}{2}m\Omega^2(eR + x_{cg}R\cos\beta)^2\end{aligned}$$

Assuming the principal axes are coincident with the blade axes $\{\hat{b}_1, \hat{b}_2, \hat{b}_3\}$, and that $I_y = I_z = I'$, the rotational kinetic energy is

$$T_{rot} = \frac{1}{2}I'\dot{\beta}^2 + \frac{1}{2}I'\Omega^2\cos^2\beta$$

The kinetic energy is the sum of the translational and rotational parts. Adding these terms and collecting parts, the kinetic energy becomes

$$\begin{aligned}T &= T_{tr} + T_{rot} \\ &= \left\{\frac{1}{2}mx_{cg}^2R^2\dot{\beta}^2 + \frac{1}{2}m\Omega^2(eR + x_{cg}R\cos\beta)^2\right\} + \left\{\frac{1}{2}I'\dot{\beta}^2 + \frac{1}{2}I'\Omega^2\cos^2\beta\right\} \\ &= \frac{1}{2}(I' + mx_{cg}^2R^2)(\dot{\beta}^2 + \Omega^2\cos^2\beta) + \frac{1}{2}me^2R^2\Omega^2 + mx_{cg}eR^2\Omega^2\cos\beta\end{aligned}$$

The potential energy is zero.

The equation of motion becomes

$$I\ddot{\beta} + I\Omega^2(\cos\beta + mx_{cg}eR^2)\sin\beta = M_A$$

where $I = I' + mx_{cg}^2 R^2$ is the blade's moment of inertia about the hinge and M_A is the aerodynamic moment in the sense of positive flapping angle β.

Linearizing the above equation of motion about $\begin{bmatrix}\beta & \dot{\beta}\end{bmatrix}^T$ yields

$$\ddot{\beta} + \Omega^2(1+\epsilon)\beta = M_A/I$$

where

$$\epsilon = \frac{mx_{cg}eR^2}{I}$$

If the blade has a uniform mass distribution then $x_{cg} = (1-e)/2$ and $I = mR^2(1-e)^2/3$, so

$$\epsilon = \frac{3e}{2(1-e)}$$

a typical value for e is 0.04 so ϵ is approximately 0.06.

Because the blade rotates with constant angular velocity Ω we can write the above equation in terms of the blade azimuth $\psi = \Omega t$.

$$\beta'' + (1+\epsilon)\beta = M_A/I\Omega^2$$

where $'$ denotes $d/d\psi$.

B.2 Aerodynamic Moment

B.2.1 Velocity Components of the Blade

The helicopter is moving forward at velocity V and the rotor is tilted with respect to the horizon by an angle α_{nf}. The plane of rotor rotation is refered to as the no-feathering plane and the axis about which it rotates is the no-feathering axis. The fixed inertial coordinates $\{\hat{n}_1, \hat{n}_2, \hat{n}_3\}$ are located in the no-feathering plane. Thus, the velocity of the helicopter can be expressed as

$$\vec{v} = V\cos\alpha_{nf}\ \hat{n}_2 - V\sin\alpha_{nf}\ \hat{n}_3$$

With respect to rotating coordinates $\{\hat{r}_1, \hat{r}_2, \hat{r}_3\}$ in the no-feathering plane the helicopter velocity is

$$\vec{v} = -V\cos\alpha_{nf}\cos\psi\ \hat{r}_1 + V\cos\alpha_{nf}\sin\psi\ \hat{r}_2 - V\sin\alpha_{nf}\ \hat{r}_3$$

where ψ is the azimuth angle of the blade with repsect to the aft of the helicopter.

In the blade reference frame $\{\hat{b}_1, \hat{b}_2, \hat{b}_3\}$ we have

$$\begin{aligned}\vec{v} = &- \left(V \cos\alpha_{nf} \cos\psi \cos\beta + V \sin\alpha_{nf} \sin\beta\right) \hat{b}_1 \\ &+ \left(V \cos\alpha_{nf} \sin\psi\right) \hat{b}_2 \\ &+ \left(V \cos\alpha_{nf} \cos\psi \sin\beta - V \sin\alpha_{nf} \cos\beta\right) \hat{b}_3\end{aligned}$$

The blade reference frame rotates with velocity

$$\vec{\omega} = \Omega \sin\beta \; \hat{b}_1 - \dot{\beta} \; \hat{b}_2 + \Omega \cos\beta \; \hat{b}_3$$

so a blade element at a location $r \; \hat{b}_1$ has velocity

$$\begin{aligned}\vec{w} &= \vec{v} + \vec{\omega} \times (r \; \hat{b}_1) \\ &= - \left(V \cos\alpha_{nf} \cos\psi \cos\beta + V \sin\alpha_{nf} \sin\beta\right) \hat{b}_1 \\ &\quad + \left(V \cos\alpha_{nf} \sin\psi + r\Omega \cos\beta\right) \hat{b}_2 \\ &\quad + \left(V \cos\alpha_{nf} \cos\psi \sin\beta - V \sin\alpha_{nf} \cos\beta + r\dot{\beta}\right) \hat{b}_3\end{aligned}$$

The velocity of the air with respect to the blade becomes $-\vec{w}$ and we must include the relative wind due to the induced velocity, $-v_i \; \hat{b}_3$. In general, the induced velocity is a function of azimuth and radius; however, for our purposes it will be sufficient to assume the induced velocity, v_i, is constant.

$$v_i = \frac{T}{2\rho A V}$$

Here T is the rotor thrust, and A is the rotor disk area. The component of the relative wind becomes

$$\begin{aligned}\text{spanwise:} \quad & U_S = V \cos\alpha_{nf} \cos\psi \cos\beta + V \sin\alpha_{nf} \sin\beta \\ \text{chordwise:} \quad & U_T = -V \cos\alpha_{nf} \sin\psi - r\Omega \cos\beta \\ \perp \text{ chord:} \quad & U_P = -V \cos\alpha_{nf} \cos\psi \sin\beta + V \sin\alpha_{nf} \cos\beta - r\dot{\beta} - v_i\end{aligned}$$

We will usually neglect the effects of the spanwise flow U_S. For small angles U_P and U_T become

$$\begin{aligned}U_P &= -V \cos\alpha_{nf} \cos\psi\beta + V \sin\alpha_{nf} - r\dot{\beta} - v_i \\ U_T &= -V \cos\alpha_{nf} \sin\psi - x\Omega\end{aligned}$$

Now define the dimensionless parameters

$$\lambda = (V \sin \alpha_{nf} - v_i)/\Omega R$$
$$\mu = V \cos \alpha_{nf}/\Omega R$$

and are termed the inflow ratio and advance ratio respectively. The parameter λ is the ratio of vertical velocity without flapping to the tip speed, and μ is the ratio of forward velocity to tip speed

The velocities U_P and U_T can then be written as

$$\begin{aligned} U_P &= \Omega R(\lambda - r\dot{\beta}/\Omega - \mu\beta \cos\psi) \\ &= \Omega R(\lambda - \tilde{r}\beta' - \mu\beta \cos\psi) \end{aligned}$$

where $\beta' = d\beta/d\psi = \dot{\beta}/\Omega$ is the flapping velocity with respect to the azimuth angle, and $\tilde{r} = r/R$ is the normalized radius. Similarly

$$U_T = \Omega R(\tilde{r} + \mu \sin\psi)$$

The angle of attack of the wind to the chord line of the blade is

$$\alpha = \theta + \frac{U_P}{U_T}$$

where θ is the incidence of the blade with respect to the no-feathering plane, and we assume the angle U_P/U_T is small.

B.2.2 Blade Flapping

The coefficient of lift C_L is proportional to the angle of attack α

$$C_L = a\alpha = a\left(\theta + \frac{U_P}{U_T}\right)$$

The differential lift acting on an elemental area of the blade $c\,dr$, where c is the chord length of the blade, is

$$dL = \frac{1}{2}C_L \rho U_T^2 c\, dr = \frac{1}{2}\rho a U_T^2 \left(\theta + \frac{U_P}{U_T}\right) c\, dr$$

The differential aerodynamic moment becomes

$$dM_A = r\,dL = \frac{1}{2}C_L\rho U_T^2 cr\,dr = \frac{1}{2}\rho a U_T^2\left(\theta + \frac{U_P}{U_T}\right)cr\,dr$$
$$= \frac{1}{2}\rho ac\Omega^2 R^4\left[\theta(\tilde{r}+\mu\sin\psi)^2 + (\lambda - \tilde{r}\beta' - \mu\beta\cos\psi)(\tilde{r}+\mu\sin\psi)\right]\tilde{r}\,d\tilde{r}$$

Integrating the above expression along the blade yields

$$M_A = \frac{1}{2}\rho ac\Omega^2 R^4\left[\theta\left(\frac{1}{4}+\frac{2}{3}\mu\sin\psi+\frac{1}{4}\mu^2\sin^2\psi\right)+\frac{1}{3}\lambda-\frac{1}{4}\beta'-\frac{1}{3}\mu\beta\cos\psi\right.$$
$$\left.+\frac{1}{2}\lambda\mu\sin\psi-\frac{1}{3}\mu\sin\psi\,\beta'-\frac{1}{2}\mu^2\cos\psi\sin\psi\,\beta\right]$$

The flapping equation was found to be

$$\beta'' + (1+\epsilon)\beta = M_A/I\Omega^2$$

introducing the above relationship for the aerodynamic flapping moment and rearranging yields

$$\beta'' + \frac{\gamma}{8}\left(1+\frac{4}{3}\mu\sin\psi\right)\beta' + \left[1+\epsilon+\frac{\gamma}{8}\left(\frac{4}{3}\mu\cos\psi+\mu^2\sin 2\psi\right)\right]\beta =$$
$$\frac{\gamma}{8}\left(1+\frac{8}{3}\mu\sin\psi+2\mu^2\sin^2\psi\right)\theta + \frac{\gamma}{8}\left(\frac{4}{3}\lambda+2\mu\lambda\sin\psi\right)$$

where $\gamma = \rho acR^4/I$ is the Lock inertia number. A typical value for γ is 6.

Strictly speaking this equation is only valid while the blade is advancing, $0 < \psi < \pi$. When the blade is retreating, $\pi < \psi < 2\pi$, there is reversed flow over some portion of the blade where the helicopter forward velocity is greater than the speed with which the blade retreats. In this situation $U_T < 0$ and occurs when

$$\tilde{r} + \mu\sin\psi < 0$$

Since the blade incidence is defined with respect to leading-edge to trailing-edge flow, the lift and flapping moments claculated in the reverse flow region are incorrect. However, these effects are small and can often be ignored for advance ratios less than 0.6, e.g. when $\mu = 0.3$ the area of reversed flow is only 2.25 % of the total rotor area and the velocities there are small.

Appendix C

Sampled-data Representations

We begin with the linear time-variant system

$$\dot{x}(t) = A(t)x(t) + B(t)u(t)$$
$$y(t) = C(t)x(t) + D(t)u(t)$$

The state transition matrix for the system Σ is

$$\Phi(t_1, t_0) = \Psi(t_1)\Psi(t_0)^{-1}$$

and the state solution for the system becomes

$$x(t) = \Phi(t, t_0)x(t_0) + \int_{t_0}^{t} \Phi(t, \tau)B(\tau)u(\tau)d\tau$$

the output solution is

$$\begin{aligned} y(t) &= C(t)x(t) + D(t)u(t) \\ &= C(t)\left\{\Phi(t, t_0)x(t_0) + \int_{t_0}^{t} \Phi(t, \tau)B(\tau)u(\tau)d\tau\right\} + D(t)u(t) \end{aligned}$$

Now consider the state (and output) to be sampled at $t = kT$, where T is the sample period. Making the substitutions, $(k+1)T \rightarrow t$ and $kT \rightarrow t_0$, and using the notation $x[k] = x(kT)$ we get

$$x[k+1] = x((k+1)T) = \Phi((k+1)T, kT)x(kT) + \int_{kT}^{(k+1)T} \Phi((k+1)T, \tau)B(\tau)u(\tau)d\tau$$

The control signal $u(t)$ is a zero-order hold such that

$$u(t) = u(kT) \qquad kT \leq t < (k+1)T$$

using this assumption the sampled state becomes

$$\begin{aligned} x[k+1] &= x((k+1)T) \\ &= \Phi((k+1)T, kT)x(kT) + \int_{kT}^{(k+1)T} \Phi((k+1)T, \tau)B(\tau)d\tau u(kT) \\ &= \Phi((k+1)T, kT)x[k] + \int_{kT}^{(k+1)T} \Phi((k+1)T, \tau)B(\tau)d\tau u[k] \\ &= A_k x[k] + B_k u[k] \end{aligned}$$

where

$$\begin{aligned} A_k &= \Phi((k+1)T, kT) \\ B_k &= \int_{kT}^{(k+1)T} \Phi((k+1)T, \tau)B(\tau)d\tau \end{aligned}$$

If we sample the output we get

$$\begin{aligned} y[k] = y(kT) &= C(kT)x(kT) + D(kT)u(kT) \\ &= C_k x[k] + D_k u[k] \end{aligned}$$

Daniel G. Cole

Education

Ph.D. in Mechanical Engineering
Virginia Polytechnic Institute & State University, December, 1998.

M.S. in Mechanical Engineering
Virginia Polytechnic Institute & State University, December, 1992.

B.S. in Mechanical Engineering, summa cum laude
Virginia Polytechnic Institute & State University, May, 1991.
Minor in Mathematics.

Professional Experience:

Research Assistant, 1998–present.
Center for Intelligent Material Systems & Structures, VPI&SU.

Instructor, 1996–1997.
Department of Mechanical Engineering, VPI&SU

Vice President & Sr. Research Scientist, 1993–1998.
Adaptive Technologies, Inc., Blacksburg, VA

Graduate Project Assistant, 1991–1995.
Department of Mechanical Engineering, VPI&SU

Selected Publications:

Saunders, W. R., D. G. Cole, C. A. Fannin, "Similitude Analysis for Piezostructures," *J. Intel. Mat. Sys. Struct.*, vol. 7, no. 2, pp. 162–167, March, 1996.

Clark, R. L., D. G. Cole and K. D. Frampton, "Phase Compensation for Feedback Control of Enclosed Sound Fields with In-bandwidth Transducers," *J. of Sound & Vib.*, 195(5), pp. 701–718, 1996.

Cole, D. G. and R. L. Clark, "Adaptive Compensation of Piezoelectric Sensoriactuators," *J. of Intel. Mat. Sys. Struct.*, vol. 5, no. 5, pp. 665–672, 1994.

Clark, R. L. and D. G. Cole, "Active Damping of Enclosed Sound Fields through Direct Rate Feedback Control," *J. Acoust. Soc. Amer.*, 97(3), pp. 1710–1716, 1995.

Saunders, W. R., D. G. Cole and H. H. Robertshaw, "Experiments in Piezostructure Modal Analysis for MIMO Feedback Control," *J. Smart Materials and Structures*, vol. 3, pp. 210–218, 1994.

Cole, D. G., W. R. Saunders and H. H. Robertshaw, "Modal Parameter Estimation for Piezostructures," *J. Vib. and Acoust.*, Dec. 1993.